

University of Windsor

## Scholarship at UWindor

---

Electronic Theses and Dissertations

Theses, Dissertations, and Major Papers

---

1984

### Bubble dynamics in viscoelastic media.

Joseph G. Mordarski  
*University of Windsor*

Follow this and additional works at: <https://scholar.uwindsor.ca/etd>



Part of the [Chemical Engineering Commons](#)

---

#### Recommended Citation

Mordarski, Joseph G., "Bubble dynamics in viscoelastic media." (1984). *Electronic Theses and Dissertations*. 1330.  
<https://scholar.uwindsor.ca/etd/1330>

This online database contains the full-text of PhD dissertations and Masters' theses of University of Windsor students from 1954 forward. These documents are made available for personal study and research purposes only, in accordance with the Canadian Copyright Act and the Creative Commons license—CC BY-NC-ND (Attribution, Non-Commercial, No Derivative Works). Under this license, works must always be attributed to the copyright holder (original author), cannot be used for any commercial purposes, and may not be altered. Any other use would require the permission of the copyright holder. Students may inquire about withdrawing their dissertation and/or thesis from this database. For additional inquiries, please contact the repository administrator via email ([scholarship@uwindsor.ca](mailto:scholarship@uwindsor.ca)) or by telephone at 519-253-3000ext. 3208.



National Library  
of Canada

Bibliothèque nationale  
du Canada

Canadian Theses Service

Services des thèses canadiennes

Ottawa, Canada  
K1A 0N4

## CANADIAN THESES

## THÈSES CANADIENNES

### NOTICE

The quality of this microfiche is heavily dependent upon the quality of the original thesis submitted for microfilming. Every effort has been made to ensure the highest quality of reproduction possible.

If pages are missing, contact the university which granted the degree.

Some pages may have indistinct print especially if the original pages were typed with a poor typewriter ribbon or if the university sent us an inferior photocopy.

Previously copyrighted materials (journal articles, published tests, etc.) are not filmed.

Reproduction in full or in part of this film is governed by the Canadian Copyright Act, R.S.C. 1970, c. C-30. Please read the authorization forms which accompany this thesis.

THIS DISSERTATION  
HAS BEEN MICROFILMED  
EXACTLY AS RECEIVED

### AVIS

La qualité de cette microfiche dépend grandement de la qualité de la thèse soumise au microfilmage. Nous avons tout fait pour assurer une qualité supérieure de reproduction.

S'il manque des pages, veuillez communiquer avec l'université qui a conféré le grade.

La qualité d'impression de certaines pages peut laisser à désirer, surtout si les pages originales ont été dactylographiées à l'aide d'un ruban usé ou si l'université nous a fait parvenir une photocopie de qualité inférieure.

Les documents qui font déjà l'objet d'un droit d'auteur (articles de revue, examens publiés, etc.) ne sont pas microfilmés.

La reproduction, même partielle, de ce microfilm est soumise à la Loi canadienne sur le droit d'auteur, SRC 1970, c. C-30. Veuillez prendre connaissance des formules d'autorisation qui accompagnent cette thèse.

LA THÈSE A ÉTÉ  
MICROFILMÉE TELLE QUE  
NOUS L'AVONS REÇUE.

# BUBBLE DYNAMICS IN VISCOELASTIC MEDIA

by

Joseph G. Mordarski

A Thesis

Submitted to the Faculty of Graduate Studies through  
the Department of Chemical Engineering in Partial  
Fulfillment of the Requirements for the Degree of  
Master of Applied Science  
at the University of Windsor

Windsor, Ontario, Canada



1984.

© Joseph George Mordarski  
All Rights Reserved

1984

**802088**

## ABSTRACT

Dynamics of air bubbles in three rheologically different fluids have been studied. The two main aspects of bubble dynamics examined were terminal velocity and coalescence. Equipment was designed to inject these bubbles automatically, as well as simultaneously without disturbing the fluid. Velocity volume data were collected for a Newtonian fluid (40% (wt) glycerol in water), and for two non-Newtonian fluids (1% (wt) Carboxymethylcellulose in water and 1% (wt) of Polyacrylamide in 50/50 glycerol and water.

No velocity discontinuity was observed in the case of the log-log plots of velocity versus volume for the three fluids. Also, there was no appreciable effect of injection period of the air bubbles upon their terminal velocities. Friction factors (drag coefficients) were also determined for bubbles travelling in the three fluids, for different Re numbers. All experimental data concerning bubble motion were obtained through a photographic technique, with a 16mm movie produced to summarize the extent of the experimental work.

The coalescence phenomena was examined for two and three air bubbles injected simultaneously in the 1% CMC and the 1% PAA solutions. In both cases, coalescence followed a regular sequence, first the trailing bubble/bubbles enter the wake of the leading bubble, then the bubble/bubbles accelerated towards the leading bubble until collision occurred. This action resulted in a thin film separating each, continuing with a film thinning process until complete coalescence.

The movie detailed that coalescence was also a symmetric phenomena under simultaneous injection with horizontal separation. An empirical relation was obtained for the bubble volume required to coalesce with a  $1.0 \times 10^{-6} \text{ m}^3$  bubble as a function of horizontal orifice separation, illustrating the delaying effect of elasticity upon bubble coalescence.

## ACKNOWLEDGEMENTS

I would like to thank all the people involved with this project and offer them my sincere gratitude. Special thanks go to my mentor, Dr. D. De K  e for his guidance in the course of this work.

To George Ryan, the technician responsible for manufacturing the equipment and to Marcella Carson for her meticulous typing of the thesis. Thanks go also to my brother, John, who provided me with company and assistance during the long experimental runs.

I would like to thank the University of Windsor and the Ontario government for the studentships received during the course of this project.

I would also like to extend my thanks to Bob Tattersall, Werner Beck, the technicians at the central design shop and to Bob Gaspar for his photographic services.

## TABLE OF CONTENTS

	<u>PAGE</u>
ABSTRACT .....	i
ACKNOWLEDGMENTS .....	iii
TABLE OF CONTENTS .....	iv
LIST OF FIGURES .....	v
LIST OF TABLES .....	vii
CHAPTER	
I. INTRODUCTION .....	1
II. LITERATURE SURVEY	
(i) Bubble Shape and Motion .....	3
(ii) Coalescence Phenomena .....	25
III. EXPERIMENTAL DETAILS	
(i) Equipment .....	34
(ii) Operation .....	76
IV. RESULTS AND DISCUSSION	
(i) Single Bubble Phenomena .....	77
(ii) Multiple Bubble Injection .....	116
V. CONCLUSIONS .....	134
VI. RECOMMENDATIONS FOR FURTHER WORK .....	136
NOMENCLATURE .....	138
REFERENCES .....	141
APPENDIX I .....	144
Experimental Results of Terminal Velocity, Volume, Diameter and Height of Bubbles in the 3 Fluids studied.	
APPENDIX II .....	155
Non-Linear Regression Computer Program Utilized in Modelling Viscosity and Primary Normal Stress Difference.	
APPENDIX III .....	159
Uncertainty Analysis and Standard Deviations of Fitted Curves	
Vita Auctoris.....	164



## LIST OF FIGURES

		<u>PAGE</u>
II-1	Generalized Correlation of Reynolds Number Versus Eötvös Number for Drops and Bubbles Rising Freely in Immiscible Newtonian Liquids for Constant Morton Numbers.	13
II-2A	Shapes of Bubbles In a Pseudoplastic Solution.	15
II-2B	Geometry of 2 Wake Models	15
II-3	A Typical Velocity-Volume Plot for a Viscoelastic Fluid	20
III-1	Cylindrical Pressure Distributor	36
III-2	Typical Orifice	36
III-3	Orifice Configuration for Multiple Bubble Injection	39
III-4	Orifice Configuration for Single Bubble Injection	39
III-5	Rotational System for Multiple Bubble System	41
III-6	"Harris Check Valve"	45
III-7	"Norgren Check Valve"	45
III-8	A Typical Spring Return Pneumatic Cylinder (Disassembled)	47
III-9	Schematic of a Pneumatic Cylinder	50
III-10	Injection System for Sample Gas Stored at Atmospheric and Non-Atmospheric Pressure	52
III-11	"MS-A" Measuring System A	56
III-12	"MS-B" Measuring System B	56
III-13	MS-A and MS-B Set Up for Simultaneous Double Bubble Experimentation	58

# LIST OF FIGURES (CONTINUED)

		<u>PAGE</u>
III-14	The Multiple Bubble Circuit	60
III-15	Schematic of Electronic Control System	64
III-16	Single Bubble Injection Apparatus With Light Diffuser	67
III-17	Schematic of Single Bubble Apparatus	70
III-18	Rheomat 30 Viscometer with Programming Unit and x-y Recorder	74
IV-1	Viscosities as a Function of the Shear Rate for The Three Test Fluids	83
IV-2	Primary Normal Stress Difference as a Function of the Shear Rate for 1% CMC and 1% PAA.	85
IV-3	Bubble Shapes in a 40% Aqueous Glycerol Solution.	92
IV-4	Eccentricity (D/H) for Newtonian and Viscoelastic Solutions.	95
IV-5	The Effect of Injection Period( $\tau$ ) on (D/H) for 1% PAA.	98
IV-6	Bubble Shapes in 1% CMC and 1% PAA	101
IV-7	Terminal Velocity as a Function of Bubble Volume for the Three Test Fluids( $\tau=10$ s)	105
IV-8	The Effect of Injection Period on Terminal Velocity for 1% PAA.	108
IV-9	Drag Coefficient versus Re for the Three Test Fluids.	111
IV-10	Bubble Coalescence with a $1.0 \times 10^{-6} \text{ m}^3$ Bubble as a Function of Orifice Separation ( $\Lambda$ ) and Injection Period( $\tau$ )	117
IV-11	Three Bubble Coalescence Phenomena	126
IV-12	Small Bubble Coalescence Phenomena	130
IV-13	Large Bubble Coalescence Phenomena	132

## LIST OF TABLES

	<u>PAGE</u>
II-1 Values of the Critical Radius Where Velocity Transition Occurs	24
III-1 Multiple Bubble Orifice Separation Distances	43
III-2 Equipment Schedule	72
IV-1 Surface Tension and Density Values	82
IV-2 Constants Utilized in De Kee Models	90
IV-3 Summary of Triple Bubble Phenomena	124

## CHAPTER I. INTRODUCTION

The motion of gas bubbles rising in a liquid interfaces with many areas of Chemical Engineering. Numerous examples of bubble motion and mass transfer in non-Newtonian fluids are of importance to the chemical industry today, particularly in the areas of polymer processing technology and foaming dynamics. A highly specialized industrial application is in the area of molten polymers. By studying the motion of gas bubbles in polymeric solutions, experimentalists are able to map velocity fields within these materials and further enhance flow phenomena present in this regime.

There has been a great deal of work published in the field of bubble dynamics for Newtonian fluids with a lower emphasis placed on the rheologically complex viscoelastic fluids. Therefore the aim of this thesis is to continue to examine single and multiple gas bubble motion in viscoelastic liquid media.

The objectives of this experimental study are to

- i) investigate the shape and rise velocities of bubbles in viscoelastic media as a function of injection period and bubble volume.
- ii) In addition, the simultaneous injection of several bubbles will be studied with respect to their possible agglomeration as a function of their relative volumes and injection distances.

- iii) Finally this thesis will attempt to provide a logical explanation for a peculiar phenomenon occurring between the bubble rise velocity and bubble volume. Experimentalists such as Astarita and Apuzzo (A1), and Acharya et al. (A2) have reported a strikingly abrupt increase in velocity after reaching a "critical volume" of ascending gas bubble .

## CHAPTER II. LITERATURE SURVEY

Bubble motion is of paramount importance in the design and maintenance of process equipment with which process engineers are involved. It is essential that the behaviour of single bubbles be comprehended before a full knowledge of interacting bubbles can be achieved. In the past, the study of gas bubble motion within viscoelastic medias has received less attention than studies involving Newtonian fluids. This is due to the rheological complexities which are inherent when dealing with non-Newtonian fluids. This chapter is divided into two distinct areas: (i) dealing with bubble shape and motion. (ii) examining bubble coalescence.

### (i) Bubble Shape and Motion

The motion of gas bubbles in viscoelastic liquids was studied by Astarita and Apuzzo (A1), among others. They reviewed existing theoretical knowledge on gas bubble motion in Newtonian liquids and expanded these concepts to viscous and viscoelastic non-Newtonian liquids. Their research provided experimental information on gas bubble motion in the low and high Reynolds number region and highlighted the appearance of a discontinuity in the ascending velocity-bubble volume relationship for elastic fluids.

Acharya et al. (A2) provided quantitative experimental data for bubbles moving in the low and high Reynolds num-

ber region and confirmed previous observations (A1) of a velocity discontinuity in non-Newtonian media.

Astarita (A3) also presented a mathematical analysis of bubble motion in a Maxwell fluid. Using dimensionless groups, he generated an order of magnitude analysis relating flow regime to elastic properties. The hypothesis of Astarita and Apuzzo (A1) that the velocity discontinuity mainly represented a changeover from a rigid interface to a free interface regime was supported by Leal et al. (L1). By comparing terminal velocity data for gas bubbles and glass spheres in aqueous polyacrylamide solutions, they provided evidence that the velocity discontinuity indeed represented from a change in interfacial conditions, from "non-slip" to "free-shear".

Calderbank et al. (C1), using an aqueous 1% polyethyleneoxide solution, provided data on bubble shape transitions as well as tailing phenomena. Their research confirmed previous findings (A1, A2, L1) related to a velocity discontinuity at a critical bubble volume. They also observed a peculiar change in shape at that instant.

Barnet et al. (B1) examined experimentally bubble motion and mass transfer in non-Newtonian fluids. Their paper outlined transitional bubble shapes in aqueous carboxymethyl cellulose (CMC) solutions and highlighted the observed relationship existing between tailing at the rear of the bubble and an increase in the drag coefficient.

Corresponding to each shape transition, they also noticed an increase in the mass transfer coefficient. Hassager (H1) claims that the phenomena of bubble tailing is related to the concept of a negative wake forming directly behind the rising bubble due to the liquid velocity being in the downward direction, away from the rising bubble.

Grace and Harrison (G1) also investigated the influence of shape on the rising velocities of large bubbles. Their paper derived equations for the rising velocities in water of elliptical cap and ovary ellipsoidal bubbles in terms of bubble volume and axes dimensions. They confirmed experimentally that elliptical cap and ovary ellipsoidal bubbles rise faster than the corresponding circular-cap and spherical-cap bubbles.

Harmathy (H2) outlined a new theory in calculating the terminal velocity of bubbles moving in a media of restricted extent. He related the terminal velocity to the drag coefficient. Since the drag coefficient is dependent upon shape, the terminal velocity eventually becomes linked to the Eötvös number. This analysis, however, is only valid for viscous fluids for Reynolds numbers greater than 500.

Empirical correlations developed by Grace et al. (G2) are given for predicting the shape regime, aspect ratio and terminal velocity of drops and bubbles based on the volume or equivalent diameter of the fluid particle and the system properties. The results are valid for both drops and



bubbles rising or falling freely under gravity in immiscible Newtonian liquids.

Garner and Hammerton (G3) examined the movement inside rising gas bubbles by the addition of ammonium chloride fog. They concluded that gas bubbles of diameter smaller than  $3.0 \times 10^{-4} \text{ m}$  ( $V = 6.28 \times 10^{-4} \text{ m}^3$ ) in water behaved as rigid spheres while bubbles of larger diameter showed vigorous internal toroidal circulation. Pertaining to droplets or gas bubbles, the existence of regular circulatory currents has been previously postulated by Hadamard (H3) and Rybczynski (R1) to be due to viscous drag of the outer fluid.

Zieminski and Raymond (Z1) experimentally studied the behaviour of a single bubble in water. The aim of their paper was to evaluate mass transfer coefficients. The reproducibility of their results appeared to be affected by the bubble detachment from the nozzles. Costes and Alran (C2) presented an excellent discussion of models for the formation of gas bubbles at a single submerged orifice in a CMC solution.

Their paper discussed models of bubble formation in non-Newtonian liquids, based on concepts given by Davidson and Schuler (D1) and Kumar and Kuloor (K1). There have also been several analytical investigations into the low and moderately high Reynolds number regime. Due to the complex rheology and presence of inertia terms in the equations of motion, it is difficult to obtain exact solutions and hence

approximate techniques have been applied. For the case of a single bubble rising in a power law fluid and in a Bingham fluid, Bhavaraju et al. (B2) used a perturbation method to obtain analytical solutions for determining the Sherwood numbers and drag coefficients. Their solutions are only valid in the creeping flow regime.

Hirose and Moo-Young (H4) obtained an approximate solution for single bubble motion in power law fluids. They (H5) also solved the problem of the creeping motion of a gas bubble in an Oldroyd fluid. Later Mashelkar (M1) obtained an approximate solution for the motion of a swarm of bubbles moving in a power law fluid by following the approach of Hirose and Moo-Young (H4) and by using Happel's free surface cell model.

Chhabra and Uhlherr (C3) examined the creeping motion of spheres through shear thinning elastic fluids described by the Carreau viscosity equation. Their analysis used a variational principle to solve the equations of motion and continuity in conjunction with the Carreau constitutive equation.

Ting (T1) utilized the Oldroyd-three-constant model for a viscoelastic liquid in determining the important parameters through which polymer viscoelasticity may affect the dynamics of a single bubble. He stressed the importance of elongational viscosity for bubbles undergoing growth or collapse processes under biaxial elongation.

Yang and Liang (Yl) investigated the dynamic behaviour of a spherical gas bubble in a creep process utilizing the generalized Maxwell model for viscoelastic behaviour. They also postulated that the effect of surface tension on bubble behaviour is entirely negligible except near its complete collapse.

The motion of a gas bubble in a liquid can be governed by: (i) Dimensionless groups (C4) such as the:

$$\text{Eötvös Number} \quad E_o = \frac{g \Delta \rho D_e^2}{\sigma} \quad (\text{II-1})$$

$$\text{Reynolds Number} \quad Re = \frac{\rho D_e \langle v \rangle}{\mu} \quad (\text{II-2})$$

$$\text{Morton Number} \quad Mo = \frac{g \mu^4 \Delta \rho}{\rho^2 \sigma^3} \quad (\text{II-3})$$

where:

- $g$  = the acceleration due to gravity ( $\text{m/s}^2$ ).
- $\sigma$  = the surface tension ( $\text{N/m}$ ).
- $D_e$  = the equivalent diameter ( $\text{m}$ ).
- $\langle v \rangle$  = the average bubble velocity ( $\text{m/s}$ ).
- $\mu$  = the dynamic viscosity ( $\text{Pa} \cdot \text{s}$ ).

$\rho_p$  = the bubble density ( $\text{kg/m}^3$ ).

$\rho$  = the density of the continuous phase ( $\text{kg/m}^3$ ).

$\Delta\rho = \rho - \rho_p$  ( $\text{kg/m}^3$ ).

(ii) Shape regime of bubble (C4, A1, G1)

- spherical
- ellipsoidal
- spherical cap

(iii) Interfacial characteristics (A1, C2, H3, R1)

- rigid interface
- free interface

(iv) Orifice characteristics (B3, C2, K1, D1)

- diameter
- shape

(v) Internal circulation (R1, Z1, G3)

- presence of
- absence of

The shapes of freely rising bubbles are dependent upon hydrodynamic forces and surface phenomena (A1, A2, L1, C2). These hydrodynamic forces and surface phenomena acquire different values depending upon the particular regime of flow as well as the interfacial characteristics of the bubble. For example, stresses set up due to differences in surface tension between the front and rear of the bubble cause a retarding effect upon bubble motion. However, as the bubble size increases, these stresses diminish, which allows the bubble to behave with a free interface, assisting bubble motion (A2). This could occur during motion in the "Levich" regime where the Reynolds number is high, the bubble spherical, and the interface is free (A2).

Although slight disagreement persists amongst researchers concerning the definitions of the conditions associated with each flow regime, most agree on the existence of four distinct regimes. Before critically examining the four flow regimes, an explanation of "free" and "rigid" interfaces is suitable. A free interface refers to a condition whereby the surface tension forces are considerably reduced with respect to the viscous stresses, usually for large bubbles, that is  $V > 1.0 \times 10^{-6} \text{ m}^3$  (B3). A bubble with a free interface has surface shear stresses considerably reduced and continuous thereby allowing momentum to be transferred across the interface res-

ulting in internal circulation.(G3). A rigid interface denotes that the interface velocity is everywhere equal to the velocity of the bubble's centre of gravity, or the bubble behaves as though the interface is rigid (A2). The four flow regimes and conditions associated with each as outlined by (A1, A2, C2) are as follows.

The Stokes regime applies for creeping flow with a spherical bubble and a rigid interface. The Hadamard regime occurs for creeping flow with a spherical bubble and a free interface. The Levich regime deals with a spherical bubble moving with a high Reynolds number, and a free interface. The conditions for flow in the Taylor regime are a high Reynolds number, a bubble with a spherical cap and a free interface. However, all these conditions occurring simultaneously under a particular flow regime, may be difficult to realize in a practical situation. Nevertheless, as evident from the introduction of the four flow regimes, a correct evaluation of the Reynolds number is paramount.

A modified Reynolds number for power law fluids has been given by Astarita and Apuzzo (A1) of the form:

$$Re = \frac{(2R)^n \rho \langle v \rangle^{2-n}}{m} \quad (II-4)$$

where:

R = the radius of the bubble (m).

m = the fluid consistency index ( $\text{kgm}^{-1}\text{s}^{n-2}$ ).

$n$  = a fluid behaviour index (dimensionless).

The Carreau viscosity Equation (II-5) has been proven to work well in describing viscosity versus shear rate for viscoelastic solutions and melts.

$$\frac{\eta - \eta_{\infty}}{\eta_0 - \eta_{\infty}} = \left[ 1 + (t_1 \dot{\gamma})^2 \right]^s \quad (\text{II-5})$$

where:

$\eta$  = the non-Newtonian viscosity (Pa.s).

$\eta_0$  = the zero shear viscosity (Pa.s).

$\eta_{\infty}$  = the infinite shear viscosity (Pa.s).

$s$  = a dimensionless parameter in the Carreau viscosity equation.

$\dot{\gamma}$  = the shear rate ( $s^{-1}$ ).

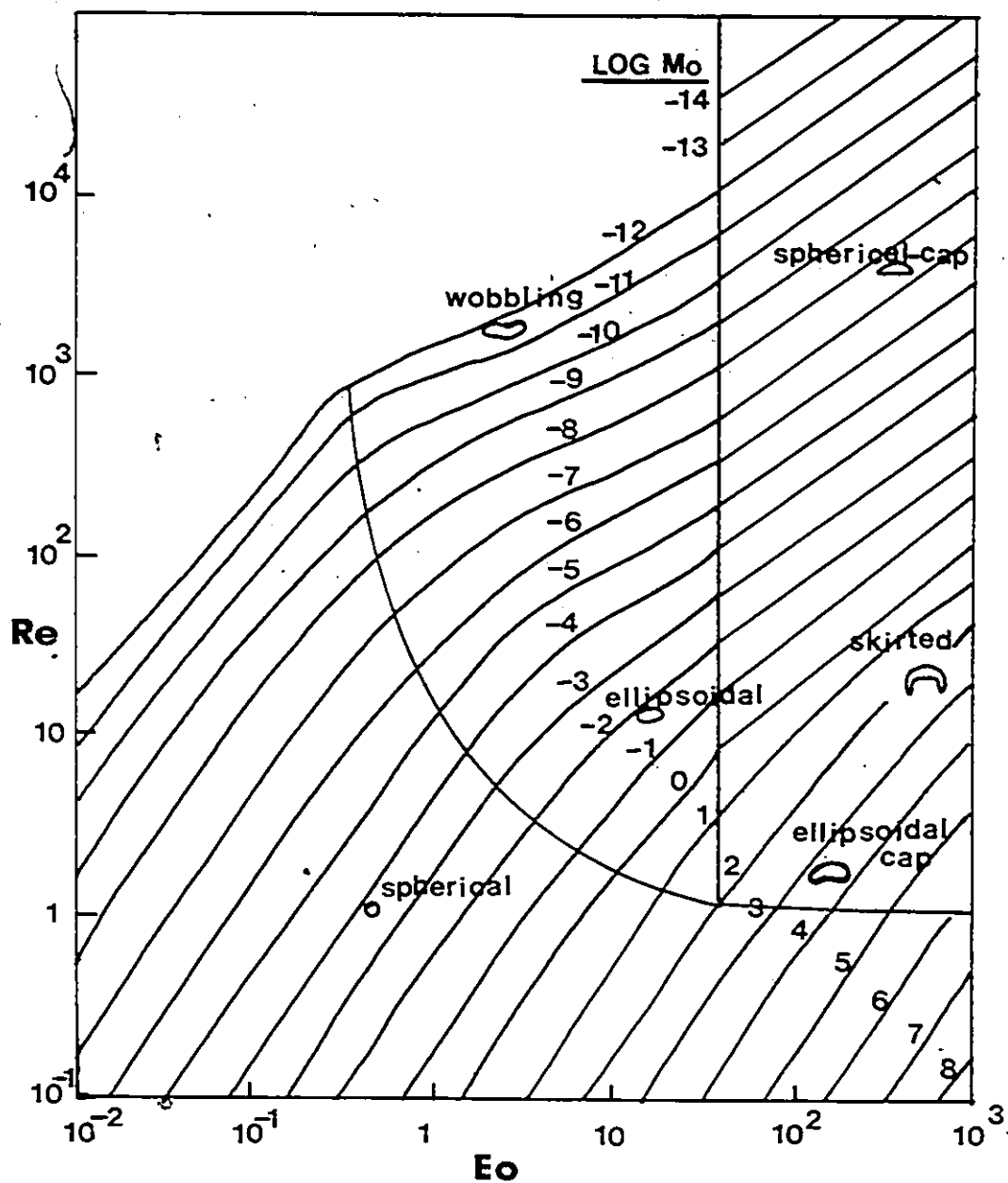
$t_1$  = a time constant (s).

Utilizing the Carreau viscosity equation, Chhabra and Uhlherr (C2) present a Reynolds number of the form:

$$Re = \frac{\rho \langle v \rangle D_e}{\eta} \quad (\text{II-6})$$

With the use of dimensionless groups such as the  $Re$ ,  $Mo$ , and  $Eo$  numbers, a generalized graphical correlation of Figure(II-1) gives one method of estimating terminal velocities of drops and bubbles for all regimes.

Bubbles which are in free rise in a liquid medium may



Figure(II-1) Generalized Correlation of Reynolds Number versus Eötvös Number for Drops and Bubbles Rising Freely in Immiscible Newtonian Liquids for Constant Morton Numbers



adopt three general configurations (C4), spherical, ellipsoidal and spherical or ellipsoidal cap. Bubbles of spherical configuration require interfacial tension and/or viscous forces to be more prominent than inertia forces. Ellipsoidal bubbles refer to bubbles which are oblate and have a convex interface. They undergo periodic dilatations and random wobbling motions. Spherical cap or ellipsoidal cap bubbles refer to large bubbles which adopt flat or indented bases.

Astarita and Apuzzo (A1) utilized aqueous viscoelastic, viscous pseudoplastic and highly elastic solutions. Typical shapes observed by them in pseudoplastic solutions are shown in Figure (II-2A). While large volume bubbles maintained the shape of a spherical cap, a peculiarity exists in the lower volume region. The dorsal surface of the bubble obtains a visible protruding tip or "cusp" at the center. No such behaviour exists for Newtonian liquids.

Astarita and Apuzzo (A1) also indicate that the gas bubbles in Carbopol and CMC revealed shape regimes of Newtonian character, passing from spherical to oblate-ellipsoid to spherical cap. They attribute the tailing phenomenon to the viscoelastic nature of the fluid.

Massager (H1), using laser doppler anemometry, investigated the tailing phenomenon and presented an interesting finding. He discovered that the liquid velocity in the wake behind the bubble was opposite in direction to normal

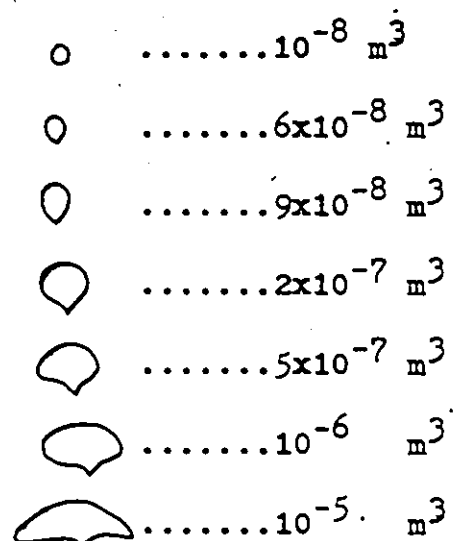


Figure (II-2A) Shapes of Bubbles in a Pseudoplastic Solution

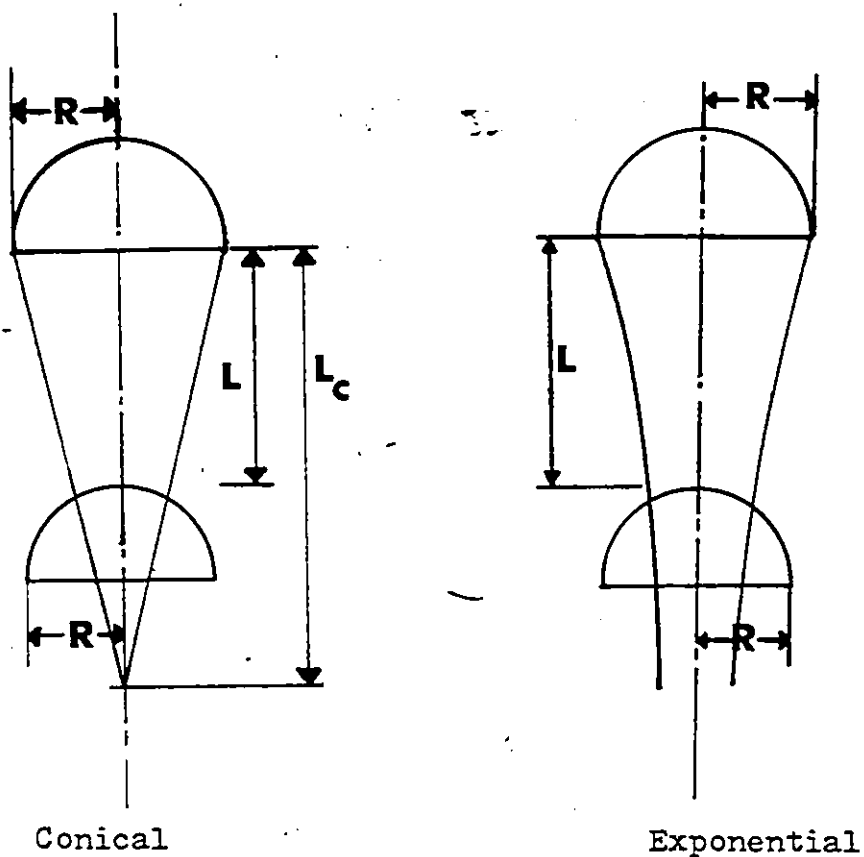


Figure (II-2B) Geometry of 2 Wake Models

wake velocity profiles in Newtonian fluids; that is, the velocity was in the downwards direction. He called this the negative wake.

For the case of a 1% polyacrylamide (PAA) solution in glycerol, the fluid behind the bubble, instead of being pulled along in the usual wake pattern is in fact recoiling, thereby producing a tail at the bubble posterior.

Leal et al. (L1) employing different concentrations of PAA noted differences in observations of bubble shape in viscoelastic media as compared to Newtonian media. With an increase in bubble volume, the bubble changed from spherical to a prolate teardrop shape and finally to a spherical cap with rounded edges and a cusped trailing surface as shown in Figure (II-2A).

Calderbank et al. (C1) observing carbon dioxide bubbles in a 1% aqueous solution of PEO (polyethylene oxide), report that shapes go from spherical to prolate spheroidal to oblate spheroid with a tail, to that of a spherical cap. Calderbank et al. (C1) also noticed the tailing phenomenon occurring for bubbles with equivalent diameters between  $2.7 \times 10^{-3} \text{ m}$  and  $2.2 \times 10^{-2} \text{ m}$ .

Acharya et al. (A2), using aqueous solutions of PEO and PAA (polyacrylamide) demonstrated that the bubbles were teardrop shaped at small Reynolds numbers. With increasing Reynolds numbers, the bubble shapes tended to be spherical, oblate spheroidal and finally spherical capped.

At small Reynolds numbers, inertia forces are negligible as compared to viscous forces, so that the surface tension keeps the bubble shape spherical. Teardrop shaped bubbles are observed due to the interaction of the elastic and surface tension forces.

Barnet et al. (B1), investigating bubble motion and mass transfer in an aqueous solution of CMC observed that as the bubble volume increased, the bubble shape went from spherical to ellipsoidal to a top shape and finally to a spherical cap. They believed the tailing phenomenon to be affected by a complex interaction of interfacial tension and internal circulation.

Batchelor and Bond (B3) contend that the characteristics of an orifice will influence the corresponding bubble shape, size and resulting motion. They assert that for circular orifices up to  $4.0 \times 10^{-4}$  m in diameter, the bubbles will be spherical. For orifices between  $4.0 \times 10^{-4}$  m and  $4.0 \times 10^{-3}$  m in diameter, the bubbles are spherical at the orifice, but upon release, rapidly assume an ellipsoidal shape. With orifice diameters exceeding  $4.0 \times 10^{-3}$  m, the bubble becomes unstable, it may assume a saucer shape or an unsymmetric shape, with the possibility also of the formation of small satellite bubbles. However, this behaviour was observed for Newtonian fluids only.

In general, the terminal velocity of a gas bubble, be it a non-Newtonian fluid, will increase with increasing

volume. Astarita and Apuzzo (A1) have shown that for viscoelastic fluids, the terminal velocity ( $v_{\infty}$ ) increases with increasing volume more rapidly than for Newtonian liquids. They have also derived some theoretical velocity-volume relationships for the viscoelastic liquids used. For the Stokes regime, they present the following relationship:

$$\langle v \rangle = \left[ \frac{\rho g}{\eta} \cdot \frac{2^{1+n}}{X_n} \left( \frac{4\pi}{3} \right)^{\frac{2-n}{3}} \right]^{\frac{1}{n}} V^{\left[ \frac{1+n}{3n} \right]} \quad (\text{II-8})$$

where:

$X_n$  = function of the flow index  $n$ .

For the Hadamard regime, no direct relationship is asserted between  $\langle v \rangle$  and  $V$ ; however, a ratio exists of the form:

$$\frac{v_{\text{Hadamard}}}{v_{\text{Stokes}}} = \left[ \frac{X_n}{X'_n} \right]^{1/n} > 1.5 \quad (\text{II-9})$$

$X'_n$  = function of the flow index  $n$ .

The Levich regime is modelled through Equation (II-8) where  $X_n$  is substituted by  $K_n$ , and  $K_n$  is represented by:

$$K_n = \frac{2^{n+3} 3^{n+1}}{1+4n} \int_0^1 (1+2\phi^2)^{(n+1)/2} d\phi \quad (\text{II-10})$$

where:

$K_n$  is a dimensionless parameter defined by Equation(II-10).

$\Phi$  is a dummy variable.

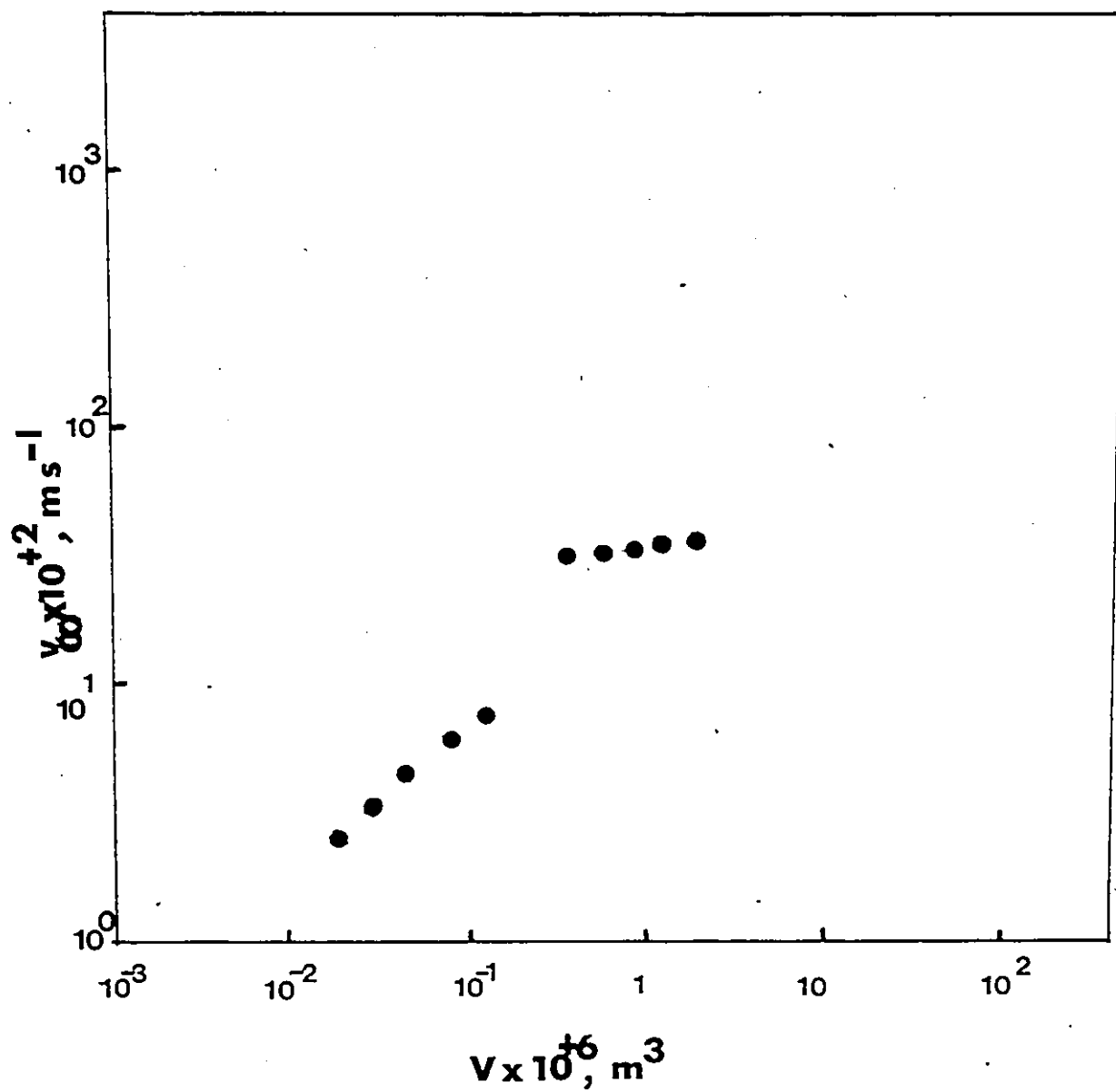
The Taylor regime is modelled by:

$$\langle v \rangle = 25.0 v^{1/6} \quad (\text{II-11})$$

Some authors (A1, A2, C1, L1, B1) report a region for non-Newtonian fluids, where there is a large increase in velocity over a small range of volume, the so-called "velocity discontinuity phenomenon". Viscoelastic fluids are prime contributors to this phenomenon. A typical representation of this phenomenon is presented in Figure(II-3).

Astarita and Apuzzo (A1) have reported a six fold jump in the terminal velocity, when a certain volume was reached with their pseudoplastic solutions (Et-497, J-100).

They have offered the hypothesis that the velocity discontinuity was due to a sudden transition from the Stokes to Hadamard region (basically from a rigid to free interface), and that viscoelasticity was somehow responsible for making the transition abrupt, rather than continuous, as for Newtonian fluids. The magnitude of the velocity jump could be largely attributed to the dependence of viscosity on shear rate similar to that found in power law fluids. They also noticed a transition in bubble shape, when  $V < V_{Cr}$



Figure(II-3) A Typical Velocity-Volume Plot for a Viscoelastic Fluid

(critical volume). Although the rear pole is cuspidal the whole bubble surface appears to be convex. When  $V > V_{cr}$  the protruding tip at the rear pole is more marked and the bubble surface appears to be concave along a horizontal circle slightly above the protruding tip. In favour of this interpretation is the fact that the shape of the  $\log \langle v_{\infty} \rangle$  versus  $\log V$  curves is the same for volumes above and below  $V_{cr}$ .

Calderbank et al. (C1) observed the same velocity phenomenon occurring at a critical volume while working with an aqueous 1% PEO solution. They observed an increase in velocity by a factor of 4 at a critical volume ( $V_{cr}$ ) of  $1.1 \times 10^{-8} \text{ m}^3$ . They also observed that the rise velocity of  $\text{CO}_2$  bubbles in non-Newtonian PEO were always lower than in distilled water. In addition, the following theoretical equations for bubble rise velocity in Newtonian fluids were employed by Calderbank et al. (C1).

$$\text{STOKES REGIME } \langle v \rangle = \frac{184}{\nu} V^{2/3} \quad (\text{II-12})$$

where:  $\nu$  is the kinematic viscosity ( $\text{m}^2/\text{s}$ ).

$$\text{HADAMARD REGIME } \langle v \rangle = \frac{126}{\nu} V^{2/3} \quad (\text{II-13})$$

$$\text{LEVICH REGIME } \langle v \rangle = \frac{42}{\nu} V^{2/3} \quad (\text{II-14})$$

$$\text{TAYLOR REGIME } \langle v \rangle = 25.0 V^{1/6} \quad (\text{II-15})$$



MENDELSON EQUATION (Ellipsoids and Spherical caps,  
free interface)

$$\langle v \rangle = \sqrt{\frac{2\sigma}{D_e \rho} + \frac{g D_e}{2}} \quad (\text{II-16})$$

DUMITRESCU EQUATION (Gas slugs, free interface)

$$\langle v \rangle = \sqrt{0.35 g D_e} \quad (\text{II-17})$$

Calderbank et al. (C1) determined that for large spherical cap bubbles in the PEO solution, the terminal rise velocities asymptotically approached the predictions of the Dumitrescu equation.

Leal et al. (L1) observed the transition occurring at a value of the equivalent critical radius approximately equal to  $2.9 \times 10^{-3} \text{ m}$ , for a 1% PAA solution. The magnitude of the velocity jump was 5-10 fold. They claim the discontinuity results from a change in interfacial conditions, from a condition of no slip to free shear at the bubble interface. They assert that only a fraction of the observed velocity jump is due to shear dependence of viscosity, the influence of elastic or normal stress effects must be included. Finally, they postulate that the stress relaxation phenomenon associated with the fluid passing around the bubble produces large tensile stress effects, which could explain the velocity discontinuity.

Acharya et al. (A2) noticed the velocity jumps with aqueous CMC, PEO, and PAA solutions, but not to the same degree as that reported by Astarita and Apuzzo (A1) and by Calderbank et al. (C1). Leal et al. (L1), and Acharya et al. (A2) also observed that solid bodies (spheres) of the same size and density difference produced no discontinuity.

In Table (II-1), a summary is prepared of the critical radius of the bubble at which this velocity discontinuity has occurred. Acharya et al. (A2) agree with the previously mentioned hypothesis that a mobile surface is required for a discontinuity to occur.

The stresses which are set up due to the difference in surface tension between the front and rear part of the bubble have a retarding influence on the bubble motion. With increased bubble size these stresses diminish in relation to the viscous stresses and the bubble tends to be mobile; that is the interface is "freed". To explain a lower magnitude velocity jump observed by their work, they suggest that Astarita and Apuzzo (A1) and Calderbank et al. (C1) created a more abrupt velocity discontinuity by using shear thinning fluids.

Acharya et al. (A2) concluded that surface effects may play a major role at which point this discontinuity will occur. They postulate that polymer molecules act as large surfactants and the flow induced gradients of these large molecules may be responsible for generating the surface stresses which oppose the circulatory motion

TABLE (II-1) . VALUES OF THE CRITICAL RADIUS WHERE VELOCITY TRANSITION OCCURS

SOLUTION	CRITICAL RADIUS $\times 10^{-2} \text{ m}$	REFERENCE
1 Polyacrylamide ET-497 (0.3%)	0.267	A1
2 Polyacrylamide ET-497 (0.7%)	0.288	A1
3 Polyacrylamide J-100 (0.25%)	0.271	A1
4 Polyacrylamide J-100 (0.5%)	0.286	A1
5 Polyethyleneoxide MSR-301 (1%)	0.134	C1
6 Polyacrylamide AP-30 (0.5%)	0.281	L1
7 Polyacrylamide AP-30 (1.0%)	0.265	L1
8 Polyacrylamide AP-30 (0.5%)	0.300	Z2
9 Polyacrylamide AP-30 (1%)	0.310	Z2
10 Polyethyleneoxide MSR-301 (0.5%)	0.243	A2
11 Polyacrylamide AP-30 (0.05%)	0.182	A2
12 Polyacrylamide AP-30 (0.1%)	0.191	A2

existing within the gas bubble.

This reasoning is also supported by Clift et al. (C4). Hence, the partial cleansing of the surface responsible for the rapid velocity change is likely to occur more abruptly in the case of a viscoelastic fluid.

Acharya et al. (A2) also disagreed with Carreau's ideas relating the discontinuity to the injection frequency. Finally, they propose an equation in the region of the velocity discontinuity. Their equation is given by:

$$\frac{v_{\text{free interface}}}{v_{\text{rigid interface}}} = 1.5 \left(\frac{3}{2}\right)^{n-1} \frac{(33n^4 - 64n^3 - 11n^2 + 97n + 16)}{4n^2 (n+1) (13 + 4n - 8n^2)} \dots\dots (II-18)$$

Garner and Hammerton (G3), working with Newtonian fluids (glycerol, white oil and water), observed a similar velocity transition taking place, but more moderate than in non-Newtonian fluids. They indicate that in fluid droplets or gas bubbles, there exists a central or internal circulation caused by the viscous drag of the outer fluid. The velocity rise with internal circulation as proposed by Hadamard should be 1.5 times that of bubbles in which no circulation (Stokes region) occurs. This correlation however, is only valid for Newtonian fluids, whereas viscoelastic fluids may obey Equation (II-18).

#### (ii) Coalescence Phenomena

Bubble coalescence is of major significance in

determining time-dependent bubble size distribution and interfacial area for many gas liquid contacting devices and gas liquid separation equipment. In a typical gas-sparged contactor or reactor, coalescence is detrimental because it decreases the surface area of the bubbles; in a separator it is desirable because it increases the size and hence the rise velocity of the bubbles.

Acharya and Ulbrecht (A4) investigated the effect of viscoelasticity on the coalescence rate of bubbles and drops using aqueous 0.5% CMC and PAA solutions. In papers by DeNevers and Wu (D2), Crabtree and Bridgewater (C5), and Narayanan et al. (N1), it has already been substantiated that increased viscosity of the ambient liquid enhances the coalescence rate. Acharya and Ulbrecht (A4) postulate that the wake region posterior to the bubble is much longer in a more viscous liquid, so that the approaching bubble is caught up in this wake at a longer distance as compared to a less viscous fluid.

They envisage three distinct stages in the coalescence phenomena. In stage one, the bubble enters a wake left behind by the leading bubble. In stage two, the trailing bubble experiencing less drag in the wake, quickly approaches the leading bubble, until they collide, with only a thin film separating each bubble. In stage three, a process of film thinning takes place until coalescence occurs. However, as Shiloh et al. (S1) point out

coalescence times should be distinguished from collision times, since two bubbles may collide and not coalesce.

Acharya and Ulbrecht (A4) discovered that due to the elasticity of CMC and PAA, the wake of a moving bubble was reduced, thereby increasing the collision time. They conclude that the elasticity of a solution will increase both the collision and coalescence times of gas bubbles.

DeNevers and Wu (D2) examined bubble coalescence with  $1 \times 10^{-2}$  -  $2 \times 10^{-2}$  m diameter bubbles in glycerine and distilled water. They assumed that each bubble trails a wake, and that the bubble coalescing from below accelerates when it enters the wake of the preceding bubble, before eventually coalescing. In their study, they assumed the two coalescing bubbles to be hemispherical in shape, equal in size and rising in the same vertical line. The only forces acting on the bubble are buoyancy and drag. Since the density of a gas is small, the product of the mass and acceleration is negligible. Hence, as the projected area of the lower bubble exposed to stagnant fluid decreases, the velocity relative to stagnant fluid must increase to keep the buoyant and drag forces equal. Their final assumption was that changes in pressure and temperature were negligible.

They present two models according to the type of wake behind the leading bubble; either a conical wake or an exponential decay wake as in Figure (II- 2B). One can

estimate time for coalescence from the terminal velocity, the initial vertical separation distance and the radius of the bubble. Since their model predicts the coalescence behaviour adequately, the assumption that buoyancy and drag forces are the only significant forces in the force balance would imply applicability to only Newtonian fluids.

Crabtree and Bridgewater (C5) studied the in-line interaction of two spherical cap bubbles for  $Mo = 2.9 \times 10^{-2}$ ,  $40 < Re < 86$  and  $1.0 \times 10^{-5} m^3 < V < 4.0 \times 10^{-4} m^3$  in a 67% aqueous solution of sucrose in water, a Newtonian solution. They utilized a wake model approach like Acharya and Ulbrecht (A4) and DeNevers and Wu (D2), to derive two equations for the coalescence time ( $T_c$ ) according to whether the velocities of the two bubbles were equal or unequal. By integrating the following equation:

$$\frac{dL}{dt} = (v_B - v_A) + \frac{v_A g}{4\pi \nu L} \quad (II-19)$$

where:

$L$  is the initial vertical separation distance of bubbles (m).

subscript A refers to the leading bubble.

subscript B refers to the trailing bubble.

For the case where  $v_A = v_B$

$$T_c = \frac{2\pi\nu}{V_{Ag}} (L^2 + \Omega) \quad (\text{II-20})$$

where:

$\Omega$  is an integration constant.

$T_c$  is the coalescence time (s).

And for the case where  $v_A \neq v_B$

$$T_c = \frac{2\pi\nu}{V_{Ag}} L^2 + \frac{L_c}{v_B - v_A} \ln (v_A - v_B) L_c + \phi \quad (\text{II-21})$$

$\phi$  is an integration constant.

$L_c$  is a critical separation distance (m)  
defined by the equation below:

$$L_c = \frac{V_{Ag}}{4\pi\nu(v_A - v_B)} \quad (\text{II-22})$$

This analysis, however, is suitable only for spherical cap bubbles. Their model also asserts a critical separation  $L_c$ ;  $L > L_c$  will guarantee that coalescence will not occur. Their experimental observations indicate that the coalescence rate decreases as the initial vertical separation distance increases.

This is expected, since the larger the separation distance, the longer the coalescence time. Assuming that the motion of bubble A is independent of the presence of bubble B, Crabtree and Bridgewater (C5) conclude the following.



For a given initial vertical separation distance, the smaller the second bubble, the longer the coalescence time. They assert that the wake is of prime importance to aligning and capturing the trailing bubble in all their trials. The model becomes poor when the trailing bubble is improperly aligned, and the shape of the trailing bubble becomes altered under the influence of the wake.

They also suggest the governing motion in wake capture is the sum of the trailing bubble's velocity plus a liquid velocity from the asymptotic wake theory. Crabtree and Bridgewater (C5) present an equation for viscous wake velocity of the form:

$$v_w = \frac{F_D}{4\pi\mu L} \text{Exp} \left[ \frac{-v_\infty r^2 \rho}{4\mu L} \right] \quad (\text{II-23})$$

where:

- $F_D$  = the drag force (N).
- $r$  = the radial spacial co-ordinate.
- $v_w$  = the wake velocity (m/s).

Bhaga and Weber (B4) studied the interaction of bubbles in a viscous aqueous sugar solution for conditions of coalescence under  $10 < \text{Re} < 100$  and  $\text{Mo} > 4 \times 10^{-3}$ . In their paper, they utilized the following wake velocity profile:

$$v_w = v_{w0} \text{Exp} \left[ \frac{-\text{Re}}{4} \left( \frac{r^2}{zD_0} \right) \right] \quad (\text{II-24})$$

where :

$v_{wo}$  is the axial wake velocity (m/s).

$z$  is the axial distance from bubble (m).

in which  $v_{wo}$  is defined by :

$$v_{wo} = \frac{v_{\infty} B}{24} \left( \frac{D_e}{z} \right) \quad (\text{II-25})$$

where: B is a dimensionless parameter defined by Equation (II-26):

$$B = \frac{E_o^{3/2}}{Mo^{1/2} Re} \quad (\text{II-26})$$

Their model utilized the aforementioned relationships, coupled with the assertion (C5) that the velocity of the trailing bubble is equal to the sum of the terminal rise velocity in isolation and the velocity in the wake of the leading bubble.

They observed that for high Morton number liquids ( $Mo > 4 \times 10^{-3}$ ), the bubble shape, drag coefficient and fluid streamlines near the bubble are only a function of the Reynolds number. Both bubbles rose vertically, with the trailing bubble overtaking the leading bubble, under conditions of both volumes equal to  $9.3 \times 10^{-6} \text{ m}^3$ . The shape and rise velocity of the leading bubble was essentially unaffected until coalescence confirming the findings of Crabtree and Bridgewater (C5). The trailing bubble was deformed, when under the influence of the

leading bubble's wake. Criteria for coalescence proposed by Bhaga and Weber (B4) are:

- (i) For coalescence to occur the instantaneous rise velocity of the trailing bubble must be greater than the terminal rise velocity (in isolation) of the leading bubble.
- (ii) Coalescence will depend upon the ratio of the terminal rise velocity of the trailing bubble to that of the leading bubble.

Narayanan et al. (N1) measured bubble positions during in-line coalescence of two bubbles in solutions of glycerine and water for  $2 < \frac{L}{D_e} < 6$ ,  $Mo$  ranging from  $1.8 \times 10^{-3}$  to 19.5, and Reynolds numbers ranging from 0.5 to 80. They also asserted that coalescence takes place in three distinct stages as outlined by Acharya and Ulbrecht (A4). For each class of bubble and corresponding bubble wake pattern, Narayanan et al. (N1), have tabulated a graphical correlation based on the ratio of individual rise velocities and a dimensionless mutual distance between each of the bubbles. Marrucci (M2) rationalizes a two stage theory of coalescence. After collision occurs between two bubbles, an initial film thinning to an equilibrium thickness takes place.

What actually occurs at this stage is a very rapid stretching of the film down to a value of the thickness where a built up concentration difference makes the balance

of the forces acting on the film statically satisfied. The value of this thickness has been calculated as a function of physical properties. Below a limiting value of a dimensionless group and generally for very dilute solutions, the quasiequilibrium film does not exist and coalescence is instantaneous. The second stage of the process, which is the slow step of the coalescence process is the further thinning of the quasi-equilibrium film. It is suggested that diffusion at the border of the film controls the thinning rate and predictive equations (for the coalescence time) are calculated accordingly.

### CHAPTER III. EXPERIMENTAL DETAILS

#### (i) EQUIPMENT

The aim of the experimental apparatus was to

(i) produce bubbles varying in volume from  $1.0 \times 10^{-8} \text{ m}^3$  to  $1.0 \times 10^{-5} \text{ m}^3$ .

(ii) inject bubbles at specified periods.

(iii) inject bubbles of varying volumes mentioned under (i) simultaneously.

Many problems were encountered in the design and subsequent construction of this multipurpose unit. Typical of the problems encountered were: obtaining useful stroboscopic photographs, injection of bubbles less than  $1.0 \times 10^{-7} \text{ m}^3$  in volume and simultaneous injection of bubbles. A number of different variables had to be determined with the experimental equipment. The "terminal" velocity of the bubbles produced their respective shape, and their volumes had to be determined accurately.

To help visualize the motion of the gas bubbles, two plexiglass tanks were constructed. One tank was solely used for simultaneous injections. The single bubble tank was square with each side  $2.03 \times 10^{-1} \text{ m}$  in length and with a height of  $6.1 \times 10^{-1} \text{ m}$ . The multiple bubble tank was also square with each side  $2.30 \times 10^{-1} \text{ m}$  in length and a height of  $7.62 \times 10^{-1} \text{ m}$ .

To inject bubbles into the fluid without disturbing

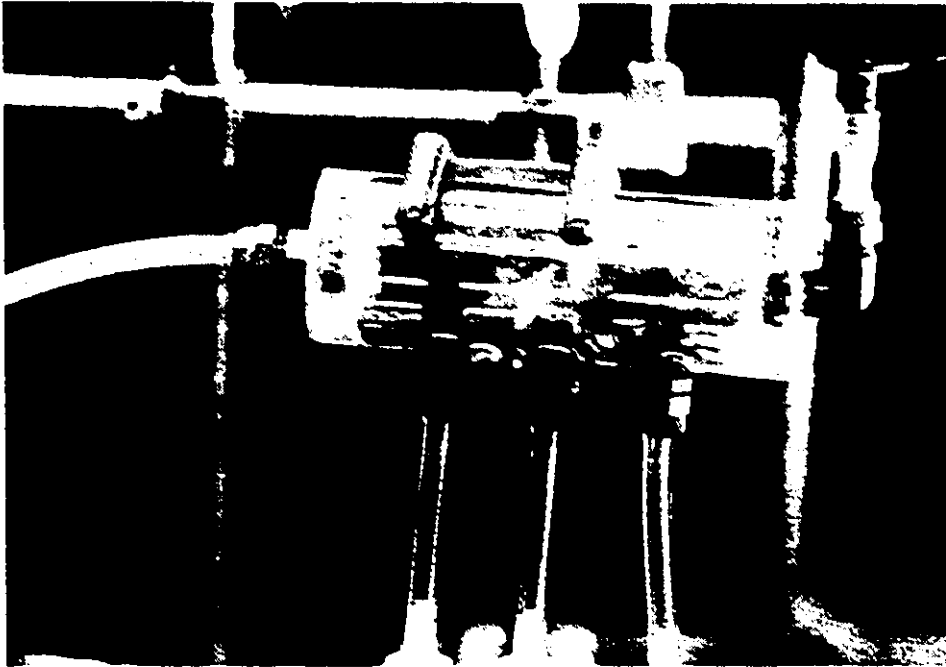
it prior to injection, the following principle was applied. The pressure exerted by the fluid upon the orifice through which the bubble would emerge was counterbalanced by an equivalent air pressure. Hence gas bubbles could be injected with minimal disturbance to the viscoelastic fluids in the tank.

To balance the head of fluid above the orifices a Union Carbide low pressure line regulator (0-20 kPa) was utilized. This regulator would allow for very fine pressure adjustment at the orifice with normal supply air pressures supplied by gas cylinders. For the single bubble case no problems were encountered, however for the multiple bubble case a pressure distributor had to be constructed. This cylindrical distributor pictured in Figure (III-1) provides ports for up to three simultaneous injections. It also distributes the incoming air supply to the orifices.

The orifice for releasing the air bubble was special in design. The lower portion was fitted with an adaptor for union with quarter inch polyflo tubing systems and the top was chamfered to prevent ripping and tearing of the exiting air bubbles. Figure (III-2) depicts a typical orifice employed in both tanks.

Figure(III-1) Cylindrical Pressure Distributor

Figure(III-2) Typical Orifice





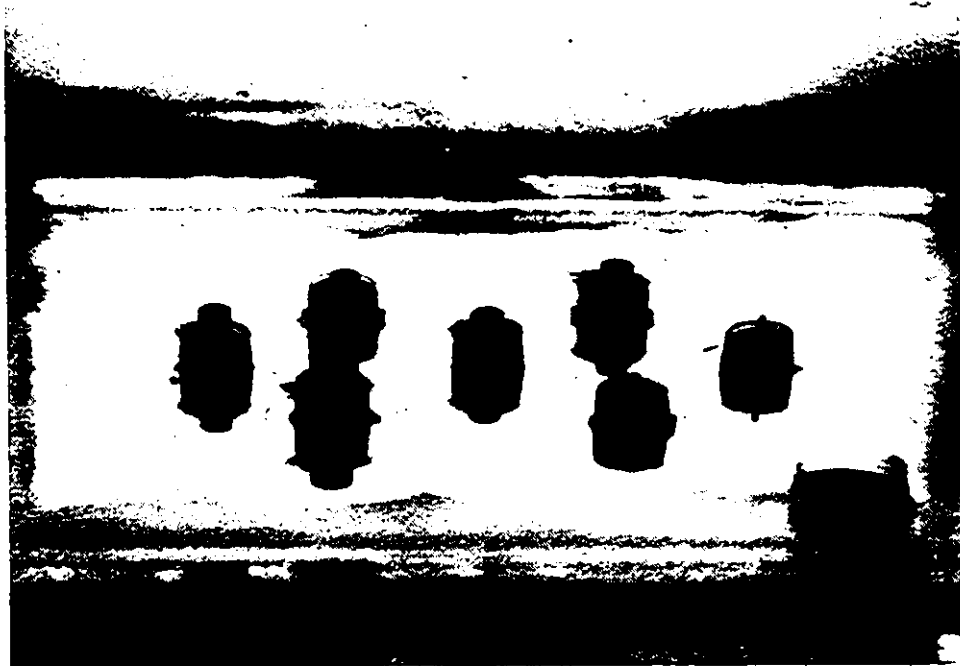
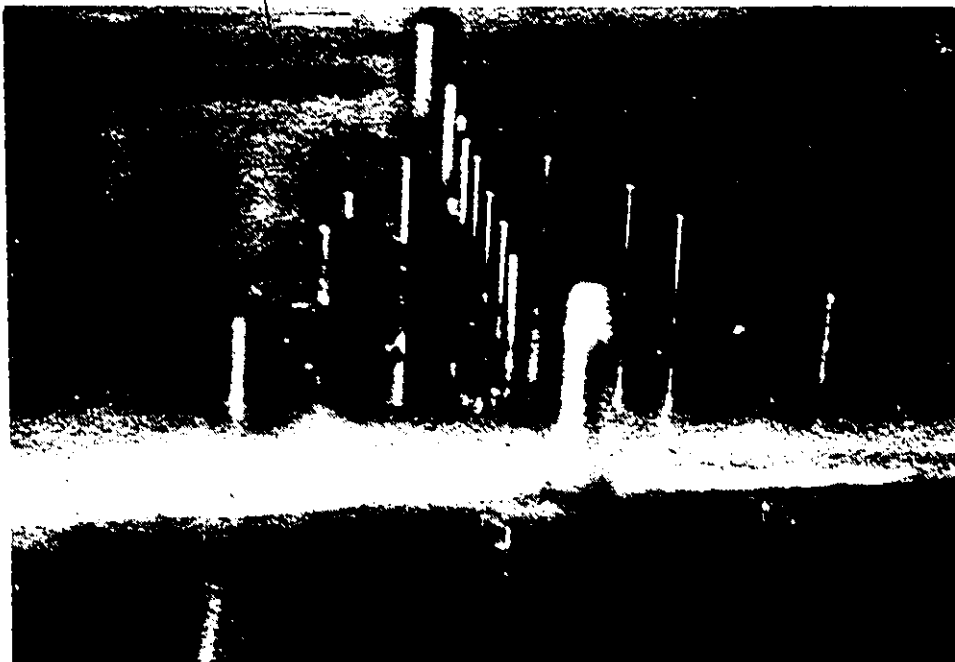
After experimentation with an orifice which was  $4.92 \times 10^{-4}$  m in diameter, it was observed that a range of orifices had to be constructed to produce the desired range of bubble volumes. Simply by trial and error orifice diameters in the range of  $6.15 \times 10^{-5}$  m -  $9.8 \times 10^{-4}$  m were selected for use in the single bubble tank.

Due to the multitude of orifices required to produce the desired volumes, multiple injection was restricted to a smaller volume range ( $V \geq 1.0 \times 10^{-6} \text{ m}^3$ ), and employed only the  $4.92 \times 10^{-4}$  m diameter orifice. Orifices were constructed from primarily stainless steel and a few were machined in brass. Figure(III-4) displays the single bubble arrangement while Figure(III-3) displays the multiple bubble arrangement.

Due to the orifice orientation in the multiple bubble system there existed the need for placing the orifices into a triangular plane. This facilitated the later union of the orifices to the injection mechanisms as well as the photographic work. Hence it was decided that the tank should have the capability of rotating in two directions. A heavy duty ball-bearing system was used for this task and is depicted in Figure(III-5).

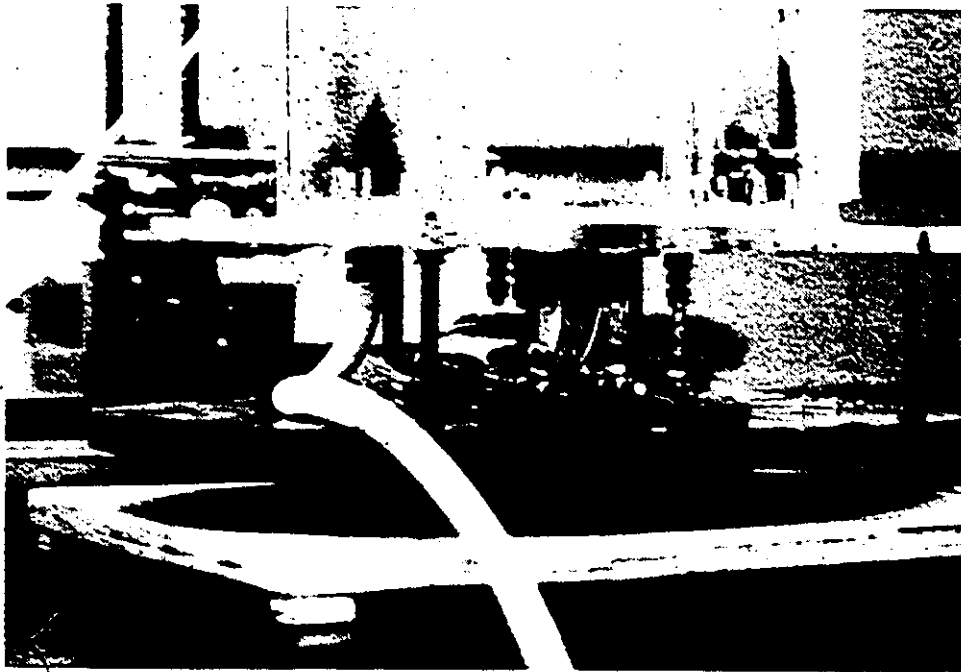
Figure (III-3) Orifice Configuration for Multiple Bubble Injection

Figure(III-4) Orifice Configuration for Single Bubble Injection



Figure(III-5) Rotational System for Multiple Bubble  
System

Figure(III-5) Rotational System for Multiple Bubble  
System



Originally a detailed design was carried out to fix one orifice and have the other two moving with respect to the fixed orifice. This way a variety of distances could be covered without the obstacle of fixed orifice locations. This system would have utilized gear and chain assemblies manufactured from plastic and stainless steel, as well as screw driven orifice movement devices. The shipping and construction times for this system were prohibitive.

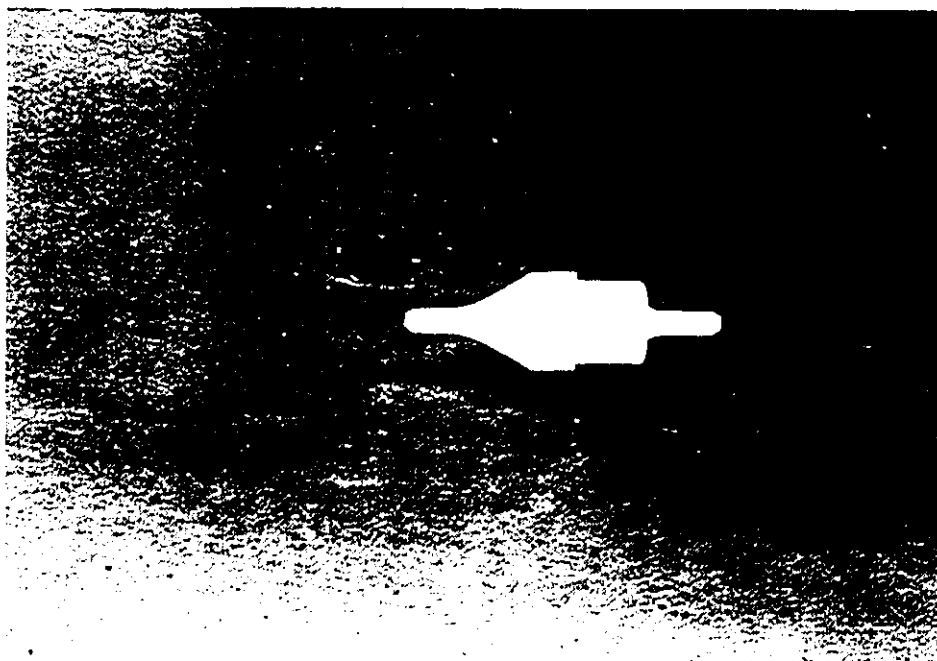
To inject the air bubbles, a novel technique was employed. In the past air bubbles were injected via a syringe, uncontrolled orifice release and a dumping cup technique. These systems would not be feasible for studying the effect of injection frequency, since it would take more than one experimenter to perform the necessary work. Hence a new system had to be developed meeting two important criteria.

One criterion of course was a variable injection pattern, while the other was the automation of the system since photographic work had to be undertaken during bubble movement in the column. The present system uses two commercially available units, a check valve and a pneumatic cylinder, pictured in Figures (III-6 to 8).

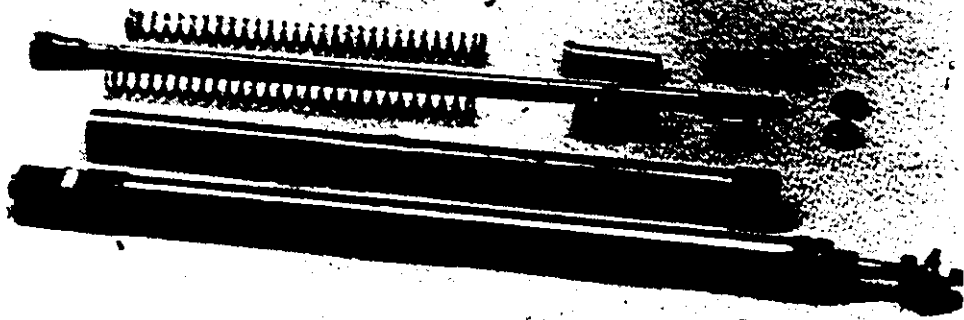
Figure (III-6) "Harris Check Valve"

Figure (III-7) "Norgren Check Valve"





Figure(III-8) A Typical Spring Return Pneumatic  
Cylinder (Disassembled)



1227

The role of the check valve is to permit the flow of liquid or gas in one direction only which is critical to the functioning of the system. The Harris check-valve shown in Figure (III-6) is made of brass and utilizes a ball and spring mechanism for operation.

The Norgren check valve shown in Figure (III-7) is made of polypropylene and utilizes a silicon cup-shield to restrict flow in one direction. This valve has a crack pressure of  $2.54 \times 10^{-2}$  m H<sub>2</sub>O while the Harris valve has a  $7.62 \times 10^{-2}$  m H<sub>2</sub>O cracking pressure.

A typical pneumatic cylinder is disassembled and depicted in Figure (III-8). This particular model which has a bore of  $6 \times 10^{-3}$  m and a stroke of  $6.0 \times 10^{-3}$  m is the smallest commercially available unit.

After experimenting with this cylinder we discovered that it was not capable of producing volumes of a magnitude less than  $0.9 \times 10^{-7}$  m<sup>3</sup>. Hence this cylinder was carefully dismantled and after detailed examination of its operation a cylinder was designed capable of producing the required bubble volumes. At first a design of a  $1 \times 10^{-3}$  m bore with a  $6.0 \times 10^{-2}$  m stroke was chosen, but after manufacturing we observed that i) it was too weak for use, since the rod had to be  $< 1.0 \times 10^{-3}$  m, ii) no piston sealing cup could be manufactured that would function adequately. Hence we settled for a bore of  $2.38 \times 10^{-3}$  m and a stroke of  $6.0 \times 10^{-2}$  m.

A typical pneumatic cylinder is pictured in Figure (III-9) along with a list of important components. The particular one shown has a  $2.54 \times 10^{-2}$  m bore and is double acting; a single-acting cylinder will have a spring located between the piston and the front flange housing.

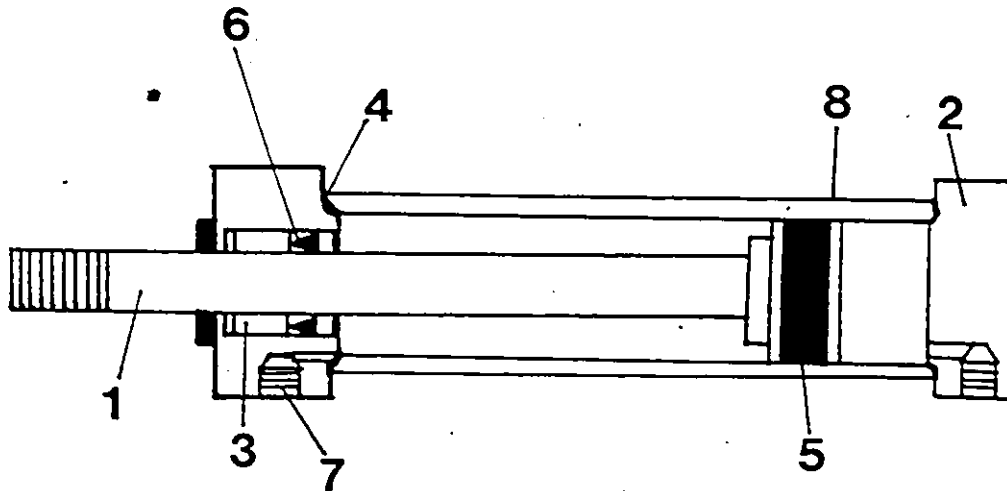


Figure (III-9) Schematic of a Pneumatic Cylinder

- (1).....Piston Rod
- (2).....Cylinder End Cap
- (3).....Rod Bushings
- (4).....Seal
- (5).....Piston Cup (Seal)
- (6).....Rod Seal
- (7).....Port
- (8).....Cylinder Barrel

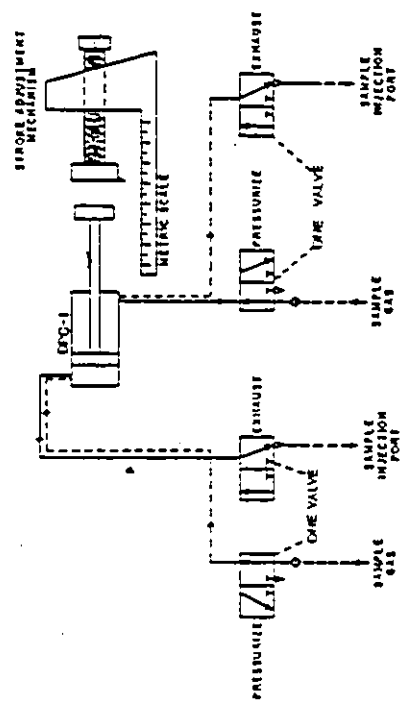
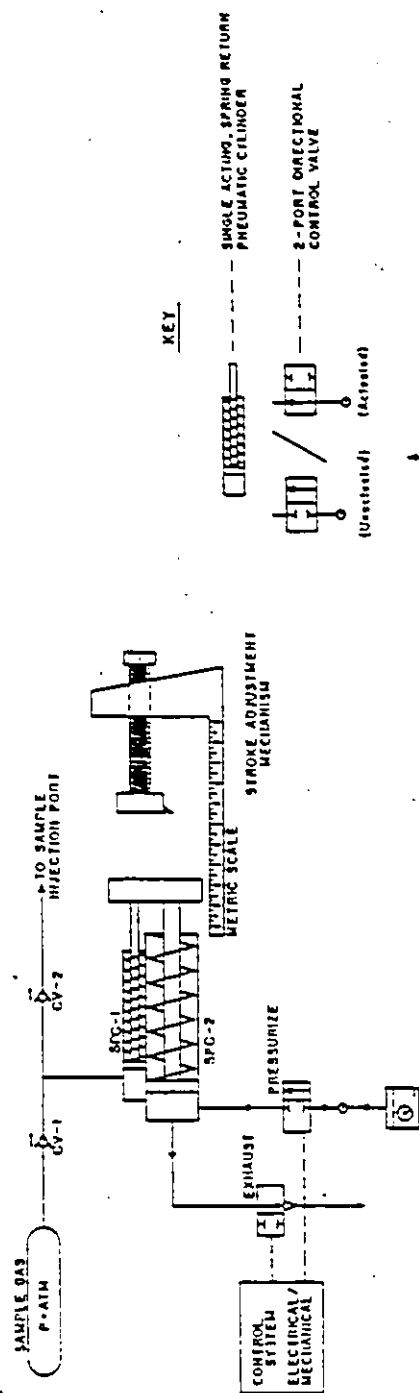
The new injection system can automatically inject a predetermined volume of gas at whatever cyclic interval selected. The heart of this injection system, as mentioned earlier, is a commercially available pneumatic cylinder usually used for its robotic movement capabilities. Normally these cylinders automatically move objects into and out of machining equipment.

We utilized the fact that these cylinders can expand and compress the gas which operates them, in a cyclic manner, for the purpose of injecting reproducible gas volumes. With the aid of solenoid valves, the exhaust from these cylinders is thus put to use. The proposed automatic injection system can take on two distinct configurations, depending on the storage pressure of the sample gas which is to be injected. For injecting sample gas stored at atmospheric or zero gauge pressure, a single acting spring return pneumatic cylinder (SPC-1) is utilized as shown in Figure(III-10 A).

In this configuration another pneumatic (SPC-2) spring return cylinder is required to generate the necessary suction and compression-injection action delivered by SPC-1. Two 2-port solenoid valves are used in conjunction with SPC-2 to initiate the required action.

Since the two cylinders are tandemly mounted, an extension or expansion action by SPC-2 introduces a suction action in SPC-1, thereby admitting sample gas

Figure (III-10) Injection Systems for Sample Gas  
Stored at Atmospheric and non-  
Atmospheric Pressure





through check valve (CV-1), into its chamber. Retraction of SPC-2 is associated with a compression and injection action by SPC-1, causing sample gas to be injected via check valve (CV-2) into a specified part.

The two solenoid valves allow the system to inject sample gas at any desired time interval. The volume of gas which is to be injected may be calibrated using a simple stroke adjustment mechanism as shown in Figure (III-10). Due to the abundance of stroke lengths and bore diameters the system displays tremendous flexibility.

A slight modification of this system is shown in Figure (III-10 A). This system is used when the gas is stored under pressure. It involves a double acting pneumatic cylinder (DPC-1) along with two 3-port solenoid valves.

In this application the sample gas actually participates in the injection control of the system. Due to the action of the 3-port solenoid valve, sample gas may be injected as the piston retracts (solid lines in Figure (III-10 B), or as the piston extends (dotted lines in Figure (III-10 B). Each valve shown is shown in two different positions. This system allows for higher injection periods as well as injection of gases other than atmospheric air.

The stroke adjustment mechanism schematically shown in Figures (III-10 A) and (III-10 B), is basically a stop for the extended pneumatic cylinder rods. The volume of bubble produced is thereby directly proportional to the stroke of the pneumatic cylinder. The extended distance or rod

travel (actual stroke) can be measured accurately with vernier calipers and a calibration graph may be drawn for each grouping of cylinder and orifice, relating volume of bubble produced to stroke length.

The stroke adjustment mechanism (MS-A) used in the single bubble experiments is shown in Figure (III-11). This mechanism was designed for allowing flexibility in changing pneumatic cylinders of different dimensions within minutes.

The stroke adjustment mechanism utilized for multiple bubble experiments (MS-B) is different in that it must accommodate three pneumatic injection cylinders leading to a sturdier design than that of MS-A. This mechanism is shown in Figure (III-12).

Experiments were carried out to determine the volume of bubble, before it coalesced with a bubble of fixed volume, while varying the injection separation distance. To accomplish this both systems were utilized (see Figure (III-13)).

By placing a check valve at the entrance to the orifice, outflow from the tank could be prevented, thereby allowing equipment manipulations to be performed without draining the tank. This connection system was also employed in the single bubble work. Figure (III-14) shows two different views of the complex multiple bubble circuit.

As outlined earlier, bubble volume is proportional

Figure (III-11) "MS-A" Measuring System A

Figure (III-12) "MS-B" Measuring System B

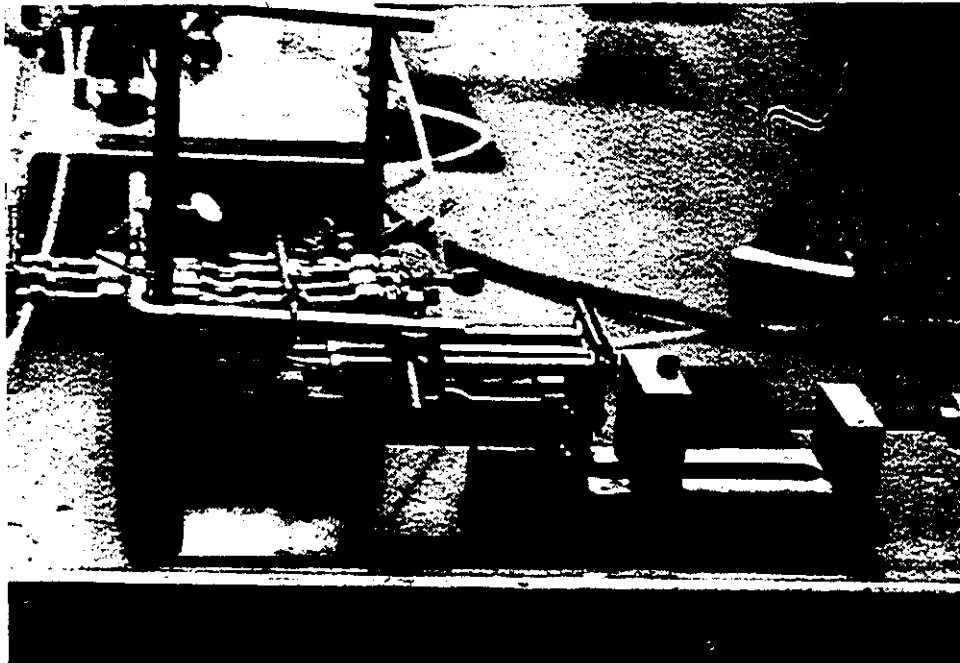
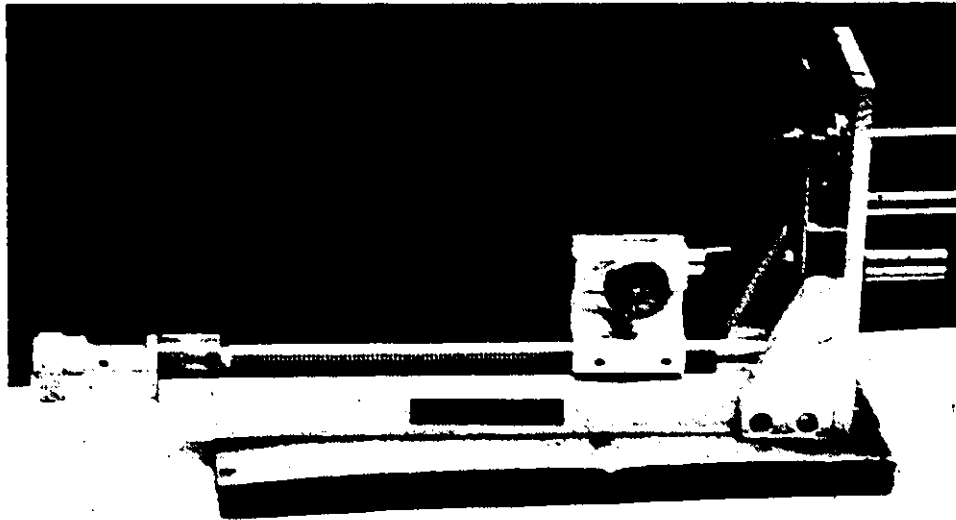


Figure (III-13) MS-A and MS-B Set Up for Simultaneous  
Double Bubble Experimentation

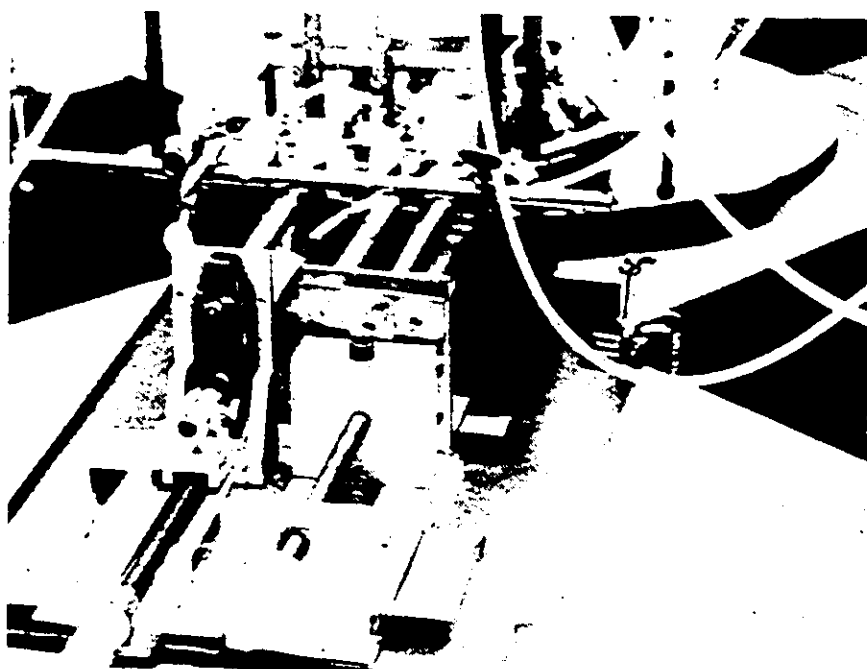
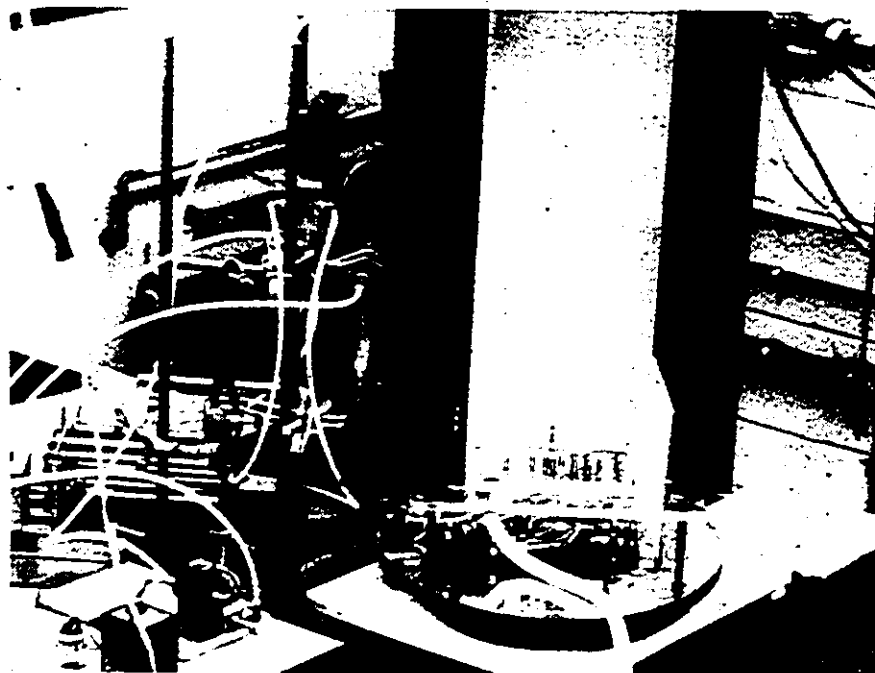
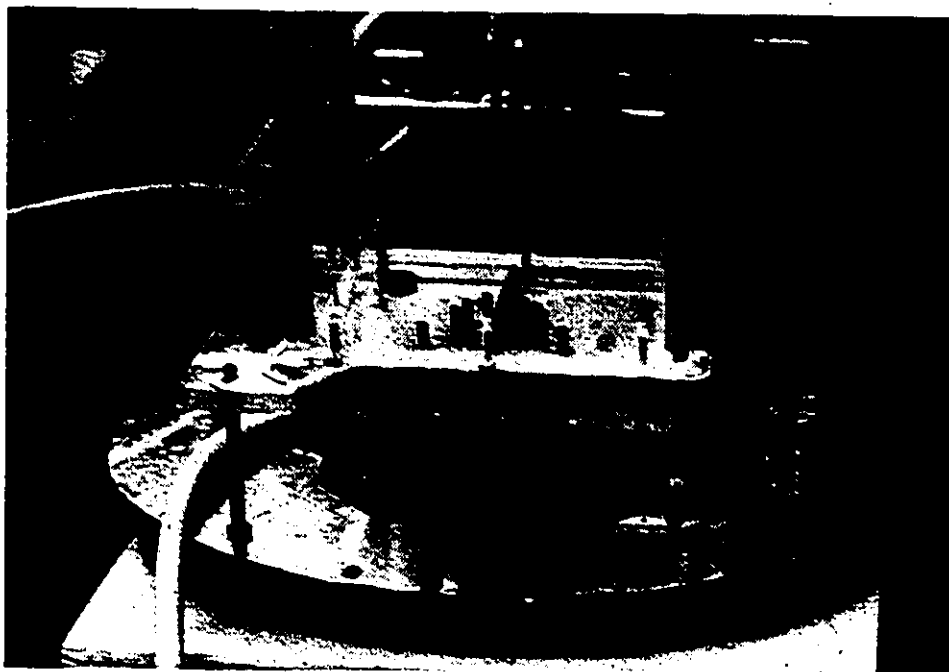


Figure (III-14) The Multiple Bubble Circuit





to the stroke of the cylinder in operation. To ascertain the volume of a bubble produced by the injection system an inverted bubble collector was built.

This device was manufactured by joining a buret to the bottom of a graduated cylinder. A funnel adaptor was also manufactured and could be inserted to capture very large bubbles ( $V > 1.0 \times 10^{-6} \text{ m}^3$ ). ✓

The volume of one bubble produced is calculated from the ratio of the total volume of liquid displaced in the collector and the total number of bubbles collected. A correction factor due to the head of fluid at a particular collection height was also applied. In this way the bubble volume was obtained at atmospheric conditions.

Since these experiments (single bubble) are aimed at examining the effect of the period of injection, the injection has to be repeated at pre-selected time intervals. Hence an electronic system was designed and assembled to accomplish this.

The system consisted of an Industrial Control Equipment 600 VAC relay and an Agastat synchronous motor timer which controlled the action of a three-way air/solenoid spool valve. Originally the equipment utilized two-way air/solenoid valves, however these valves malfunctioned and were replaced with a single, more expensive three-way valve.

There was also the need for a portable control unit (PCU) which had a manual override and an electric counter to facilitate in maintaining proper bubble count as well as overriding pre-selected injection periods. This system was capable of delivering injection periods of 1-60 seconds (by seconds) and 1-60 minutes (by minutes).

A detailed schematic of this electronic control system is shown in Figure(III-15). This particular control system since its inception into the project proved to be very reliable.

To measure the velocity of the ascending gas bubbles a photographic technique was employed. A stroboscope and a specially equipped Ricoh -35mm camera, fitted with an 80-200mm Sigma Macro-zoom lens and a Ricoh XR electronic


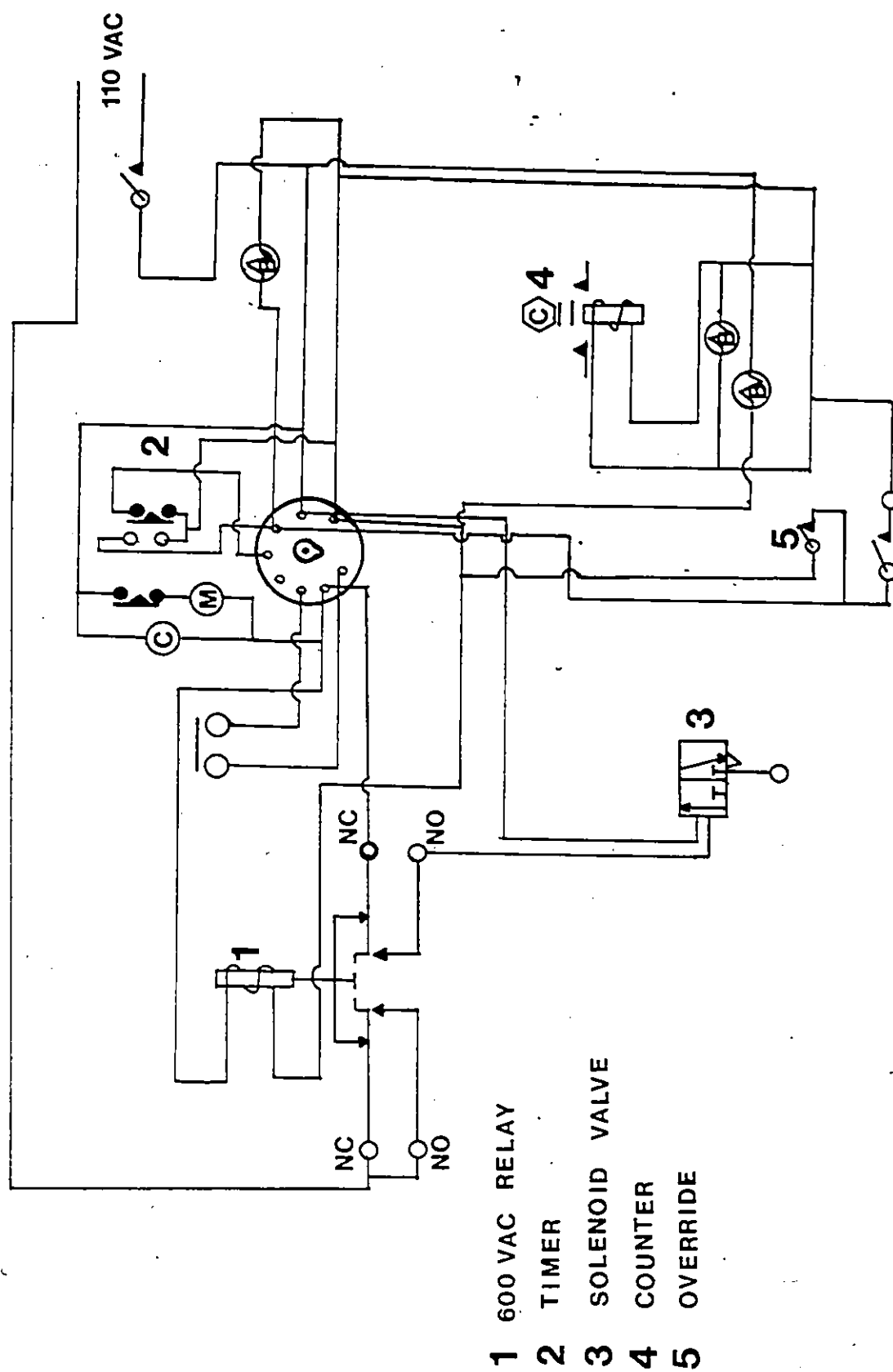


Figure (III-15 ) Schematic of Electronic Control System



winder, were used to capture the moving bubble on film.

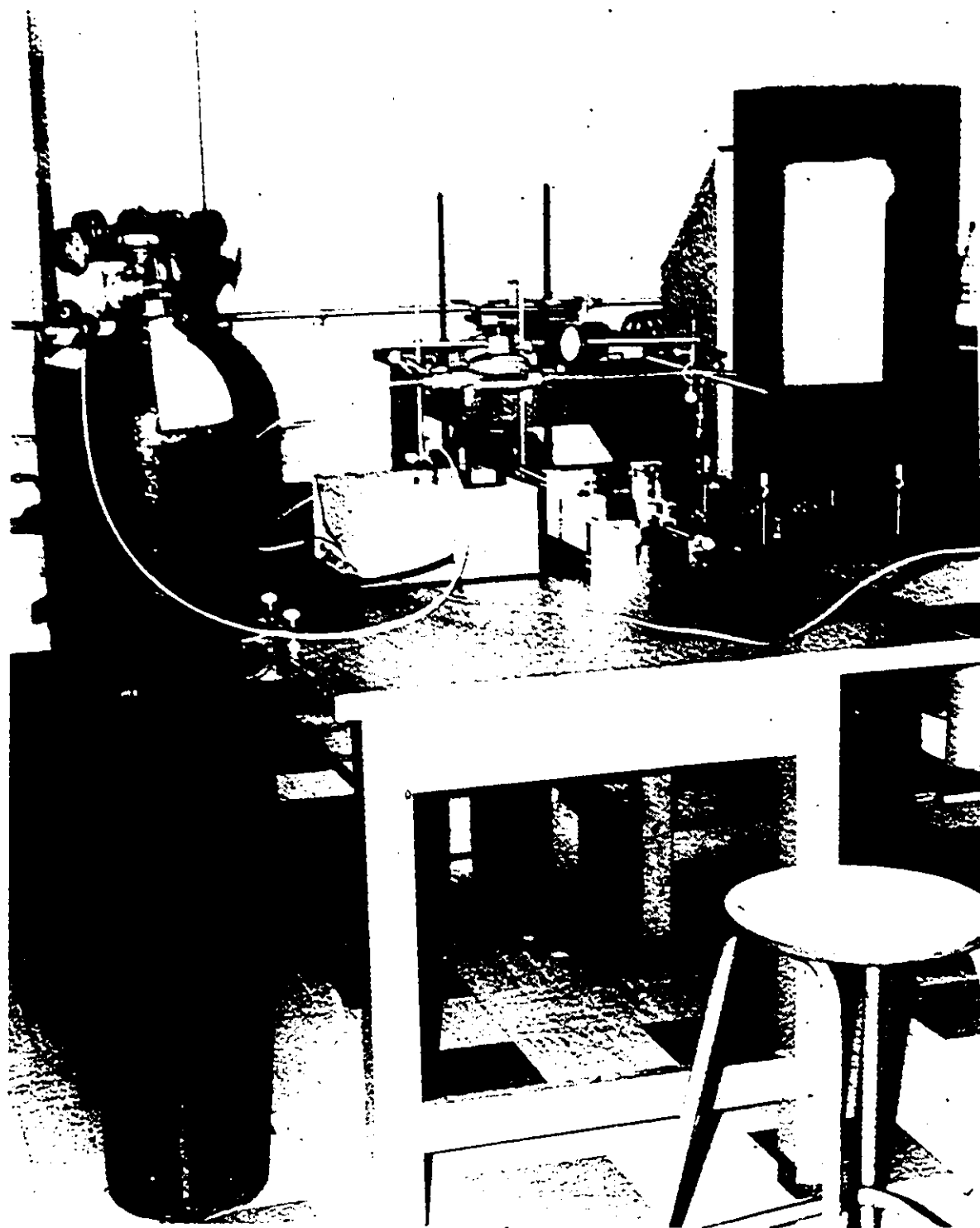
The rising bubble was intermittently illuminated in a completely dark room by the stroboscope set at a known frequency (calibrated with a frequency counter at 6.0 Hz). Depending on the shutter speed, the camera would capture the moving bubble as a series of simultaneous still bubbles.

Many different camera/stroboscope orientations were tried before the desired photographic effects were achieved. Finally it was decided that illumination from the rear with the camera directly in front of the tank provided the best contrasts. A light diffuser had to be constructed to permit the stroboscopic light to be adequately diffused before entering the camera, thereby producing useful contrasts on the film.

The light diffuser consisted of a trapezoidal unit with each side radiating out from the strobe (behind the tank) to cover the full cross section of the tank, as shown in Figure (III-16). The interior was lined with reflective silver paper, with the posterior open to the strobe and the front covered by a layer of cheesecloth and tissue paper. Also a layer of reflective silver paper covered two sides of the plexiglass tank parallel to the light diffuser, to aid in illuminating all regions of the ascending bubble.

Since the light emitted by the strobe was of low

Figure(III-16) Single Bubble Injection Apparatus  
with Light Diffuser



intensity the film selected was HP5 used with Ilford's Microphen developer. In this way one was permitted to use an f-stop of f-11, providing enough depth of field and contrast to clearly ascertain the bubble from the background. The whole synthesis procedure of developing the photographic technique based on this particular strobe and camera took approximately 4 months of experimentation.

By knowing the stroboscopic frequency and the distance between bubbles on the negative, one could obtain an average velocity. To aid in measuring the distances between the bubbles, scales were affixed to the front of the tank. The negatives were then processed and projected via a slide projector upon a screen, greatly magnifying all dimensions, to increase the accuracy of the distance measurement.

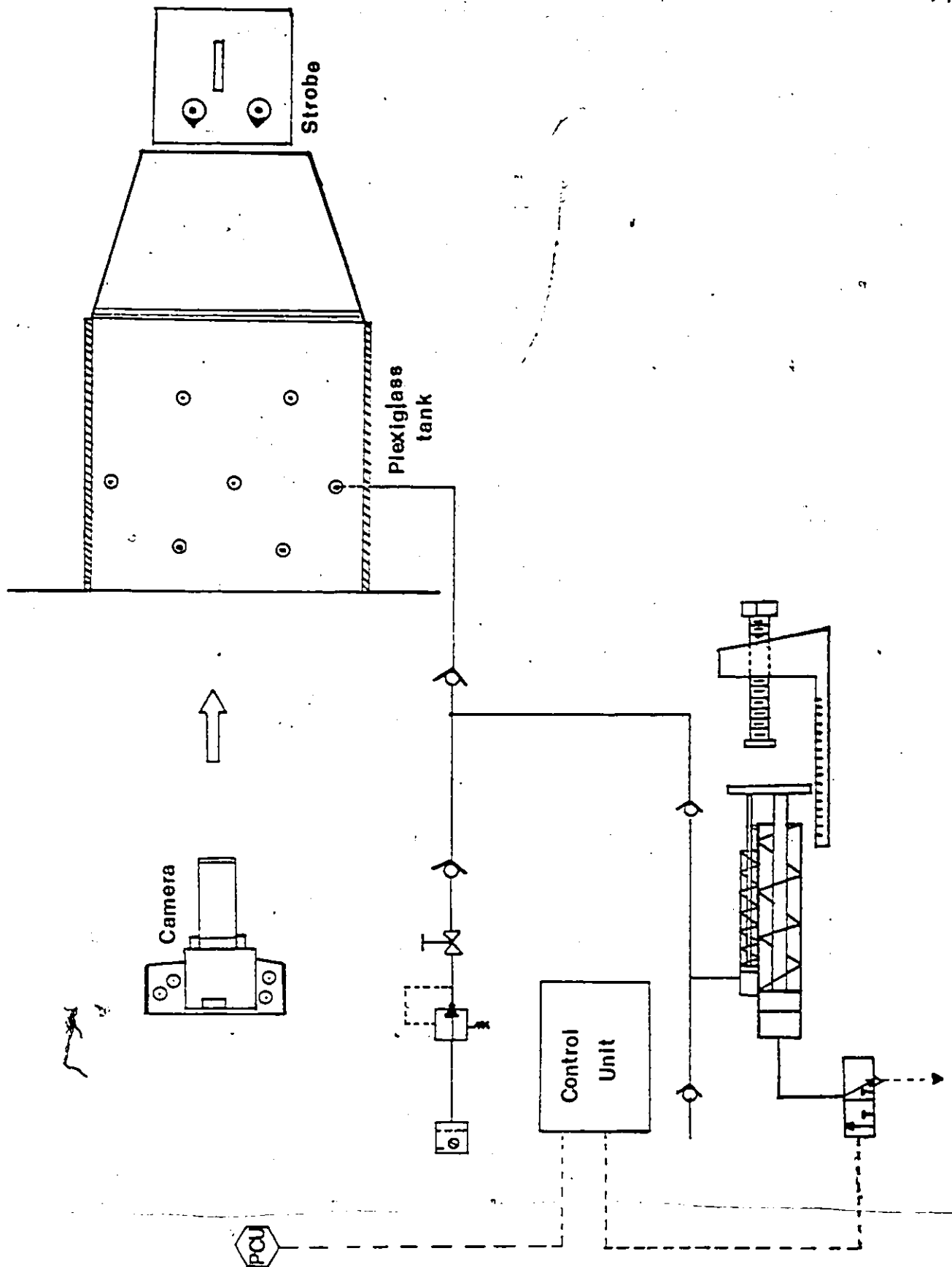
Since one of the objectives of this experimentation is to examine the relationship between terminal velocity and volume it is paramount in utilizing that region in the tank where bubbles travel with a constant velocity. This terminal velocity region was discovered by experimental velocity measurements taken at various heights in the tank.

A darkroom to process film was also assembled and proved to be very helpful in lowering turnaround time on processing film. Due to long shutter speeds employed, usually one second, it was necessary to have the camera mounted on a tripod to prevent vibrations.

A schematic of the entire single bubble system is depicted in Figure (III-17). The multiple injection system



Figure(III-17) Schematic of Single Bubble Apparatus



is basically of the same orientation except for the paraphernalia associated with the pressure distributor and stroke adjustment mechanism discussed earlier.

A photograph of the (single bubble) experimental apparatus was shown in Figure (III-16). A complete list of the experimental equipment utilized in this project is given in Table (III-2).

TABLE (III-2)

Equipment Schedule

ITEM	MANUF. OR SUPPLIER	IDENTIFICATION
RICOH -35 mm CAMERA	TUREK LTD.	MODEL NO. KR-10
SIGMA MACROZOOM LENS	TUREK LTD.	MODEL NO. 641-458
RICOH ELECTRIC WINDER	TUREK LTD.	MODEL NO. XR-1
STROBOSCOPE	SARGENT-WELCH SCIENTIFIC CO. LTD.	CAT. NO. S77545
CHECK VALVE	ESSEX WELDERS SUPPLY	MODEL NO. 50VR
CHECK VALVE	CHECKER INDUSTRIAL LTD.	MODEL NO. 4LD-061 -D00
PNEUMATIC CYLINDER $6.0 \times 10^{-2}$ m (6mm)	NOPAK CANADA LTD.	MODEL NO. CIB6-605
PNEUMATIC CYLINDER $1.1 \times 10^{-2}$ m (7/16") bore $1.43 \times 10^{-2}$ m (9/16") bore	INDUSTRIAL AIR AND HYDRAULIC EQUIPMENT COMPANY.	MODEL NO. 023 MODEL NO. 013
PNEUMATIC CYLINDER $8.0 \times 10^{-2}$ m (8mm) bore	PESTO INC.	MODEL NO. ESN-8 SDP
PNEUMATIC CYLINDER $1.27 \times 10^{-2}$ m (1/2")	CANADIAN POWER AND RUBBER SUPPLY CO.	MODEL NO. DCPS -05-3
AGASTAT ELECTRIC TIMER	PETERSONS ELECTRONICS LTD.	MODEL NO. STMNHAG
THREEWAY SOLENOID VALVE	CHECKER INDUSTRIAL	MODEL NO. H41AA02 -HSE-HD0
LOW PRESSURE LINE REGULATOR	UNION CARBIDE LTD.	MODEL NO. SSC-1
PNEUMATIC CYLINDER $2.54 \times 10^{-2}$ m (1") bore	WINDSOR FACTORY SUPPLY	MODEL NO. CM 112 x3
ELECTRIC RELAY	INDUSTRIAL CONTROL EQUIPMENT	MODEL NO. A-102

The three fluids investigated were:

- (i) 40% (wt) of glycerol in water
- (ii) 1% (wt) of CMC in water
- (iii) 1% (wt) of PAA in a 50% (wt) mixture of glycerol and water.

In addition, an anti-bacteria agent, phenylmercuric acetate was added to each to prevent biological degradation of the solutions. Their viscosities were obtained by using the CONTRAVES-RHEOMAT 30 viscometer shown in Figure( III-1 ).

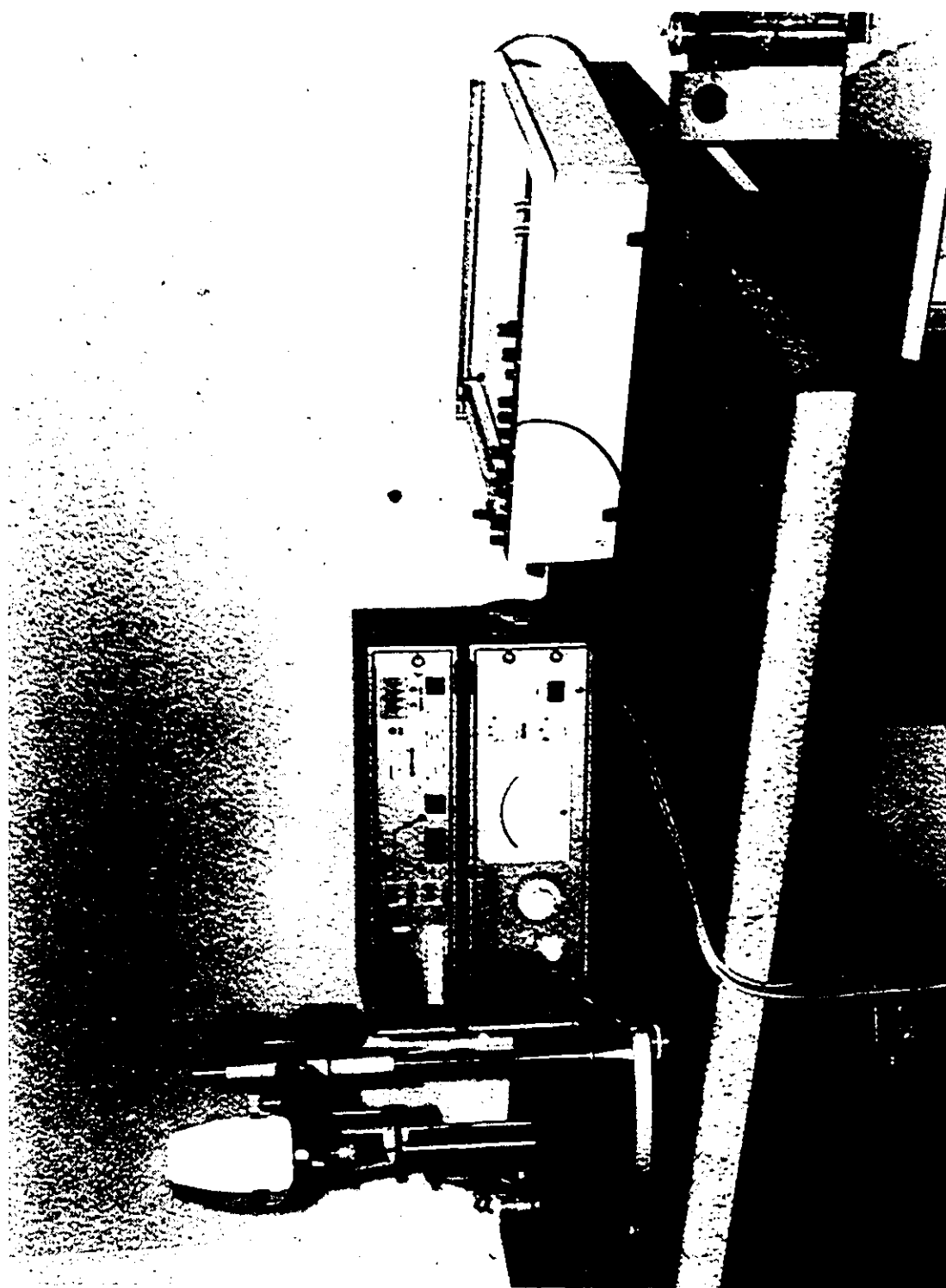
The RHEOMAT 30 is a rotational viscometer. The rotating measuring body is driven by a DC motor, the speed of which is precisely controlled by a closed loop servosystem.

The torque required to maintain the rotational speed of the measuring body is measured and recorded. Since the shear rate is a function of the rotational speed and measuring system dimensions and shear stress are a function of the applied torque, the flow behaviour and viscosity of the test substance can be evaluated.

This unit utilized basically two types of measuring systems, the coaxial cylinders and the cone and plate. Each have their own advantages and disadvantages and are used primarily on the basis of the type of rheological data required.

When coupled to an x-y recorder and a programming

Figure(III-18) Rheomat 30 Viscometer with Programming  
Unit and x-y Recorder



unit, the RHEOMAT 30 is a powerful tool to evaluate a multitude of rheological phenomena. This unit is designed for medium and high shear rates thus functioning poorly as a low shear viscometer.

Additional data on steady state viscosity and primary normal stress measurements were obtained with a far superior unit, a Weissenberg rheogionometer located in Montreal.

#### B. OPERATION:

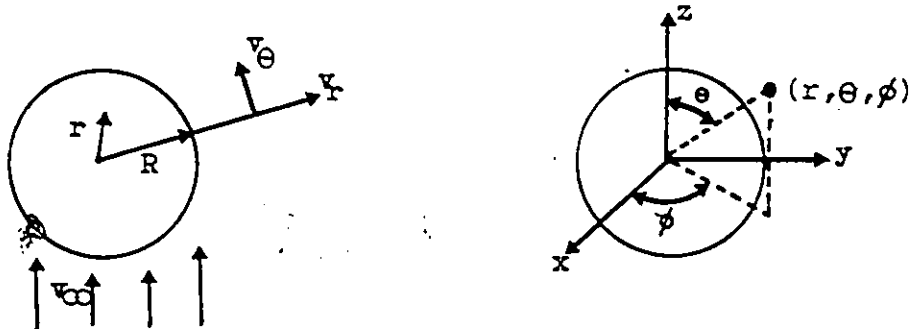
Since the apparatus is automatic, the experimenter has only to pressurize the necessary injection lines, adjust the stroke adjustment mechanism to a certain volume and select an injection period. The equipment will then inject the selected bubble volume at the desired injection period.

This now allows the experimenter to position the camera and strobe to take the necessary pictures. When beginning experimentation, after the equipment has not been used for some period of time, it is advantageous to purge injection lines with low pressure and then adjust the pressure distribution system so as to just balance the head of the fluid in the tank.

## CHAPTER IV. RESULTS AND DISCUSSION

### (i) SINGLE BUBBLE PHENOMENA

Bird (B5) has given a set of equations for the motion of a fluid about a solid, stationary sphere which is analogous to the case of the motion of a sphere in a stationary liquid. His solution is valid for creeping flow which restricts the  $Re$  to be less than one, thereby allowing the viscous forces to predominate over the inertial forces. Other restrictions placed on the problem are a non-rotating, solid sphere fixed in position within a Newtonian fluid. Utilizing the following coordinate representation;



the well known "creeping flow" solutions for the shear stress distribution ( $\tau_{r\theta}$ ), pressure distribution ( $P$ ), and velocity components ( $v_r$ ,  $v_\theta$ ) have been analytically found to be:

$$\tau_{r\theta} = \frac{3}{2} \frac{\mu v_\infty}{R} \left( \frac{R}{r} \right)^4 \sin\theta \quad (IV-1)$$

$$P = P_0 - \rho g z - \frac{3}{2} \frac{\mu v_\infty}{R} \left( \frac{R}{r} \right)^2 \cos\theta \quad (IV-2)$$

$$v_r = v_\infty \left[ 1 - \frac{3}{2} \left( \frac{R}{r} \right) + \frac{1}{2} \left( \frac{R}{r} \right)^3 \right] \cos\theta \quad (IV-3)$$

$$v_\theta = -v_\infty \left[ 1 - \frac{3}{4} \left( \frac{R}{r} \right) - \frac{1}{4} \left( \frac{R}{r} \right)^3 \right] \sin\theta \quad (IV-4)$$



Now by integrating the pressure (P) and shear stress ( $\tau_{\theta}$ ) distributions over the surface of the sphere, Stoke's Law may be derived analytically to be:

$$F_D = 6\pi\mu v_{\infty} R \quad (\text{IV-5})$$

where,  $F_D$  (N) is the drag force associated with fluid movement.

The drag force can be expressed as a product of an area, kinetic energy and a friction factor,  $f$ . For a sphere this representation becomes:

$$F_D = (\pi R^2) \left( \frac{1}{2} \rho v_{\infty}^2 \right) f \quad (\text{IV-6})$$

Now substituting for Stoke's Law Equation (IV-5) one may arrive at an expression for  $f$ , namely:

$$f = \frac{24}{\text{Re}} \quad (\text{IV-7})$$

Next the motion of a spherical drop in a Newtonian fluid with internal circulation will be examined. For the motion of a spherical drop, the symbols will carry a prime to differentiate them against the properties of the fluid. The following conditions apply for a spherical drop with internal circulation:

At  $r=0$ :  $v_r' \neq \infty$   $v_\theta' \neq \infty$

At  $r=R$ :

$$\begin{aligned} v_\theta &= v_\theta' \\ v_r &= v_r' \\ \tau_{r\theta} &= \tau_{r\theta}' \end{aligned}$$

From the equations of continuity and motion, Hadamard (H3) has derived the following equation for the terminal velocity of a drop.

$$v_\infty = \frac{2(\rho - \rho')(\mu + \mu') g R^2}{3\mu(2\mu + 3\mu')} \quad (\text{IV-8})$$

Similarly one can obtain an expression for the drag force,  $F_D$

$$F_D = \frac{2\pi(2\mu + 3\mu')\mu R v_\infty}{(\mu + \mu')^2} \quad (\text{IV-9})$$

The motion of a bubble in a liquid may be described in the following way. Using Hadamard's terminal velocity expression, Equation (IV-8) and neglecting  $\mu', \rho'$  since  $\mu' \rho' \ll \mu \rho$  we arrive at an expression for the terminal velocity of a bubble with circulation.

$$v_\infty = \frac{\rho g R^2}{3\mu} \quad (\text{IV-10})$$

Similarly the drag force  $F_D$  can be evaluated to be:

$$F_D = 4\pi R \mu v_{\infty} \quad (\text{IV-11})$$

which is  $2/3$  of the value for a solid sphere. For a non-spherical bubble a factor  $C$  may be utilized to account for the eccentricity.  $C$  is a function of  $(D/H)$  where  $H$  is the height of the bubble, and  $D$  is the maximum width of the bubble.

$$F_D = 4\pi R \mu v_{\infty} C \quad (\text{IV-12})$$

The friction factor  $f$ , can be expressed in the same way as outlined earlier, however the drag force for a bubble of volume  $V$  can be represented by:

$$F_D = \rho V g \quad (\text{IV-13})$$

Substituting this expression into Equation (IV-6) and solving for the friction factor  $f$ , the following is attained:

$$f = \frac{8g V}{\pi D^2 v_{\infty}^2} \quad (\text{IV-14})$$

This expression may be utilized for the viscoelastic fluids as well (L3). The Reynolds number for the viscoelastic fluids will be described by the following relation:

$$Re = \frac{\rho v_{\infty} D}{\eta_0} \quad (\text{IV-15})$$

where  $\eta_0$  is a constant and is numerically equal to the sum of  $\eta_p$  parameters in De K  e's viscosity equation which will be outlined later in this discussion.

An effective viscosity  $\eta_{eff}$  may also be defined in an analogous manner leading to a Reynolds number of the form

$$Re = \frac{\rho v_{\infty} D}{\eta_{eff}} \quad (IV-16)$$

where units of  $\eta_p$  and  $\eta_{eff}$  are Pa.s. With this effective viscosity, we can obtain a shift factor,  $k'$ , which will determine the necessary shift to line up the viscoelastic friction factor curve to that of the Newtonian case ( $f = 24/Re$ ). Algebraically, by equating the Reynolds numbers of Equations (IV-15 and IV-16)

$$\left[ \frac{v_{\infty} D \rho}{\eta_{eff}} \right] = \left[ \frac{v_{\infty} D \rho}{\eta_0} \right] k' \quad (IV-17)$$

the effective viscosity may be determined to be:

$$\eta_{eff} = \frac{\eta_0}{k'} \quad (IV-18)$$

The derivation of these equations will now establish a foundation for examining the phenomena observed during

experimentation. Before entering upon a discussion of these phenomena it will be appropriate to examine some of the properties associated with these fluids.

There was a sharp contrast in the measured viscosities of the three solutions while the solution densities and surface tension shown in Table (IV-1) were comparable. The reason for this lies in the fact that the two non-Newtonian solutions are primarily  $H_2O$  and  $H_2O$ -glycerol and one would expect their surface tensions and densities to be comparable to pure  $H_2O$  and glycerol solutions. However the primary normal stress difference and viscosities were significantly different for the non-Newtonian fluids, hence a more detailed examination is required for explaining these last two solution properties, one involving chemical structure.

Table (IV-1) Surface Tension and Density Values

Fluid	Surface Tension (N/m)	Density ( $kg/m^3$ )
A. 40% Glycerol	0.061	1091
B. 1% CMC	0.057	1001
C. 1% PAA	0.071	1128
D. $H_2O$	0.074	1000
E. Glycerol	0.063	1261

Depicted in Figures (IV-1) and (IV-2) are graphs of the viscosities and primary normal stress differences as a function of the shear rate,  $\dot{\gamma}$  for the three fluids studied and predictions for each utilizing De K  e's model .

Figure (IV-1) Viscosities As a Function of the Shear  
Rate for The Three Test Fluids.

————— De Kée Model (Equation IV-20)

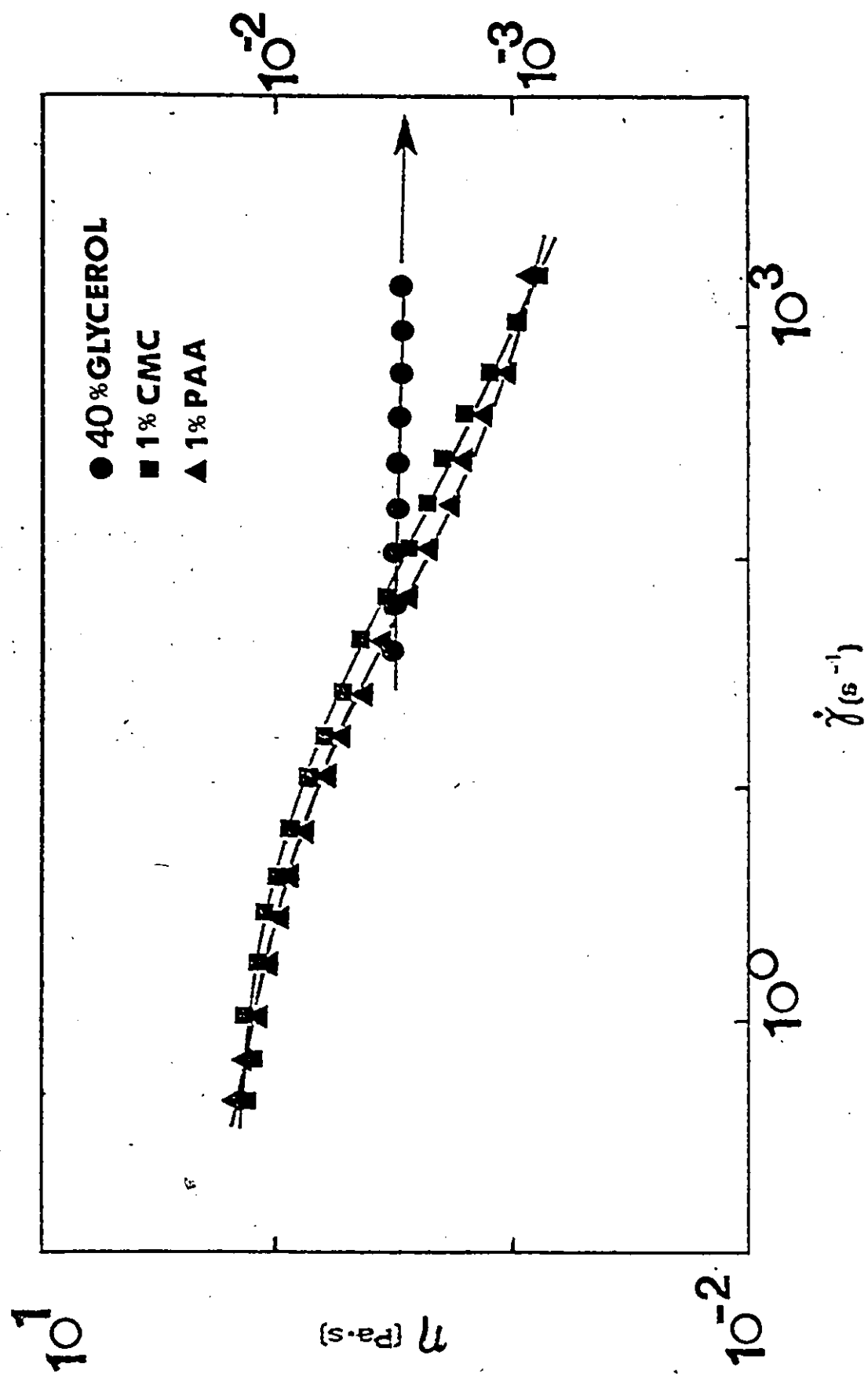
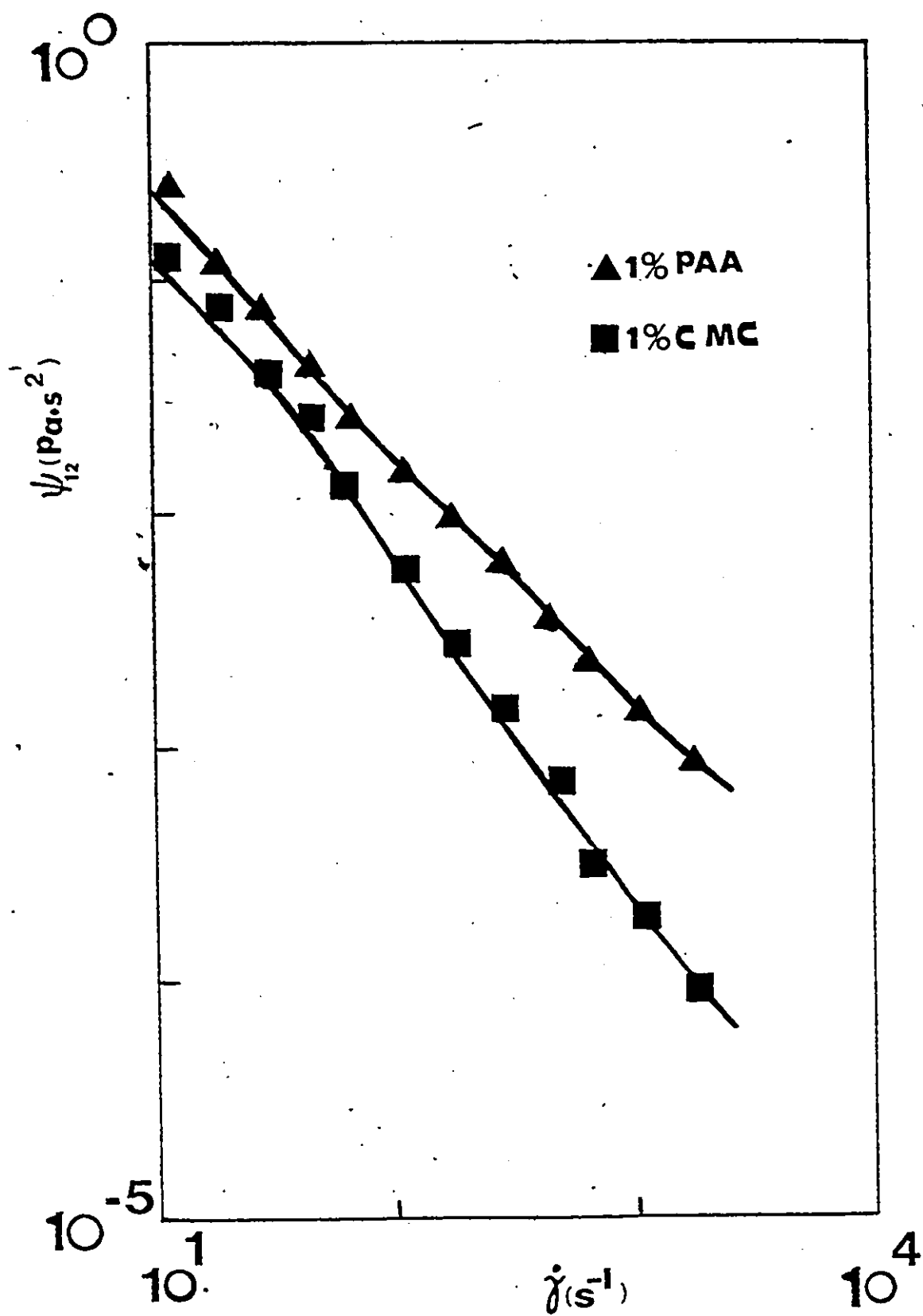


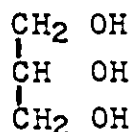
Figure (IV-2) Primary Normal Stress Difference As a  
Function of the Shear Rate for 1% CMC  
and 1% PAA.

—————:De K   Model (Equation IV-21)





Glycerol used in the Newtonian solution is an organic alcohol, with the following molecular representation:

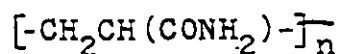


It is composed of short, straight chains of very low molecular weight ( $M=92$ ) and is quite soluble in water. At low concentration ( 50% wt) the molecules being so short and straight behave independently of each other and offer little resistance to shear. Glycerol like water is a Newtonian fluid whereby the viscosity ( $\eta$  or  $\mu$ ) is independent of the shear rate ( $\dot{\gamma}$ ). Glycerol and water also exhibit no primary normal stress differences, which is typical of all Newtonian fluids.

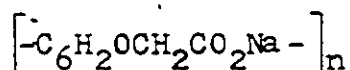
The two viscoelastic liquids used, namely, 1% CMC and 1% PAA in glycerol- $\text{H}_2\text{O}$  contain macromolecules, which are long chain molecules, with very high molecular weights. These linear polymers are long covalently bonded structures which tend to coil up and uncoil when placed in solution. The coiled chains tend to create/destroy specific junction points or entanglements when placed under shear. The lifetime of these entanglements is characteristic of the polymer studied and contributes significantly to the viscosity and primary normal stress differences exhibited. Since the value of viscosity and primary normal stress difference is dictated by the resultant motion of the polymer molecule as a whole. Properties such as molecular weight, chain length and configuration, and degree of entanglement

contribute to the viscosity and primary normal stress difference.

In the case of the glycerol solution the molecular chains all have equal length, however, the viscoelastic solutions, contain chains of varying length and are classified on an average molecular weight (MW) basis. Since entanglements increase greatly in complexity as the chain length increases, one expects an increase of viscosity with increasing molecular weight. The polyacrylamide used in this experimental work had a MW of 500,000 to 600,000 and contained the following repeating unit:



The carboxymethylcellulose utilized in this work contained the following repeating unit:



However, no information could be obtained pertaining to its molecular weight.

As can be seen from Figure (IV-1), the Newtonian fluid viscosity is clearly independent of the shear rate as well as being lower for all shear rates, as compared to the two viscoelastic fluids. The two viscoelastic fluids were also pseudoplastic. An explanation for this phenomenon is given in Lodge's (14) network theory for polymers. His theory basically states that non-Newtonian fluids contain long chain molecules which tend to get entangled.

Entanglements retard movements of long molecules. Hence the viscosity is high. By increasing the shearing force, molecules disentangle (uncoil) and orient themselves, making it easier for them to slide along - hence viscosity drops. Lodge's network theory can also be applied to the primary normal stress coefficient as plotted in Figure (IV-2). The coefficient  $\psi_{12}$  is defined as:

$$\psi_{12} = \left( \frac{\tau_{11} - \tau_{22}}{\dot{\gamma}^2} \right) \text{ Pa} \cdot \text{s}^2 \quad (\text{IV-19})$$

where:  $\tau_{11}$ ,  $\tau_{22}$  are normal stresses (Pa)  
and decreases with increasing shear rate.

To model the viscosity and primary normal stress difference coefficient, De K  e's model was used.

The model has the following form:

$$\eta = \sum_p \eta_p e^{-t_p \dot{\gamma}} + \eta_{\infty} \quad (\text{IV-20})$$

$$(t_p = 10 t_{p+1})$$

where the constants  $\eta_{\infty}$ ,  $\eta_p$  and  $t_p$  are determined by a non-linear regression computer program given in Appendix II.

The primary normal stress difference is given by:

$$\psi_{12} = 2 \sum_p \eta_p \lambda_p e^{-c t_p \dot{\gamma}} + \psi_{\infty} \quad (\text{IV-21})$$

where the constants  $\psi_{\infty}$ ,  $\lambda_p$  and  $c$  can also be determined using a non-linear regression program.  $\lambda_p$  can be obtained in terms of  $\eta_p$  as follows:

$$\lambda_p = \frac{\lambda_3 \eta_p}{\eta_3} \quad (\text{IV-22})$$

Table(IV-2) Constants utilized in De Kée Models

FLUID	40% GLYCEROL	1% CMC	1% PAA
$\eta_1$ (Pa.s)	$3.31 \times 10^{-3}$	0.628	1.167
$\eta_2$ (Pa.s)		0.582	0.316
$\eta_3$ (Pa.s)		0.106	0.109
$t_1$ (s)		0.168	0.210
c		2.61	0.383
$\lambda_3$ (s)		0.0224	0.0168
$\eta_\infty$ (Pa.s)		0.080	0.089
$\psi_\infty$ (Pa.s <sup>2</sup> )		$1.0 \times 10^{-4}$	$1.10 \times 10^{-6}$

The evaluated constants for the two models for each of the fluids are given in Table (IV-2). The function  $\psi_{12}$  is related to elasticity by the parameters  $c$  and  $\lambda_p$ . The Newtonian fluid has no elasticity; that is  $\psi_{12} = 0$ . Elasticity precludes that the polymer chains tend to highly curved configurations between entanglements (T2). Owing to these conformations the distance between the ends is much less than that of equivalent linear lengths. Deformation or stretching of the polymer straightens out the molecules, which tend to return again to an equilibrium curved state when the deformation force is removed. As we shall see later elasticity plays an important role in determining the shape of bubbles in the viscoelastic solutions.

Figure (IV-3) shows pictures of bubbles which were in free rise in the 40% glycerol solution. Scales were provided for estimating the relative sizes of the bubbles. For bubbles shown in frames A and B, the scale on the left is applicable, while for frames C and D, one should refer to the scale on the right. Bubbles of approximately  $1 \times 10^{-8} \text{ m}^3$  were spherical. However, the pictures lacked proper quality at this volume.

Figure(IV-3) Bubble Shapes in a 40% Aqueous Glycerol Solution.

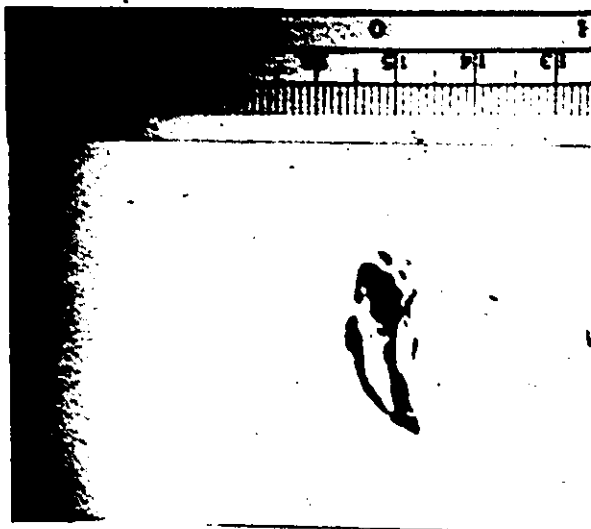
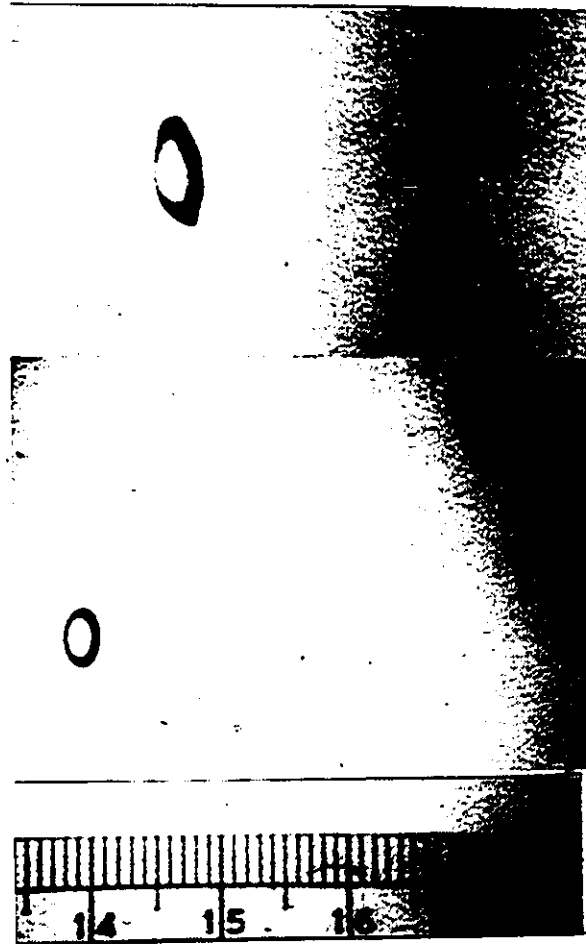
A -  $5 \times 10^{-8} \text{ m}^3$

B -  $1 \times 10^{-7} \text{ m}^3$

C -  $1 \times 10^{-6} \text{ m}^3$

D -  $2 \times 10^{-6} \text{ m}^3$

Note: For bubbles A,B the scale on the left applies while for bubbles C,D the scale on the right is utilized.

**D****C****B****A**



The bubbles rising in glycerol below a volume of  $5 \times 10^{-8} \text{ m}^3$  tended to rise in a vertical path, while all volumes between  $5 \times 10^{-8}$  and  $2 \times 10^{-6} \text{ m}^3$  would oscillate about their axis during ascent. Bubble volumes at  $1 \times 10^{-8} \text{ m}^3$  -  $4 \times 10^{-8} \text{ m}^3$  were spherical shaped, then formed ellipsoidal shapes at higher volumes and at a volume of  $1 \times 10^{-6} \text{ m}^3$  acquired a spherical cap shape. Bubbles greater than  $1 \times 10^{-6} \text{ m}^3$  in volume achieved highly random spherical cap shapes that would dilatate greatly changing overall dimensions significantly. The interplay of surface tension, inertia, viscous forces in conjunction with internal circulation controlled the bubble shapes. Depicted in Figure (IV-4) is a graph of (D/H) for 1%CMC and 40%Glycerol.

At this time it would be advantageous to define  $T$  as the injection period.  $T$ , pertains to the number of bubbles injected per unit time. For the case of the 40% glycerol solution there is considerable scatter in the data because of the random shape dilatations observed in this solution. There is however a tendency for the (D/H) ratio to increase with increasing volume. An empirical curve may be fitted to the data for the 40% glycerol solution of the form

$$(D/H) = 29.60 V^{0.18} \quad (\text{IV-23})$$

where:

D = diameter of bubble (maximum horizontal dimension) m

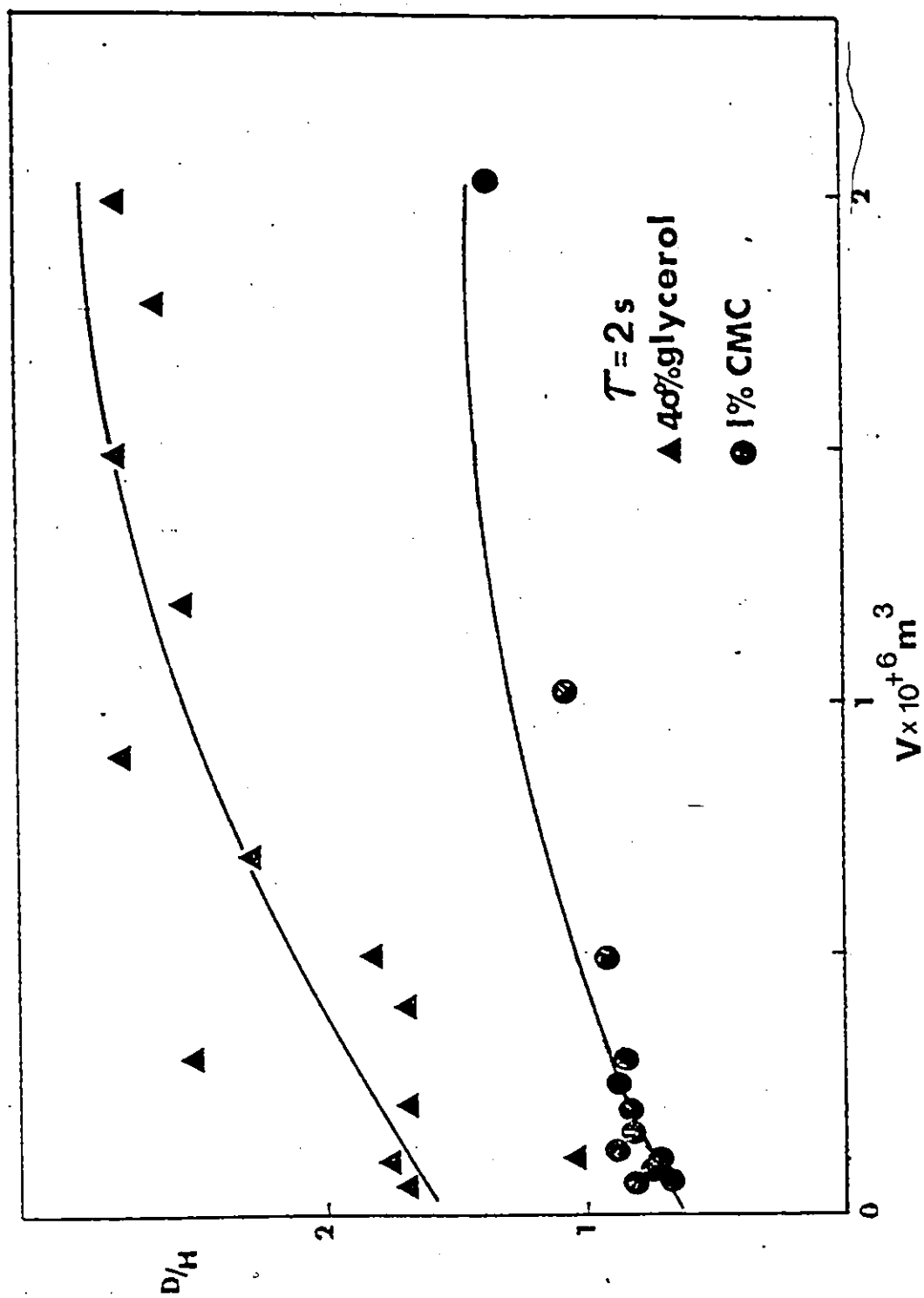
H = height of bubble (maximum vertical dimension) m

$\frac{D}{H}$  = Dimensionless

V = Volume of bubble ( $\text{m}^3$ )

Figure (IV-4) Eccentricity (D/H) for Newtonian  
and Viscoelastic Solutions

————: Empirical Model (Equation  $\overline{\text{IV}}-23$  and  $\overline{\text{IV}}-24$ )



The viscoelastic solution (1% CMC) also demonstrated the same trend. In this case the empirical equation is given by:

$$(D/H) = 18.36 V^{0.20} \quad (IV-24)$$

In Figure (IV-5) the effect of injection period on  $(D/H)$  is examined. The experimental work has shown that there is little effect of injection period on  $(D/H)$ . A similar empirical equation for the 1% PAA case yields:

$$(D/H) = 28.18 V^{0.22} \quad (IV-25)$$

Experimental data are listed in Appendix 1. Clift et al. (C4) mention that increased flattening of bubbles or an increasing  $(D/H)$  ratio results from increased inertia forces directly attributed to the increased terminal velocities.

Bhaga and Weber (B4) claim that for a high Morton (Mo) number the shape is only a function of  $Re$ , since at low volumes, surface tension and viscous forces are more predominant.

Figure (IV-5) The Effect of Injection Period  
(  $\tau$  ) on (D/H) for 1% PAA

—————: Empirical Model (Equation IV-25)

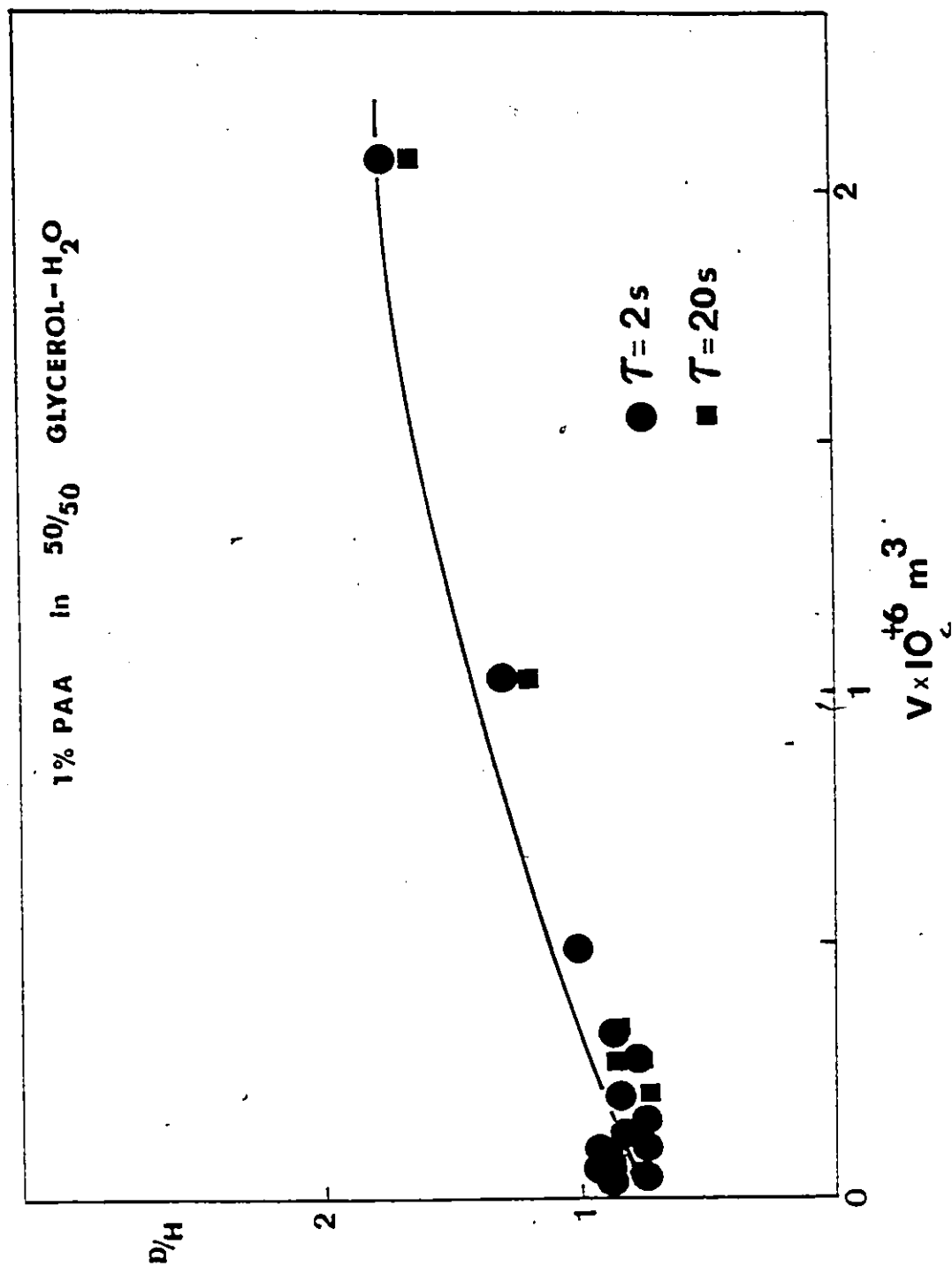


Figure (IV-6) shows bubble shapes observed in the 1% CMC and the 1% PAA solutions. Both viscoelastic fluids were responsible for approximately the same shape transitions although bubbles in the 1% CMC solution appeared blurry, probably because of the opaqueness of the CMC solution. With an increase in bubble volume, the air bubbles changed from spherical (not photographed) to prolate teardrop shaped into an oblate cusped shape and finally to a spherical cap. The tailing phenomena was observed for bubble volumes of  $5 \times 10^{-8} \text{ m}^3$  to  $2 \times 10^{-6} \text{ m}^3$  confirming previous reports (A1, A2, C1, L1, H1).

Perhaps the best explanation for this phenomenon is due to Barnett et al. (B1), who cite that a hole (momentum defect) develops at the rear of the bubble resulting from the fluid being displaced by the bubble and failing to recover quickly enough. This effect is peculiar only to elastic non-Newtonian fluids as detailed by Calderbank et al. (C1). The explanation for it stresses the time dependency of the elasticity of the fluid also known as stress relaxation. For low to moderate shear rates ( $\dot{\gamma} = 1.2$  to  $158 \text{ s}^{-1}$ ) the stress relaxation time was about 3 seconds for the CMC solution at  $\dot{\gamma} = 22.3 \text{ s}^{-1}$  and 6 seconds for the PAA solution at  $\dot{\gamma} = 22.3 \text{ s}^{-1}$ . For the small bubble volumes,  $5 \times 10^{-8} \text{ m}^3$  to  $1 \times 10^{-6} \text{ m}^3$  there is an interplay of forces such as interfacial tension and elasticity to govern their shape. The viscoelasticity of the PAA and CMC solutions maintains a smooth bubble contour at large bubble volumes. This is not the case for the Newtonian solution. The pattern of rise is also significantly

Figure(IV-6) Bubble Shapes in 1%CMC and 1%PAA

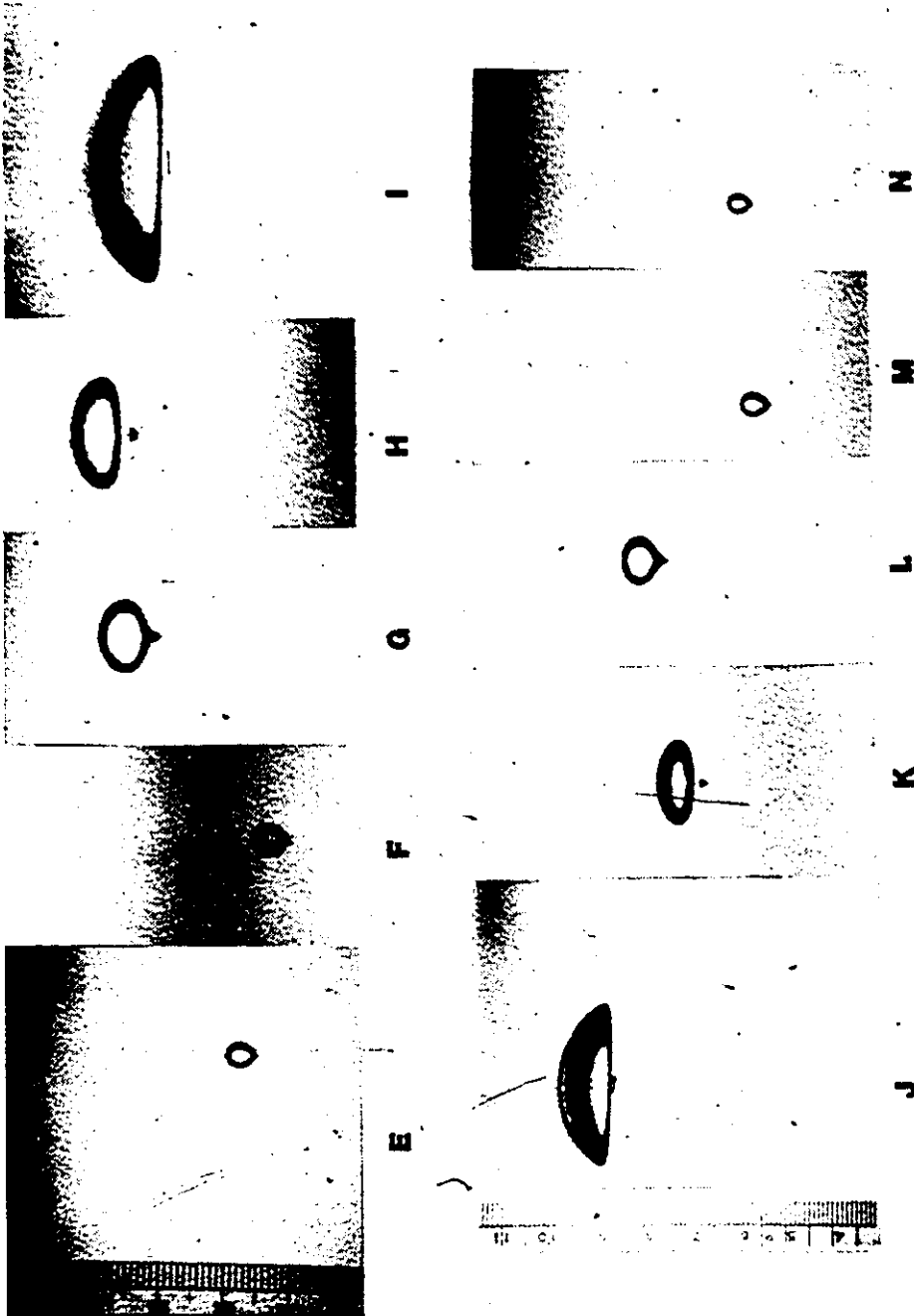
1% CMC

E -  $5 \times 10^{-8} \text{ m}^3$   
F -  $1 \times 10^{-7} \text{ m}^3$   
G -  $1 \times 10^{-6} \text{ m}^3$   
H -  $2 \times 10^{-6} \text{ m}^3$   
I -  $1 \times 10^{-5} \text{ m}^3$

1% PAA

J -  $1 \times 10^{-5} \text{ m}^3$   
K -  $2 \times 10^{-6} \text{ m}^3$   
L -  $1 \times 10^{-6} \text{ m}^3$   
M -  $1 \times 10^{-7} \text{ m}^3$   
N -  $5 \times 10^{-8} \text{ m}^3$





different from the one observed for the Newtonian fluid. All bubble volumes rise in a vertical trajectory with no observed instability in their motions. The bubbles in viscoelastic fluids showed evidence of circulatory activity at the surface (front) of the large bubbles. As the surface molecules of the bubble move outwards and downwards from the forward stagnation point, a new surface forms. The energy required per unit time to form the surface is  $2\pi R O v_t$ , where  $v_t$  is the tangential velocity of the surface (G3). This energy is balanced by the closing of the rear surface and any excess surface energy that is generated is released in the form of internal circulation. Hughes and Gilliland (H6) pointed out that circulation becomes appreciable whenever the skin friction becomes the dominant surface force. The internal circulation of gas inside the bubbles depends on the accumulation of surface active impurities at the interface, with observed internal velocities of the order of 1% of the terminal velocities (C4). Surfactants to some extent are even contained within distilled water and tend to reduce internal motion by rendering the interface rigid. Surfactants such as Sodium Lauryl Sulfate also have an effect on the terminal velocity (C4). The terminal velocity of drops was found to decrease as the concentration of surfactant increased as observed by Edge and Grant (C4). There are also indications that shape deformations tend to decrease internal circulation significantly (C4). They (C4) also mention that traces of surface-active impurities may have a profound effect on reducing the internal circulation, thereby significantly

increasing the drag and drastically reducing overall mass transfer. Levich and Frumkin (L3), proposed the following explanation for the absence of circulation. They state that surface active substances tend to accumulate at the interface between two fluids, thereby affecting the surface tension. When a bubble (drop) moves through a continuous medium, absorbed surface active materials are swept to the rear, leaving the frontal region relatively uncontaminated. The concentration gradient results in a tangential gradient of surface tension which in turn causes a tangential stress tending to retard surface motion. In this experimental work no attempt was made at isolating the effects of surfactants.

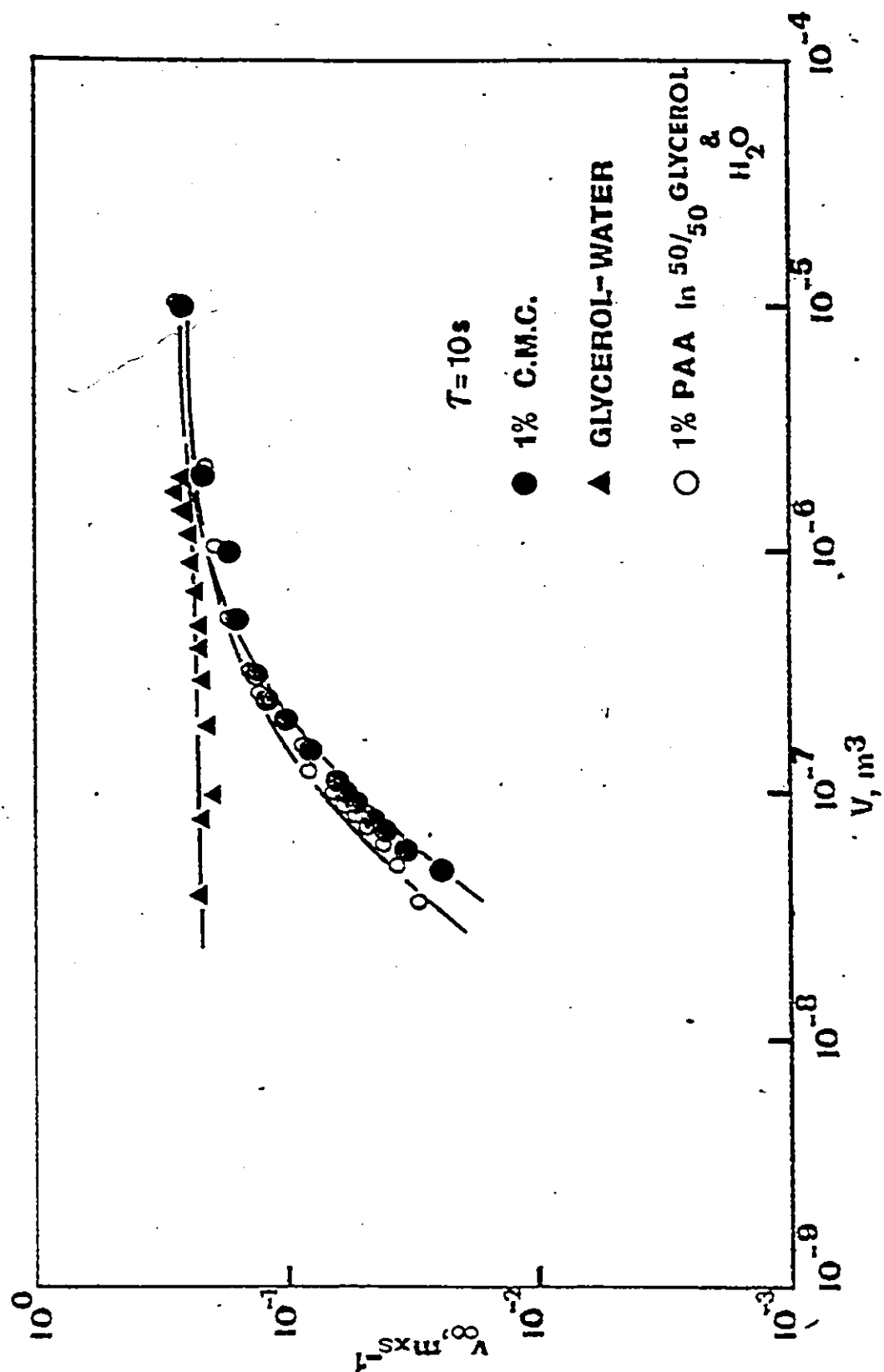
The terminal velocity of the air bubbles increased with increasing volume for all fluids. This result is shown in Figure (IV-7) and in Appendix 1. Consistent with other experimentors (A1, C1, L1) the terminal velocity ( $v_{\infty}$ ) increases more rapidly for the viscoelastic fluids than for the Newtonian fluid. Garabedian (G4) remarked that rising bubbles adopt a stable shape which leads to an asymptotic rising velocity.

Bubbles rising in a viscoelastic fluid have a lower velocity than bubbles rising in a Newtonian fluid. To explain this occurrence a force balance must be performed on the bubble. One may, by equating the gravity force to the drag and buoyancy forces obtain the terminal velocity for the bubble as:

$$v_{\infty} = \frac{2R^2(\Delta\rho)g}{9\mu} \quad (\text{IV-26})$$

Figure (IV-7) Terminal Velocity As a Function of  
Bubble Volume for The Three Test  
Fluids (  $\tau = 10s$  )

—————: Empirical Model (Equations IV-27 to IV-29)



This solution is not applicable to viscoelastic systems but does demonstrate the inverse dependency of viscosity upon terminal velocity. Judging from the Reynolds number evaluated for the viscoelastic solutions, bubble dynamics is confined to a low shear-rate range ( $\dot{\gamma} = 1-10\text{s}^{-1}$ ). At this shear rate range, the viscosity of CMC and PAA is much higher than the corresponding 40% glycerol solution viscosity, hence the terminal velocity of air bubbles in glycerol (40%) solution would be higher than in the case of the viscoelastic solutions. Empirical equations relating the velocity and volume were obtained for the three fluids (as shown below), based on a generalization of Equation (II-8).

40% Glycerol

$$\langle v_{\infty} \rangle = 18.226(V + 1.58 \times 10^{-6})^{1/3} \quad (\text{m/s}) \quad (\text{IV-27})$$

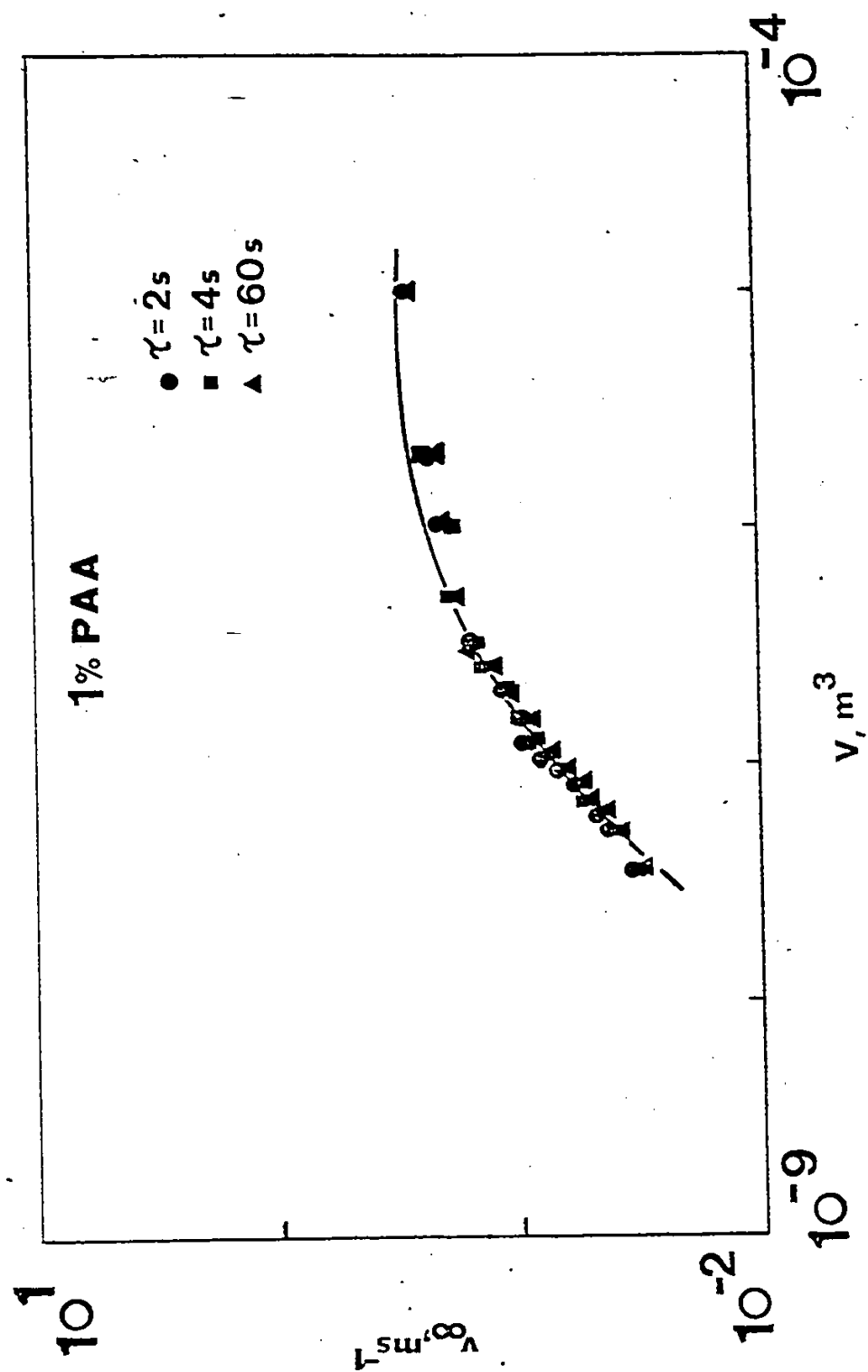
$$\text{1\% CMC } \langle v_{\infty} \rangle = 16.52(V - 4.59 \times 10^{-8})^{1/3} \quad (\text{m/s}) \quad (\text{IV-28})$$

$$\text{1\% PAA } \langle v_{\infty} \rangle = 18.43(V - 4.56 \times 10^{-8})^{1/3} \quad (\text{m/s}) \quad (\text{IV-29})$$

The velocity-volume curves shown for CMC and PAA did not contain a velocity discontinuity as reported by Astarita and Apuzzo, Calderbank et. al., Acharya et al. and Leal et al. (A1, C1, A2, L1). The discontinuity did not appear even when experimentation was carried out at irregular injection periods. One objective of this work was to see the effect of injection period upon the terminal velocity of the air bubbles, as shown in Figure (IV-8). Clearly

Figure (IV-8) The Effect of Injection Period  
On Terminal Velocity for 1% PAA.

————: Empirical Model (Equation IV-29)



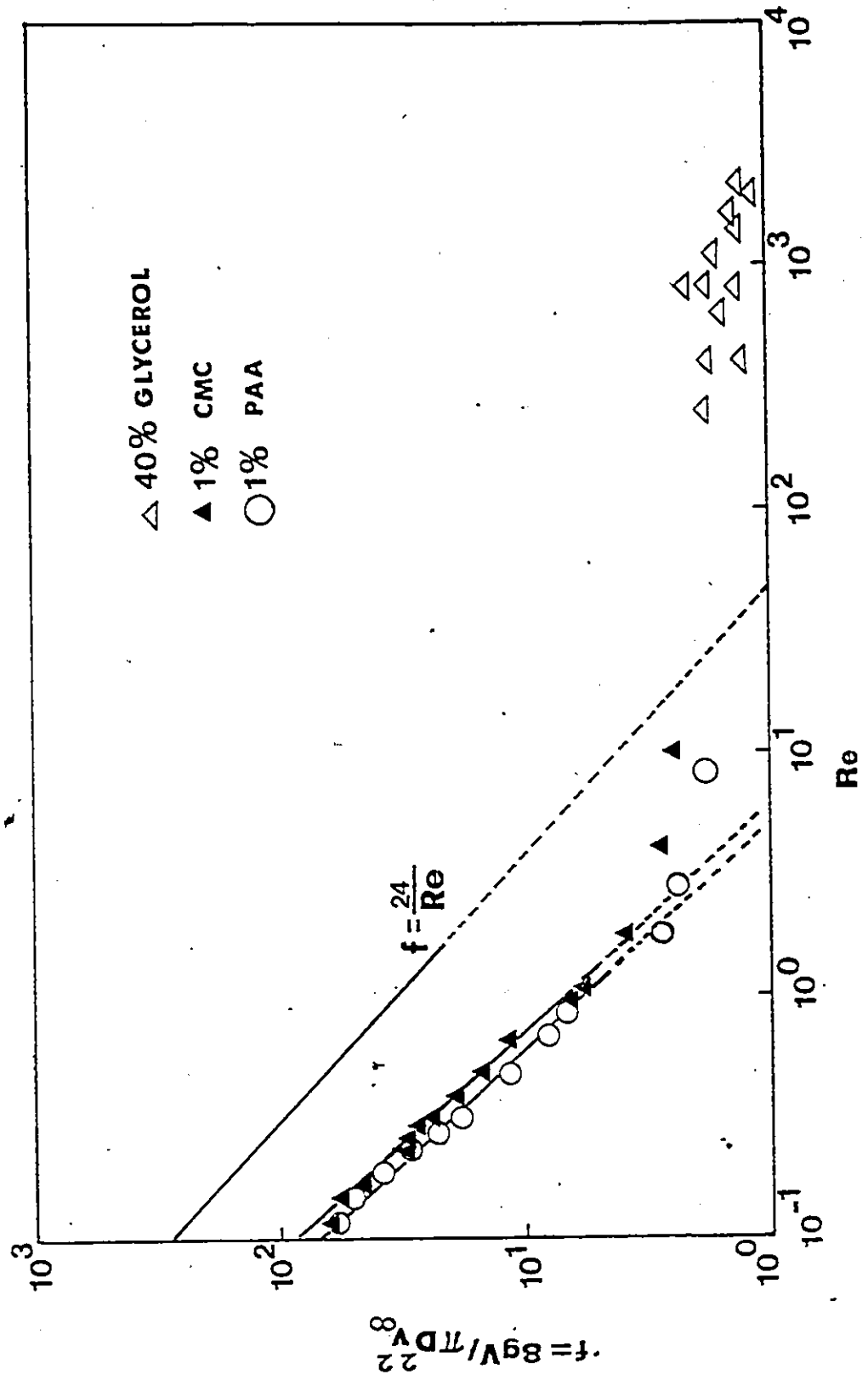


there is only normal scatter in the velocity-volume data leading to the conclusion that the injection period ( $\tau$ ), seems to have very little effect on the terminal velocities. The study of this parameter ( $\tau$ ) was based on a hypothesis to explain the velocity discontinuity based on the transient behaviour of macromolecules. In network theories one assumes that the macromolecules form a network of temporary junctions. When the solution is in motion, the molecules slide past each other losing and forming junctions. On cessation of steady simple shear, the stress depends on the change in concentration of segments. Hence  $\tau$ , the injection period has a direct effect on the prevailing stress. Since this concentration decreases in exponential fashion, the relaxation functions decrease more rapidly with increasing  $\dot{\gamma}_0$ , the initial shear rate (D5). The air bubbles travelling through the stagnant viscoelastic solution provide the initial shear rate ( $\dot{\gamma}_0$ ).

The drag coefficient,  $f$ , was also evaluated via Equation (IV-14). Figure (IV-9) shows Stokes Law for comparison with the Re-drag curves for our test fluids. The drag coefficient for glycerol is outside the boundaries established for creeping flow—namely a spherical bubble travelling with low velocity (or  $Re < 1$ ).

Figure (IV-9) Drag Coefficient Versus  $Re$  for The  
Three Test Fluids

————: Empirical Model (Equations  $\overline{IV-31}$  and  $\overline{IV-32}$ )



To fulfill the creeping flow assumption for elastic non-Newtonian fluids one deviates from the classical creeping flow hypothesis that the inertia terms in the equation of motion are negligible as compared to the internal stress terms. This translates into a low Reynolds number analysis of the problem. For elastic fluids the Weissenberg number has to be evaluated, since high Weissenberg numbers may result in creeping flow conditions even at comparatively high Reynolds numbers (A3).

The Weissenberg number can be expressed as:

$$W_s = \frac{\mu v_0}{R E} \quad (IV-30)$$

The drag coefficients were calculated for CMC and PAA as a function of  $Re$ , respectively as:

$$f = \frac{7.0}{Re} \quad (IV-31)$$

$$f = \frac{6.0}{Re} \quad (IV-32)$$

Clift et al. (C4) show that the drag coefficient for bubbles lies below the rigid sphere curve (Stokes Law) when internal circulation is present. The drag is dominated by deformation. The drag curves would also lie below the rigid sphere curve if we were dealing with cylinders instead of spheres (B5). The shift factors ( $k'$ ) for CMC and PAA, which would align the viscoelastic friction data to Stokes Law, were found to be:

$$k'_{CMC} = 3.43 \quad (IV-33)$$

$$k'_{PAA} = 4.00 \quad (IV-34)$$

This factor precludes that the viscoelastic friction data are approximately three times lower than the rigid sphere data in a Newtonian fluid. The effective viscosities ( $\eta_{eff}$ ) at low  $\dot{\gamma}$  were also calculated and found to be:

$$\eta_{eff, CMC} = 0.383 \text{ Pa.S} \quad (IV-35)$$

$$\eta_{eff, PAA} = 0.400 \text{ Pa.S} \quad (IV-36)$$

The drag phenomena observed in this experimental work can be analyzed through the ideas put forth by Barnett et al. (B1). They state that a "hole" or momentum defect results when a fluid passing over a sphere fails to recover quickly enough. This process sets up an adverse pressure gradient and a wake develops. The energy transfer required to create the wake in a Newtonian fluid is much less than in the corresponding non-Newtonian fluid due to the absence of elastic forces. Hence, due to elasticity, the drag experienced by the bubble in a viscoelastic fluid would be greater than that experienced in a Newtonian fluid. To complete the comparison, a line was fitted to the Newtonian case of the form:

$$f = \frac{6.595}{Re^{0.216}} \quad (IV-37)$$

The last point examined in this section is the possibility of wall effects. Warshay et al. (W1) present a correlation to correct for wall effects of the form:

$$\frac{\langle v \rangle}{v_{\infty}} = \left[ 1 - \left( \frac{D_e}{D_c} \right)^2 \right]^{1.43} = \frac{1}{K} \quad (\text{IV-38})$$

where:

- $D_e$  = equivalent diameter of bubble (m)
- $D_c$  = diameter of chamber (m)
- $K$  = correction factor for wall effects

Since the experimental tank has orifices located unsymmetrically because of the decision to fabricate a square vessel for photographic reasons, this correlation would only provide an order of magnitude analysis. The correlation also does not take into account the non-Newtonian nature of the two fluids studied by this work. However, the correction factor K is about 1.2 for the largest volume bubble produced (approx.  $1.0 \times 10^{-5} \text{ m}^3$ ), while K is about 1.1 for a  $2.0 \times 10^{-6} \text{ m}^3$  bubble.

## (ii) MULTIPLE BUBBLE INJECTION

The multiple bubble experimental results are primarily qualitative in nature with only three parameters examined, relative bubble volumes, injection period and orifice separation ( $\Lambda$ ). The data may be divided into two main groups, based on the type of coalescence experimentation performed. In the first group, one bubble was fixed at  $1.0 \times 10^{-6} \text{ m}^3$  in volume and a subsequent bubble was injected simultaneously at different horizontal coordinates (orifice separation,  $\Lambda$ ) and different volumes until it reached a volume ( $V_c$ ) which coalesced with the fixed volume bubble. In Figure (IV-10)  $V_c$ , the coalescent volume ( $\text{m}^3$ ) is plotted against  $\Lambda$ , the orifice separation (m). Data are shown for different injection periods. The plot consists of results for PAA and CMC only, because no coalescence phenomena could be realized in the Newtonian case. Due to the severe oscillations and dilatations of the bubbles formed in this fluid, bubbles did not coalesce. They would disintegrate upon collision. The viscoelastic coalescence data when fitted on semi-log coordinates produced models of the form:

$$\underline{1\% \text{ CMC}} \quad V_c = (6.52 \times 10^{-7}) \text{ Exp } (60.68 \Lambda) \quad (\text{IV-39})$$

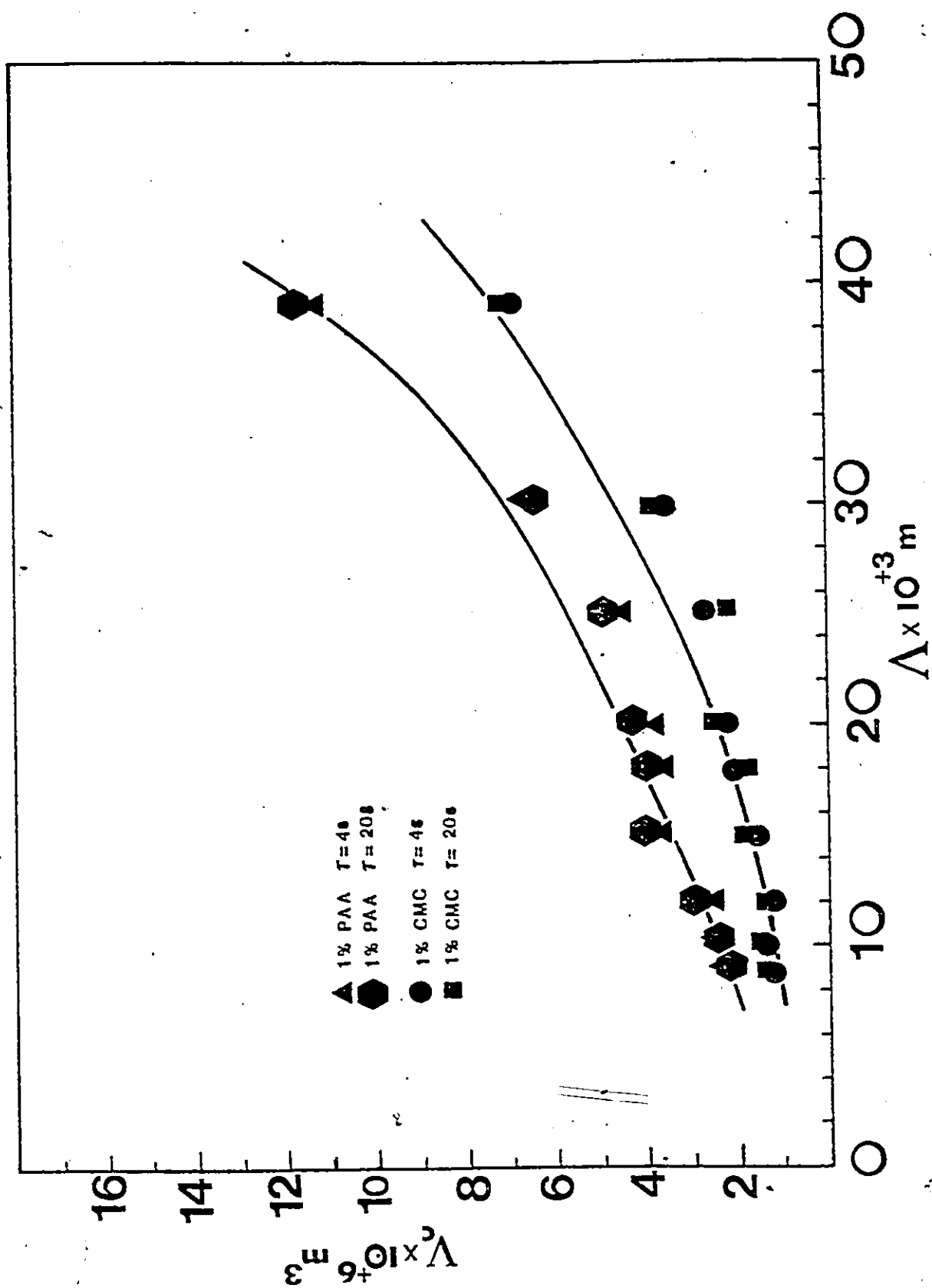
$$\underline{1\% \text{ PAA}} \quad V_c = (1.50 \times 10^{-6}) \text{ Exp } (49.89 \Lambda) \quad (\text{IV-40})$$

These empirical models show that  $V_c$  and  $\Lambda$  are related. A greater coalescent volume is required for greater separa-

Figure (IV-10) Bubble Coalescence With a  $1.0 \times 10^{-6} \text{ m}^3$   
Bubble As a Function of Orifice  
Separation (  $\Delta$  ) and Injection  
Period (  $\tau$  ).

—————: Empirical Model (Equations IV-39 and IV-40)





tion upon injection. Multiplying the CMC curve by a factor of about 2 will approximately allow a superposition of CMC and PAA curves. This factor seems to be proportional to the relaxation times of the two viscoelastic solutions.

Since for moderate shear rates ( $\dot{\gamma} = 1.2-158 \text{ s}^{-1}$ ) the stress relaxation time was of the order of 3 seconds for the CMC solution and 6 seconds for the PAA solution. Injection period  $(\tau)$  was not found to be a significant parameter in controlling coalescence for this two bubble phenomenon. The coalescence curve for the more elastic PAA solution is higher than that of the CMC solution on Figure (IV-10). It must be stressed that the coalescent volume  $V_c$  is the minimum volume of bubble required to coalesce with a  $1.0 \times 10^{-6} \text{ m}^3$  bubble just before escaping the terminal velocity region.

Coalescence, as mentioned earlier is a three stage process. In the first stage the trailing bubble enters the wake behind the leading bubble. Depending upon its size, the trailing bubble experiences less drag in the wake and accelerates towards the leading bubble. An order of magnitude analysis may be performed utilizing Batchelor's far wake velocity solution (A4) to examine the accelerations in this region. The far wake solution takes on the following form:

$$v_w(r,z) = \frac{v_{A\infty}}{32} f\left[\frac{D}{z}\right] \text{Re} \exp\left[-\frac{1}{4} \frac{\rho^v v_{A\infty} r^2}{\eta_0 z}\right] \quad (\text{IV-41})$$

$v_w(r,z)$  = the wake velocity (m/s)

$z$  = the axial distance measured from rear of bubble (m)

$v_{A\infty}$  = the terminal velocity of the leading bubble (m/s)

$r$  = the radial distance (m)

Now by inserting Equations (IV-15, IV-31, IV-32) into Equation (IV-41) one can obtain an approximation to the wake velocity in the viscoelastic fluids. By differentiating this new equation with respect to time an acceleration may be realized. Typical wake velocities calculated from Equation (IV-41) with  $r=0$  and  $z=0.01$  m are 0.051 m/s and 0.053 m/s for a  $1.0 \times 10^{-6} \text{ m}^3$  bubble and 0.212 m/s and 0.193 m/s for a  $10.0 \times 10^{-6} \text{ m}^3$  bubble in 1% CMC and 1% PAA, respectively.

Then ensuing bubbles collide as a result and are separated by a thin liquid film, or sometimes they separate completely from each other. In the third stage, the ambient liquid is drained from the interfacial film until this bursts and coalescence occurs. Acharya et al. (A4) mention that greater the elasticity, the longer the drainage time of the separating film between two bubbles. Even when two bubbles collide they could separate or not coalesce. This phenomenon was noticed for both viscoelastic fluids many times in the multiple bubble experiments, especially when bubbles were of approximately the same size.

In the behaviour of a free surface bounded by a gas, the molecules of the liquid are influenced by the cohesive forces of the liquid alone, since the corresponding forces from the gas on these liquid molecules are negligible. The resultant force is directed inwards. However, conditions change when bubbles coalesce and the surface of the liquid (interfacial film) will then be acted on by forces from the contiguous media. By producing a larger surface contact area, more surface energy is required to create more surface, and since surface energy is inversely proportional to interfacial area, the surface free energy starts to decrease. If free energy (surface) be zero or negative according to Adamson (A5) the tendency would be to disperse one phase into the other (i.e. coalescence). Along this thin surface region there is diffusion and Brownian motion resulting in an interchange of

molecules between the surface and bulk region. Elasticity appears to prolong the coalescence process. A characteristic of films is their resilience to mechanical disturbance. Gibbs (A5) considered this important property to be associated with the elasticity of the film  $E$ , represented by:

$$E = \frac{2}{d \ln A} \frac{d\sigma}{d \ln A} \quad \text{Nm}^{-2} \quad (\text{IV-42})$$

where:  $A$  = area of film ( $\text{m}^2$ ).

Qualitatively,  $E$  gives a measure of the ability of a film to adjust its surface tension under applied stress. When a bubble is deformed from a spherical shape its persistence on remaining intact depends on the elasticity of the film to permit variations in surface tension. This now allows us to consider the effect of chemical potential, operating at the interface. Due to the Gibbs effect any disturbance of the interfacial film accompanying an increase of its surface will reduce the surface excess temporarily. Surface excess may be defined in the following manner:

$$d\sigma = -\sum \Gamma_i du_i \quad (\text{IV-43})$$

where:

$u_i$  = chemical potential ( $\text{Nm.moles}^{-1}$ )

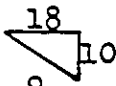

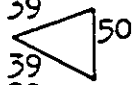
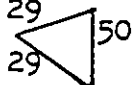
$\Gamma_i$  = surface excess ( $\text{moles.m}^{-2}$ )

The surface tension rises as a consequence and this increase of tension (proportional to  $E$ ) counteracts further extension of the surface thus tending to restore the initial equilibrium. The temporary rise in surface tension due to a decrease in the local surface excess is lessened by a replenishing of the absorbed species from the bulk liquid by diffusion and Brownian motion.

Davies and Rideal (D4) claim the higher the viscosity of the fluid the slower will be the drainage. They claim that the rate of thinning is related to the drainage rate, with a thicker film producing a faster drainage rate. This behaviour of film thinning and drainage is also governed by radial squeezing flow occurring between the two bubble interfaces. Within a short time the integrity of the film declines and after reaching a certain film thickness as shown by Marrucci (M2) the film collapses and bubbles coalesce.

In the second part of experimentation with multiple bubble phenomena, three bubble coalescence was examined. Three bubbles of equal volume were injected at different orifice separations and configurations for two injection periods. A summary of the results is presented in TABLE (IV-3). As can be seen from the data the elasticity of 1% PAA prevents coalescence until a higher volume is produced in comparison to the 1% CMC solution. However the injection period has a large influence on the coalescence volumes. When  $T$  was less than or equal to one second the coalescence volume was much smaller than for the lower injection periods in all cases, independent of the spatial distances or pattern. The table illustrates only the minimum volume necessary for coalescence of all three bubbles within the endpoint of the terminal velocity region.

Table(IV-3) Summary of Triple Bubble Phenomena

Test Fluids		1%CMC		1%PAA	
Separation	Pattern	$\tau \leq 1s^{-1}$	$\tau > 1s^{-1}$	$\tau \leq 1s^{-1}$	$\tau > 1s^{-1}$
*		**	**	**	**
9/9	Linear	NC	1.04	NC	1.72
15/15	Linear	3.37	6.08	8.1	11.6
30/30	Linear	8.0	11.20	11.64	NC
30/15	Linear	3.4	11.14	4.4	11.42
30/9	Linear	2.01	4.56	3.7	8.23
18/10		2.44	3.52	4.88	10.7
9/10		1.58	2.60	4.45	6.86
20/20	Linear	6.8	10.9	8.9	NC
25/25	Linear	8.14	NC	10.6	NC
39/39/50		9.72	NC	10.7	NC
29/29/50		6.50	NC	7.56	NC

\* Note Distances Given are  $\times 10^{-3}m$

\*\* Volumes  $\times 10^{-6}m^3$

NC = no coalescence (complete)

If the bubbles produce shearing stresses resulting in deformations to the bulk viscoelastic liquid at a rate superceding transient relaxations (D5) viscous resistances will be greatly diminished thereby allowing bubbles to impact with greater force (i.e., greater accelerations).

This shock will enhance the enlargement of film surfaces and reduce the coalescence times considerably. Also more surface contact area is created when three bubbles collide so by reasoning provided by Adamson (A5) quicker coalescence times should exist for the three bubble cases in comparison to similar two bubble cases. Triangular or closed patterns provided more interaction than linear patterns and in some cases lowered the coalescence volumes. More experimentation has to be performed in this area to quantify any definite trends. However, as the separation between orifices ( $\Lambda$ ) increases the volume required for complete coalescence also increases for both 1% CMC and 1% PAA. The mode of coalescence for three bubbles is practically the same as for the two bubble case, except occasionally two bubbles will coalesce first and the third coalescing with the product of the first two.

This is depicted in Figure (IV-11) where two bubbles have coalesced already (both  $1.0 \times 10^{-5} \text{ m}^3$  in volume) at an injection-period of  $1/2 \text{ s}$  and a linear separation of  $3.0 \times 10^{-2} \text{ m}$  in 1% PAA.

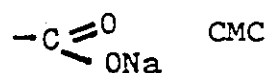
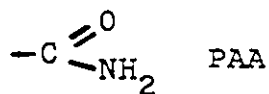


Figure (IV-11) Three Bubble Coalescence Phenomena

(The two bubbles on the right have already coalesced, both  $1.0 \times 10^{-5} \text{ m}^3$  in volume, at an injection period of  $\frac{1}{4}$ s and a linear separation of  $3.0 \times 10^{-2} \text{ m}$  in 1% PAA)



Shown in Figures (IV-12) and (IV-13) are photographs of the sequence involved in two and three bubble coalescence. In general the bubble below travels in the wake of the leading bubble achieving a velocity equal to its own terminal velocity plus the wake velocity of the leading bubble, then accelerates greatly toward it. By virtue of the bubble relative volumes, the bubbles collide and form a thin interfacial film between them, film thinning and drainage occur and the bubbles coalesce. In the case of three bubble coalescence, however, the central bubble manages to position itself ahead of the other two bubbles. The three bubbles initially after injection repel each other and the outer two bubbles acquire a radial velocity component, literally pushing themselves away from the central bubble. The central bubble rises on an axial trajectory only. Hence this manipulation allows for the central bubble to position itself slightly ahead of the other two bubbles. This repulsive action may be a result of vortex or wake interaction, elastic effects or possibly some type of electrostatic phenomenon. Monolayers may become charged dependent on the ionic properties of the polymer solution. The polymers used in this work may be considered ionizable because of their side groups:



Hence, conditions for charged monolayers could exist. Bikerman (A5) has published results on the electrical conductivity of bubbles and if applied to this situation, three bubble repulsion could be explained as simply an electrostatic phenomenon. More experimentation in this area would be welcome. From Figures (IV-12) and (IV-13) the lower bubble will change its trajectory immensely and even undergo large deformations to collide with the leading bubble. An explanation for this action may possibly be derived considering pressure variations in boundary layer theory.

Figure(IV-12)Small Bubble Coalescence PhenomenaTOP ROW:

1% PAA

$$V_1 = 4.70 \times 10^{-6} \text{ m}^3$$

$$V_2 = 1.0 \times 10^{-6} \text{ m}^3$$

$$\Lambda = 2.4 \times 10^{-2} \text{ m}$$

$$\tau = 4 \text{ s}$$

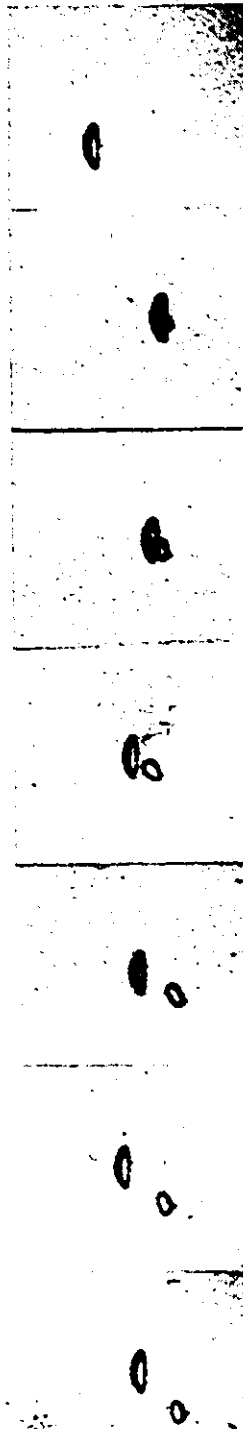
BOTTOM ROW:

1% CMC

$$V_1 = V_2 = V_3 = 1.5 \times 10^{-6} \text{ m}^3$$

$$\Lambda = 9.0 \times 10^{-3} \text{ m}$$

$$\tau = 1/2 \text{ s}$$



2



Figure(IV-13). Large Bubble Coalescence PhenomenaTOP ROW:1%PAA

$$V_1 = 9.33 \times 10^{-6} \text{ m}^3$$

$$V_2 = 3.53 \times 10^{-6} \text{ m}^3$$

$$\Lambda = 2.4 \times 10^{-2} \text{ m}$$

$$\tau = 10\text{s}$$

BOTTOM ROW:1%CMC

$$V_1 = V_2 = V_3 = 7.5 \times 10^{-6} \text{ m}^3$$

$$\Lambda = 3.0 \times 10^{-2} \text{ m}$$

$$\tau = 1\text{s}$$





## CHAPTER V. CONCLUSIONS

The viscosity and primary normal stress difference were measured for the two elastic fluids used in this work. The non-Newtonian viscosity for the 1% CMC and 1% PAA solution was, by order of magnitude, quite similar, whereas the primary normal stress difference was greater in the case of PAA under the shear rate range measured.

The shape and motion of the air bubbles were governed by hydrodynamic forces, surface tension, elasticity and viscosity. No velocity discontinuity was observed by plotting the logarithm of velocity against the logarithm of volume in the case of the two non-Newtonian fluids and the Newtonian glycerol solution. Also, there was no appreciable effect of injection period upon terminal velocity and the eccentricity ( $D/H$ ) for the air bubbles.

The eccentricity ( $D/H$ ) for the bubbles increased with increasing volume as a result, predominantly, of inertia. The eccentricity data for the glycerol solution were scattered because of the random shape dilations the bubbles undertook in this solution.

Furthermore, the friction factors as a function of the Reynolds number were determined using the three fluids. The two non-Newtonian fluids 1% CMC and 1% PAA revealed friction factor curves lower than that described by Stoke's Law due to their non-spherical shape.

Coalescence was seen to occur in three stages for both the simultaneous injection of two and three bubbles. In stage one a bubble or bubbles enter the region behind the

leading bubble with both axial and radial velocity components. Experiencing less drag in this region behind the leading bubble, the trailing bubble/bubbles accelerate significantly until collision takes place with a thin film separating the bubbles.

In stage three a process of film thinning takes place leading to rupture of the film and coalescence. From the corresponding photography and 16mm movie film on these bubble dynamics, it was obvious that the coalescence phenomena is symmetrical. Therefore, a model based on a symmetrical wake could be used to account for the velocity and acceleration present in this region.

An empirical graph relating the volume necessary for coalescing with a  $1.0 \times 10^{-6} \text{ m}^3$  bubble as a function of the initial horizontal orifice separation distance was drawn demonstrating the delaying effect of elasticity on coalescence.

## CHAPTER VI. RECOMMENDATIONS FOR FURTHER WORK

- (i) More experimentation is required with various elastic solutions of varying concentrations to substantiate this work's claim of no velocity discontinuity.
- (ii) Since the experimental apparatus can be manipulated to inject different gases, it would be advantageous to study bubbles of monatomic, polyatomic and inert gases.
- (iii) Chemicals which influence the surface chemistry of bubbles (surfactants) should be added to various elastic fluids to further understand their behaviour.
- (iv) Dimensional analysis is required in modelling the velocity and coalescence phenomena discovered by this work.
- (v) High speed movie work would be helpful in explaining more confidently the phenomena witnessed..
- (vi) The graphical correlation based on two bubble coalescence should be extended to cover more bubbles injected simultaneously and different gases so as to aid in designing distributor plates and other gas liquid contact devices.

- (vii) Weakly evident from the movie on bubble coalescence, bubbles upon injection would veer away eventually acquiring greater mutual separations as compared to initial injection separation. It would be interesting to observe this phenomena with solutions more electrolytic in character and possibly explain it in terms of electrostatic forces between the gas and liquid.
- (viii) The injection of one bubble of a certain gas and another bubble of a different gas would examine the behaviour of multigas coalescence phenomena, as yet untested.
- (ix) Laser doppler anamometry could be used to examine the velocity distributions surrounding these rising bubbles in elastic fluids.
- (x) Synthetic blood or a reasonable substitute could be used in place of the elastic solutions to examine the behaviour of bubbles in the human circulatory system.
- (xi) Lastly, this automatic injection system could lead to an improved method of mixing gas-liquid components; tests should be carried out to discern under what conditions it would be feasible.

NOMENCLATURE

A	Area of the film ( $m^2$ )
B	Dimensionless parameter defined by equation (II-26)
C	Constant in equation ( <u>IV</u> -12)
c	Constant in De K��e Pnsd model equation ( <u>IV</u> -31)
D	Diameter of bubble (m)
D <sub>c</sub>	Diameter of chamber (m)
D <sub>e</sub>	Equivalent diameter of bubble (m)
E <sub>o</sub>	E��tvos number
E	Elasticity of the film ( $Nm^{-2}$ )
f	Friction factor as defined by equation ( <u>IV</u> -6)
F <sub>D</sub>	Drag force on bubble (N)
g	Acceleration due to gravity ( $ms^{-2}$ )
H	Height of bubble (m)
K	Correction factor for wall effects equation ( <u>IV</u> -38)
K <sub>n</sub>	Dimensionless parameter defined by equation (II-10)
k'	Shift factor defined by equation ( <u>IV</u> -17)
L	Separation (vertical) between bubbles (m)
L <sub>c</sub>	Critical vertical separation distance (m)
m	Fluid consistency index ( $kgm^{-1}s^{n-2}$ )
Mo	Morton number
n	Fluid behaviour index
P	Pressure ( $Nm^{-2}$ )
r	Radial spacial coordinate (m)
R	Radius of bubble (m)

Re	Reynolds number
$R_{ec}$	Critical equivalent radius of bubble (m)
s	Dimensionless parameter in equation (II-5) (s).
t	Reciprocal of stroboscopic frequency (s).
$t_1$	Time constant in equation ( <u>IV</u> -5) (s).
$t_p$	Constants in De Kée Pnsd equation ( <u>IV</u> 20-21) (s).
$T_c$	Coalescence time (s)
$u_i$	Chemical potential of species i (Nm.moles <sup>-1</sup> )
v	Velocity of bubble (m/s).
$v_A, v_B$	Velocity of leading bubble. Velocity of trailing bubble (m/s).
$v_{A\infty}$	Terminal velocity of leading bubble (m/s).
$v_{\infty}$	Terminal velocity of bubble (m/s).
$v_t$	Tangential velocity of surface (m/s).
$v_{wo}$	Axial wake velocity (m/s).
$v_w$	Wake velocity in vertical direction (m/s).
V	Volume of bubble (m <sup>3</sup> )
$V_A, V_B$	Volume of leading, trailing bubble (m <sup>3</sup> )
$V_c$	Coalescent volume (m <sup>3</sup> )
$V_{cr}$	Critical volume (m <sup>3</sup> )
$w_i$	Uncertainty in value i.
Ws	Weissenberg number
$X_n, X'_n$	Pseudoplasticity correction factor for index n.
$\Delta x$	Distance travelled by bubble within time t (s).
z	Axial distance (m)

GREEK SYMBOLS

$\sigma$	Surface tension (N/m)
$\rho$	Density of continuous phase ( $\text{kg/m}^3$ )
$\rho_p$	Density of particle ( $\text{kg/m}^3$ )
$\Delta\rho$	Density difference between 2 phases ( $\text{kg/m}^3$ )
$\dot{\gamma}$	Shear rate ( $\text{s}^{-1}$ )
$\dot{\gamma}_0$	Initial shear rate ( $\text{s}^{-1}$ )
$\lambda_p$	Constants in De Kée Pnsd equation ( <u>IV</u> 21-22) (s).
$\eta$	Non-Newtonian viscosity (Pa.s)
$\eta_0$	Zero shear viscosity (Pa.s)
$\eta_{\infty}$	Infinite shear viscosity (Pa.s)
$\eta_p$	Constants in De Kée viscosity and Pnsd equations ( <u>IV</u> 20-22).
$\eta_{\text{eff}}$	Effective viscosity defined by equation ( <u>IV</u> -18) (Pa.s).
$\psi_{12}$	Primary normal stress coefficient ( $\text{Pa.s}^2$ )
$\mu$	Newtonian viscosity of continuous phase (Pa.s)
$\nu$	Kinematic viscosity of continuous phase ( $\text{m}^2/\text{s}$ )
$T$	Injection Period (s)
$\tau_0$	Shear stress (Pa.)
$\Phi$	Dummy variable in equation (II-10)
$\Omega$	Integration constant in equation (II-20)
$\phi$	Integration constant in equation (II-21)
$\Lambda$	Horizontal orifice separation (m)
$\Gamma_1$	Surface excess ( $\text{moles.m}^{-2}$ )
$\langle \rangle$	Average of property specified
$\psi_{\infty}$	Constant in De Kée Pnsd equation ( <u>IV</u> -21) ( $\text{Pa.s}^2$ ).
$\tau_{11}, \tau_{22}$	Normal stresses (Pa)
$\hat{\sigma}$	Standard deviation

### REFERENCES

- A1 - Astarita G. and Apuzzo G., A.I.Ch.E.J., II, 815 (1965).
- A2 - Acharya A., Mashelkar R., and Ulbrecht J., Chem. Eng. Sci., 32, 813 (1977).
- A3 - Astarita G., Ind. Eng. Chem. Fund., 5, 549 (1966).
- A4 - Acharya G. and Ulbrecht J., A.I.Ch.E. J., 24, 348 (1978).
- A5 - Adamson A., Physical Chemistry of Surfaces (3rd Edition) John Wiley & Sons, 1976.
- B1 - Barnett S., Humphrey A. E., and Litt M., A.I.Ch.E., 12, 253 (1966).
- B2 - Bharvaraju S., Mashelkar R., and Blanch H., A.I.Ch.E. J., 24, 1063 (1978).
- B3 - Batchelor G. K., Bond I. H., Surveys in Mechanics, Cambridge Press, 1956.
- B4 - Bhaga D. and Weber M.E., Chem. Eng. Sci., 35, 2467 (1980).
- B5 - Bird R., Stewart W., and Lightfoot E., Transport Phenomena, John Wiley & Sons, New York, 1960.
- B6 - Burdon R. S., Surface Tension and Spreading of Liquids (2nd Edition), Cambridge University Press, 1949.
- C1 - Calderbank R. H., Johnson S. L. and Loudon J., Chem. Eng. Sci., 25, 235 (1970).
- C2 - Costes J. and Alran C., Int. J. Mphse. Flow., 4, 535 (1978).
- C3 - Chhabra R. P. and Uhlherr P. H., Rheol. Acta, 19, 187 (1980).
- C4 - Clift R., Grace J.R. and Weber M., Bubble Drops and Particles, Academic Press (1978).



REFERENCES (Continued)

- C5 - Crabtree J. R. and Bridgewater J., Chem. Eng. Sci., 26, 839 (1971).
- D1 - Davidson J. and Schuler B. D., Trans. Inst. Chem. Eng., 58, 144 (1960).
- D2 - DeNevers N. and WU. J. L., A.I.Ch.E. J., 17, 182 (1971).
- D3 - De Kée D., Carreau P. J., J. of Rheol., 24 (3), 319-324 (1980).
- D4 - Davies J. T., Rideal E. K., Interfacial Phenomena (2nd Edition) Academic Press. New York, 1963.
- D5 - De Kée D., Carreau P. J., J. of Non-Newtonian Fluid Mech., 6, 127 (1979).
- G1 - Grace J. and Harrison D., Chem. Eng. Sci., 22, 1337 (1967).
- G2 - Grace J., Wairegi T. and Nguyen T., Trans. Inst. Chem. Engrs., 54, 167 (1967).
- G3 - Garner F. and Hammerton D., Chem. Eng. Sci., 1, 3 (1954).
- G4 - Garabedian P. R., Proc. R. Soc. A241, 423 (1957).
- H1 - Hassager O., Nature, 279, 402 (1979).
- H2 - Harmathy T., A.I.Ch.E. J., 6, 281 (1960).
- H3 - Hadamard J., Acad. Sci. Paris, 152, 1735 (1911).
- H4 - Hirose T. and Moo-Young M., Can. J. Chem. Eng., 47, 265 (1969).
- H5 - Hirose T. and Moo-Young M., Ind. Eng. Chem. Fund., 11, 281 (1972).
- H6 - Hughes R. R., Gilliland E. R., Chem. Engng. Prog. 48, 497 (1952).
- K1 - Kumar R. and Kuloor N. R., Can. J. Chem. Eng., 48, 383 (1969).
- K2 - Kline S.J. and F.A. McClintock., Mech. Eng., 3 (1953)

REFERENCES (Continued)

- L1 - Leal L. G., Acrivos A. and Skoog J., Can. J. Chem. Eng., 44, 569 (1971).
- L2 - Lee J. and Ssali G. W. K., VDI-Berichte, 182 (1972)
- L3 - Levich, V., Physiochemical Hydrodynamics, Prentice-Hall, 1962.
- L4 - Lodge A. S., Elastic Liquids, Academic, New York, 1964.
- M1 - Mashelkar R. A., A.I.Ch.E. J., 24, 1070 (1978).
- M2 - Marrucci G., Chem. Eng. Sci., 24, 975 (1969).
- M3 - Mordarski J., De Kée D., Chemical Engineering, March 7, 1983.
- N1 - Narayanan S., Goosens L. and Kossen N., Chem. Eng. Sci., 29, 2091 (1974).
- P1 - Prandtl L. and Tietjens O., Fundamentals of Hydro and Aeromechanics, Dover Publications Inc. New York, 1957.
- R1 - Rybczynski W., Bull. Acad. Sci. Graco., A40 (1911).
- S1 - Shiloh K. S., Sideman S. and Resnick W., Can. J. Chem. Eng., 51, 542 (1973).
- S2 - Schlichting H. R., Boundary Layer Theory (6th Edition), McGraw-Hill Co., 1968.
- S3 - Shih F. S., Ph.D. Thesis, University of Cincinnati (1968).
- T1 - Ting R. Y., A.I.Ch.E. J., 21, 810 (1975).
- T2 - Treolar L.R.G., Introduction to Polymer Science, Wykeham Publications. New York, 1970.
- W1 - Warshay M., Bogusz E., Johnson M. and Kintner R., Can. J. Chem. Eng., 29 Feb. (1959).
- Y1 - Yang W. J. and Liang C.Y., J. Appl. Phys., 43, 3060 (1972).
- Z1 - Zieminski S. and Raymond D., Chem. Eng. Sci., 17, 23 (1968).
- Z2 - Zana E., Ph.D. Thesis, California Institute of Technology (1975).

Appendix I

Experimental Results of Terminal Velocity,  
Volume, Diameter and Height of Bubbles in  
the 3 Fluids Studied.

40% (wt) Glycerol

$V \times 10^{+6} \frac{m}{s}$ I.P. (S)	TERMINAL VELOCITY $\times 10^{+2} \frac{m}{s}$			D/H (DIMENSIONLESS)		
	2	10	30	2	10	30
0.04	22.63	22.81	22.63	1.72	1.57	1.50
0.08	21.85	21.92	21.74	1.79	1.81	1.75
0.10	20.75	20.66	20.48	1.44	1.37	1.70
0.20	21.86	21.32	21.20	1.70	1.81	1.93
0.30	22.39	21.97	21.86	2.56	2.36	2.40
0.40	22.81	22.75	22.93	1.70	1.74	2.03
0.50	23.35	23.27	22.88	1.05	1.96	1.96
0.70	24.45	24.21	22.43	2.37	2.27	2.57
0.90	25.16	24.43	25.00	2.81	2.51	2.50
1.20	25.57	25.57	27.36	2.56	2.89	3.10
1.50	26.83	26.23	26.71	2.82	2.78	2.97
1.80	27.49	28.20	28.14	2.66	2.79	2.65
2.0	27.66	27.66	27.55	2.82	2.96	2.57

40% (wt) Glycerol

$V \times 10^{+6}$ I.F. $\eta$ (S)	AVERAGE DIAMETER $\times 10^{+6}$ m			AVERAGE HEIGHT $\times 10^{+2}$ m		
	2	10	30	2	10	30
0.04	0.43	0.33	0.39	0.25	0.21	0.26
0.08	0.40	0.56	0.49	0.23	0.31	0.28
0.10	0.49	0.59	0.63	0.34	0.43	0.37
0.20	0.75	0.87	0.85	0.44	0.48	0.44
0.30	1.18	1.11	1.13	0.46	0.47	0.47
0.40	1.02	1.08	1.10	0.60	0.62	0.54
0.50	1.11	1.04	0.98	0.60	0.53	0.50
0.70	1.35	1.39	1.44	0.57	0.61	0.56
0.90	1.60	1.73	1.70	0.57	0.69	0.68
1.20	1.79	1.85	1.80	0.70	0.64	0.58
1.50	2.12	2.20	2.17	0.75	0.79	0.73
1.80	1.97	2.21	2.28	0.74	0.79	0.86
2.0	2.23	2.25	2.34	0.71	0.76	0.91

1% (wt) CMC

$V \times 10^{+6}$ I.F. $\tau$ (s)	TERMINAL VELOCITY $\times 10^{+2} \text{ m/s}$					
	1	2	6	10	20	60
0.050	2.94	2.70	2.50	2.50	2.50	--
0.061	3.57	3.57	3.13	3.57	3.57	3.57
0.071	4.54	4.35	4.17	4.17	4.76	5.0
0.081	4.55	5.0	5.0	4.76	5.0	4.76
0.091	5.56	5.0	5.26	5.56	5.56	5.56
0.104	6.25	6.25	6.25	6.25	6.25	6.25
0.12	6.25	6.25	7.14	6.25	6.25	7.14
0.152	8.33	8.33	8.33	8.33	9.09	8.33
0.203	10.63	10.69	10.72	10.69	10.48	10.18
0.254	11.97	12.16	12.28	12.28	11.47	11.37
0.310	13.53	13.56	13.41	13.77	13.98	14.01
0.51	16.37	16.17	16.46	16.46	16.76	16.27
1.03	12.16	18.56	18.76	18.96	18.56	18.76
2.04	22.15	21.86	21.86	21.86	21.66	21.86
10.41	30.53	28.54	28.29	28.14	27.94	27.55

1% (wt) CMC

$\eta_{sp}/c$ $\times 10^6$ I.P. (S)	AVERAGE DIAMETER $\times 10^{12}$ m					
	1	2	6	10	20	60
0.050		0.40	0.40	0.40	0.40	
0.061		0.40	0.42	0.41	0.42	
0.071		0.47	0.46	0.46	0.48	
0.081		0.45	0.45	0.45	0.42	
0.091		0.48	0.51	0.49	0.52	
0.104		0.51	0.50	0.52	0.50	
0.12		0.58	0.56	0.60	0.60	
0.152		0.60	0.62	0.60	0.61	
0.203	0.70	0.67	0.68	0.68	0.71	0.69
0.254	0.72	0.80	0.79	0.76	0.79	0.71
0.310	0.81	0.83	0.85	0.85	0.87	0.84
0.51	0.87	0.89	0.91	0.93	0.92	0.90
1.03	1.16	1.21	1.15	1.19	1.19	1.2
2.04	1.67	1.62	1.63	1.66	1.61	1.61
10.41	3.18	3.20	3.22	3.23	3.25	3.29

1% (wt) CMC

$V \times 10^{-6} \text{ m}^3$ I.P. (S)	AVERAGE HEIGHT $\times 10^{-2} \text{ m}$					
	1	2	6	10	20	60
0.050		0.48	0.49	0.48	0.49	
0.061		0.52	0.52	0.52	0.50	
0.071		0.61	0.60	0.61	0.61	
0.081		0.60	0.62	0.61	0.62	
0.091		0.65	0.65	0.65	0.65	
0.104		0.68	0.70	0.68	0.70	
0.12		0.65	0.68	0.70	0.70	
0.152		0.72	0.72	0.72	0.72	
0.203	0.82	0.79	0.81	0.83	0.81	0.80
0.254	0.87	0.91	0.91	0.88	0.86	0.88
0.310	0.98	0.97	0.98	0.98	0.97	0.95
0.51	0.99	0.97	1.00	0.99	0.99	1.00
1.03	1.11	1.11	1.08	1.12	1.10	1.12
2.04	1.23	1.18	1.19	1.18	1.21	1.12
10.41	1.51	1.43	1.44	1.42	1.44	1.35

A



1% (wt) CMC

$V \times 10^{16} \frac{m}{s}$ I.P. $\tau$	D/H (DIMENSIONLESS)					
	1	2	6	10	20	60
0.050		0.83	0.82	0.83	0.82	
0.061		0.77	0.81	0.78	0.84	
0.071		0.77	0.77	0.75	0.78	
0.081		0.75	0.73	0.74	0.67	
0.091		0.74	0.78	0.75	0.8	
0.104		0.75	0.71	0.76	0.71	
0.12		0.89	0.81	0.86	0.86	
0.152		0.83	0.86	0.83	0.85	
0.203	0.85	0.85	0.84	0.82	0.87	0.86
0.254	0.83	0.88	0.87	0.86	0.91	0.81
0.310	0.83	0.86	0.87	0.87	0.89	0.88
0.51	0.88	0.92	0.91	0.94	0.93	0.9
1.03	1.05	1.09	1.06	1.06	1.08	1.07
2.04	1.36	1.37	1.37	1.41	1.33	1.35
10.41	2.11	2.24	2.24	2.27	2.26	2.43

$V \times 10^{+6} \frac{m}{s}$		1% (wt) PAA					
$\frac{I.P.}{(S)}$		TERMINAL VELOCITY $\times 10^{+2} \frac{m}{s}$					
		2	4	6	10	20	60
0.035		3.17	3.14	3.06	3.02	3.05	3.08
0.051		4.26	3.92	3.82	3.82	3.78	3.82
0.061		4.66	4.26	4.22	4.23	4.29	4.39
0.072		5.19	5.13	5.03	5.06	4.86	5.24
0.082		5.66	5.76	5.69	5.59	5.79	5.09
0.093		6.59	6.25	6.22	6.12	6.25	6.45
0.102		7.89	7.19	6.86	6.72	7.22	7.06
0.122		9.21	8.54	8.48	8.38	8.28	8.54
0.152		9.18	9.31	9.18	9.15	9.21	8.91
0.21		11.75	11.55	11.24	11.18	11.11	12.23
0.26		13.07	13.83	13.54	14.01	13.24	13.20
0.31		15.90	15.07	15.53	14.67	15.60	15.61
0.52		18.12	17.89	18.03	18.0	17.03	17.93
1.04		21.06	20.69	21.03	20.96	20.52	20.59
2.08		22.80	22.74	22.73	22.87	22.91	22.88
10.28		28.53	28.64	28.44	28.47	28.54	28.61

$V \times 10^{+6_m}$ I.P. (S)		1% (wt) PAA						
		AVERAGE DIAMETER $\times 10^{+2_m}$						
		2	4	6	10	20	60	
0.035		0.41	0.39	0.37	0.39	0.40	0.39	
0.051		0.42	0.42	0.40	0.39	0.40	0.41	
0.061		0.44	0.42	0.44	0.42	0.41	0.43	
0.072		0.45	0.47	0.45	0.48	0.46	0.48	
0.082		0.45	0.49	0.43	0.46	0.48	0.48	
0.093		0.49	0.46	0.49	0.47	0.53	0.51	
0.102		0.51	0.48	0.51	0.49	0.50	0.47	
0.122		0.55	0.48	0.49	0.48	0.48	0.56	
0.152		0.55	0.53	0.59	0.56	0.55	0.53	
0.21		0.61	0.60	0.53	0.59	0.61	0.58	
0.26		0.69	0.73	0.69	0.73	0.76	0.71	
0.31		0.77	0.78	0.78	0.77	0.80	0.83	
0.52		0.94	0.93	0.96	1.01	0.93	0.97	
1.04		1.33	1.29	1.36	1.32	1.32	1.28	
2.08		1.90	1.87	1.84	1.86	1.81	1.85	
10.28		3.61	3.61	3.63	3.57	3.59	3.60	

1% (wt) PAA

V x 10 <sup>+6</sup> I.P. (S)	AVERAGE HEIGHT x 10 <sup>+2</sup> m						
	1	2	6	10	20	60	
0.035	0.47	0.45	0.46	0.47	0.46	0.49	
0.051	0.53	0.51	0.49	0.51	0.50	0.49	
0.061	0.50	0.48	0.53	0.49	0.49	0.49	
0.072	0.52	0.59	0.55	0.56	0.56	0.58	
0.082	0.52	0.59	0.60	0.57	0.58	0.55	
0.093	0.64	0.60	0.59	0.67	0.61	0.60	
0.102	0.65	0.63	0.62	0.68	0.61	0.65	
0.122	0.68	0.70	0.66	0.70	0.68	0.74	
0.152	0.72	0.72	0.74	0.70	0.69	0.69	
0.21	0.72	0.81	0.77	0.74	0.77	0.81	
0.26	0.86	0.83	0.88	0.92	0.87	0.84	
0.31	0.90	0.93	0.92	0.93	0.92	0.95	
0.52	1.00	0.94	0.99	1.00	0.99	0.98	
1.04	1.05	1.08	1.11	1.09	1.11	1.05	
2.08	1.08	1.11	1.11	1.14	1.12	1.14	
10.28	1.35	1.31	1.25	1.23	1.20	1.28	

1% (wt) PAA

$V \times 10^{-6} \frac{3}{n^2}$ I.P. (S)	D/H DIMENSIONLESS						
	2	4	6	10	20	60	
0.035	0.87	0.86	0.80	0.83	0.87	0.80	
0.051	0.79	0.82	0.82	0.76	0.80	0.84	
0.061	0.88	0.88	0.83	0.86	0.84	0.88	
0.072	0.87	0.87	0.82	0.86	0.82	0.83	
0.082	0.87	0.83	0.72	0.81	0.83	0.83	
0.093	0.76	0.77	0.83	0.70	0.87	0.85	
0.102	0.78	0.76	0.82	0.72	0.82	0.72	
0.122	0.81	0.69	0.74	0.69	0.71	0.76	
0.152	0.76	0.74	0.80	0.8	0.8	0.77	
0.21	0.85	0.74	0.69	0.8	0.8	0.72	
0.26	0.80	0.88	0.79	0.8	0.87	0.85	
0.31	0.86	0.84	0.85	0.83	0.87	0.87	
0.52	0.94	0.99	0.97	1.01	0.94	0.99	
1.04	1.27	1.19	1.23	1.21	1.19	1.22	
2.08	1.76	1.68	1.67	1.63	1.62	1.62	
10.28	2.67	2.76	2.9	2.9	3.0	2.8	

## Appendix II

Non-Linear Regression Computer Program  
Utilized in Modelling Viscosity and  
Primary Normal Stress Difference

```

SUBROUTINE ATFRIV (XXXXXXXXXX JCE M.
C NON-LINEAR REGRESSION PROGRAM
C *****
1 DIMENSION X(50),Y(50),W(50),CX(10)
2 DIMENSION RX(50,10),RY(50),RZ(50),PERCENT(50)
3 DIMENSION P(10),PG(10),PA(10),PART(10),DIFF(10)
4 REAL LAMDA
5 LOGICAL FAIL
6 COMMON A,E
7 A=1E-150
8
9
10 130 FORMAT(1P1)
11 WRITE(6,5)
12 5 FORMAT(' THE FOLLOWING DATA WERE READ IN AS INPUT',/,
13 ' IT IS PRINTED FOR THE PURPOSE OF CHECKING THE INPUT DATA',//)
14 READ(5,10) NCATA,NP
15 WRITE(6,15) NCATA,NP
16 15 FORMAT(2I6)
17 READ(6,10) (I=1,NP)
18 WRITE(6,25) (PG(I),I=1,NP)
19 25 FORMAT(1X,10F12.7)
20 35 FORMAT(2F20.10)
21 DO 30 I=1,NCATA
22 READ(5,10) X(I),Y(I)
23 WRITE(6,35) Y(I),X(I)
24 30 CONTINUE
25
26 C
27 C
28 C
29 C
30 C
31 C
32 C
33 C
34 C
35 C
36 C
37 C
38 C
39 C
40 C
41 C
42 C
43 C
44 C
45 C
46 C
47 C
48 C
49 C
50 C
51 C
52 C
53 C
54 C
55 C
56 C
57 C
58 C
59 C
60 C
61 C
62 C
63 C
64 C
65 C
66 C
67 C
68 C
69 C
70 C
71 C
72 C
73 C
74 C
75 C
76 C
77 C
78 C
79 C
80 C
81 C
82 C
83 C
84 C
85 C
86 C
87 C
88 C
89 C
90 C
91 C
92 C
93 C
94 C
95 C
96 C
97 C
98 C
99 C
100 C
101 C
102 C
103 C
104 C
105 C
106 C
107 C
108 C
109 C
110 C
111 C
112 C
113 C
114 C
115 C
116 C
117 C
118 C
119 C
120 C
121 C
122 C
123 C
124 C
125 C
126 C
127 C
128 C
129 C
130 C
131 C
132 C
133 C
134 C
135 C
136 C
137 C
138 C
139 C
140 C
141 C
142 C
143 C
144 C
145 C
146 C
147 C
148 C
149 C
150 C
151 C
152 C
153 C
154 C
155 C
156 C
157 C
158 C
159 C
160 C
161 C
162 C
163 C
164 C
165 C
166 C
167 C
168 C
169 C
170 C
171 C
172 C
173 C
174 C
175 C
176 C
177 C
178 C
179 C
180 C
181 C
182 C
183 C
184 C
185 C
186 C
187 C
188 C
189 C
190 C
191 C
192 C
193 C
194 C
195 C
196 C
197 C
198 C
199 C
200 C
201 C
202 C
203 C
204 C
205 C
206 C
207 C
208 C
209 C
210 C
211 C
212 C
213 C
214 C
215 C
216 C
217 C
218 C
219 C
220 C
221 C
222 C
223 C
224 C
225 C
226 C
227 C
228 C
229 C
230 C
231 C
232 C
233 C
234 C
235 C
236 C
237 C
238 C
239 C
240 C
241 C
242 C
243 C
244 C
245 C
246 C
247 C
248 C
249 C
250 C
251 C
252 C
253 C
254 C
255 C
256 C
257 C
258 C
259 C
260 C
261 C
262 C
263 C
264 C
265 C
266 C
267 C
268 C
269 C
270 C
271 C
272 C
273 C
274 C
275 C
276 C
277 C
278 C
279 C
280 C
281 C
282 C
283 C
284 C
285 C
286 C
287 C
288 C
289 C
290 C
291 C
292 C
293 C
294 C
295 C
296 C
297 C
298 C
299 C
300 C
301 C
302 C
303 C
304 C
305 C
306 C
307 C
308 C
309 C
310 C
311 C
312 C
313 C
314 C
315 C
316 C
317 C
318 C
319 C
320 C
321 C
322 C
323 C
324 C
325 C
326 C
327 C
328 C
329 C
330 C
331 C
332 C
333 C
334 C
335 C
336 C
337 C
338 C
339 C
340 C
341 C
342 C
343 C
344 C
345 C
346 C
347 C
348 C
349 C
350 C
351 C
352 C
353 C
354 C
355 C
356 C
357 C
358 C
359 C
360 C
361 C
362 C
363 C
364 C
365 C
366 C
367 C
368 C
369 C
370 C
371 C
372 C
373 C
374 C
375 C
376 C
377 C
378 C
379 C
380 C
381 C
382 C
383 C
384 C
385 C
386 C
387 C
388 C
389 C
390 C
391 C
392 C
393 C
394 C
395 C
396 C
397 C
398 C
399 C
400 C
401 C
402 C
403 C
404 C
405 C
406 C
407 C
408 C
409 C
410 C
411 C
412 C
413 C
414 C
415 C
416 C
417 C
418 C
419 C
420 C
421 C
422 C
423 C
424 C
425 C
426 C
427 C
428 C
429 C
430 C
431 C
432 C
433 C
434 C
435 C
436 C
437 C
438 C
439 C
440 C
441 C
442 C
443 C
444 C
445 C
446 C
447 C
448 C
449 C
450 C
451 C
452 C
453 C
454 C
455 C
456 C
457 C
458 C
459 C
460 C
461 C
462 C
463 C
464 C
465 C
466 C
467 C
468 C
469 C
470 C
471 C
472 C
473 C
474 C
475 C
476 C
477 C
478 C
479 C
480 C
481 C
482 C
483 C
484 C
485 C
486 C
487 C
488 C
489 C
490 C
491 C
492 C
493 C
494 C
495 C
496 C
497 C
498 C
499 C
500 C
501 C
502 C
503 C
504 C
505 C
506 C
507 C
508 C
509 C
510 C
511 C
512 C
513 C
514 C
515 C
516 C
517 C
518 C
519 C
520 C
521 C
522 C
523 C
524 C
525 C
526 C
527 C
528 C
529 C
530 C
531 C
532 C
533 C
534 C
535 C
536 C
537 C
538 C
539 C
540 C
541 C
542 C
543 C
544 C
545 C
546 C
547 C
548 C
549 C
550 C
551 C
552 C
553 C
554 C
555 C
556 C
557 C
558 C
559 C
560 C
561 C
562 C
563 C
564 C
565 C
566 C
567 C
568 C
569 C
570 C
571 C
572 C
573 C
574 C
575 C
576 C
577 C
578 C
579 C
580 C
581 C
582 C
583 C
584 C
585 C
586 C
587 C
588 C
589 C
590 C
591 C
592 C
593 C
594 C
595 C
596 C
597 C
598 C
599 C
600 C
601 C
602 C
603 C
604 C
605 C
606 C
607 C
608 C
609 C
610 C
611 C
612 C
613 C
614 C
615 C
616 C
617 C
618 C
619 C
620 C
621 C
622 C
623 C
624 C
625 C
626 C
627 C
628 C
629 C
630 C
631 C
632 C
633 C
634 C
635 C
636 C
637 C
638 C
639 C
640 C
641 C
642 C
643 C
644 C
645 C
646 C
647 C
648 C
649 C
650 C
651 C
652 C
653 C
654 C
655 C
656 C
657 C
658 C
659 C
660 C
661 C
662 C
663 C
664 C
665 C
666 C
667 C
668 C
669 C
670 C
671 C
672 C
673 C
674 C
675 C
676 C
677 C
678 C
679 C
680 C
681 C
682 C
683 C
684 C
685 C
686 C
687 C
688 C
689 C
690 C
691 C
692 C
693 C
694 C
695 C
696 C
697 C
698 C
699 C
700 C
701 C
702 C
703 C
704 C
705 C
706 C
707 C
708 C
709 C
710 C
711 C
712 C
713 C
714 C
715 C
716 C
717 C
718 C
719 C
720 C
721 C
722 C
723 C
724 C
725 C
726 C
727 C
728 C
729 C
730 C
731 C
732 C
733 C
734 C
735 C
736 C
737 C
738 C
739 C
740 C
741 C
742 C
743 C
744 C
745 C
746 C
747 C
748 C
749 C
750 C
751 C
752 C
753 C
754 C
755 C
756 C
757 C
758 C
759 C
760 C
761 C
762 C
763 C
764 C
765 C
766 C
767 C
768 C
769 C
770 C
771 C
772 C
773 C
774 C
775 C
776 C
777 C
778 C
779 C
780 C
781 C
782 C
783 C
784 C
785 C
786 C
787 C
788 C
789 C
790 C
791 C
792 C
793 C
794 C
795 C
796 C
797 C
798 C
799 C
800 C
801 C
802 C
803 C
804 C
805 C
806 C
807 C
808 C
809 C
810 C
811 C
812 C
813 C
814 C
815 C
816 C
817 C
818 C
819 C
820 C
821 C
822 C
823 C
824 C
825 C
826 C
827 C
828 C
829 C
830 C
831 C
832 C
833 C
834 C
835 C
836 C
837 C
838 C
839 C
840 C
841 C
842 C
843 C
844 C
845 C
846 C
847 C
848 C
849 C
850 C
851 C
852 C
853 C
854 C
855 C
856 C
857 C
858 C
859 C
860 C
861 C
862 C
863 C
864 C
865 C
866 C
867 C
868 C
869 C
870 C
871 C
872 C
873 C
874 C
875 C
876 C
877 C
878 C
879 C
880 C
881 C
882 C
883 C
884 C
885 C
886 C
887 C
888 C
889 C
890 C
891 C
892 C
893 C
894 C
895 C
896 C
897 C
898 C
899 C
900 C
901 C
902 C
903 C
904 C
905 C
906 C
907 C
908 C
909 C
910 C
911 C
912 C
913 C
914 C
915 C
916 C
917 C
918 C
919 C
920 C
921 C
922 C
923 C
924 C
925 C
926 C
927 C
928 C
929 C
930 C
931 C
932 C
933 C
934 C
935 C
936 C
937 C
938 C
939 C
940 C
941 C
942 C
943 C
944 C
945 C
946 C
947 C
948 C
949 C
950 C
951 C
952 C
953 C
954 C
955 C
956 C
957 C
958 C
959 C
960 C
961 C
962 C
963 C
964 C
965 C
966 C
967 C
968 C
969 C
970 C
971 C
972 C
973 C
974 C
975 C
976 C
977 C
978 C
979 C
980 C
981 C
982 C
983 C
984 C
985 C
986 C
987 C
988 C
989 C
990 C
991 C
992 C
993 C
994 C
995 C
996 C
997 C
998 C
999 C
1000 C

```

```

71      CC 110 J=1.NP
72      110  RX(1,J)=PART(J)
73      100  RY(1)=YSTAR-Y(1)
74      CALL REG(RX,RY,NCATA,NP,DIFF1)
75      C    FIND NEW VALUE OF PARAMETERS
76      CC 120 I=1.NP
77      120  P(1)=P(1)+DIFFACT*DIFF(1)
78      C    THE FOLLOWING STATEMENTS MAY BE USED TO CHECK THE CONVERGENCE OF
79      C    THE ROUTINE BY REMOVING THE 'C' IN COLUMN 1 AND PRINT OUT THE
80      C    RESULTS OF EVERY ITERATION
81      125  WRITE(6,125)X
82      125  FORMAT(' ITERATION NUMBER', 14, /)
83      140  PRINT 215, I, PG(1), P(1), DIFF(1)
84      140  WRITE(6,125)X
85      145  FORMAT(' ITERATION NUMBER', 14, /)
86      145  WRITE(6,125)X
87      140  CC 140 I=1.NP
88      140  WRITE(6,125) I, PG(1), P(1), DIFF(1)
89      140  CC 150 I=1.NP
90      C    *****
91      C    NOTE CHANGED BASIS FOR CONVERGENCE
92      C    TOL=1 REFERS TO 10% CHANGE, TOL=2 REFERS TO 1% CHANGE, ETC.
93      C    IF (ABS(DIFF(1)).GE.ABS(P(1))*TOL) GO TO 160
94      C    *****
95      150  CONTINUE
96      155  FAIL=.FALSE.
97      155  WRITE(6,125)X
98      155  FORMAT(' SYSTEM CONVERGES AFTER', 14, ' ITERATIONS', //)
99      155  1 ' FINAL VALUES OF PARAMETERS ARE', //)
100      160  GO TO 200
101      160  CONTINUE
102      165  FAIL=.TRUE.
103      165  WRITE(6,125)X
104      165  FORMAT(' SYSTEM FAILS TO CONVERGE AFTER', 14, ' ITERATIONS', //)
105      165  1 ' FINAL VALUES OF PARAMETERS ARE', //)
106      170  WRITE(6,125)X
107      170  FORMAT(' PARAMETER          GUESS VALUE          FINAL VALUE          LAST
108      170  1 ' DIFFERENCE', //)
109      170  CC 210 I=1.NP
110      210  WRITE(6,215)I, PG(1), P(1), DIFF(1)
111      215  FORMAT(' 10, JE20, 7)
112      SUM=0.0
113      CC 250 I=1.NCATA
114      250  Z=X(I)
115      250  CALL MODEL(Z,P,NP,PART,YSTAR)
116      250  RZ(1)=YSTAR
117      250  IF (YSTAR.EC.0.0) YSTAR=1.0E-10
118      250  RY(1)=YSTAR-Y(1)
119      250  SUM=SUM+(1)*RY(1)*RY(1)
120      250  PERCENT(1)=RY(1)/YSTAR*100
121      250  CONTINUE
122      255  WRITE(6,255)
123      255  FORMAT(' 14, //, 3X, 'CATA', 6X, 'INDEPENDENT', 3X, 'DEPENDENT', 12X,
124      255  1 'WEIGHT', 12X, 'CALCULATED', 10X, 'ABSOLUTE', 7X, 'PERCENT', //,
125      255  2 3X, 'PCINT', 7X, 'VARIABLE', 10X, 'VARIABLE', 11X, 'VARIABLE',
126      255  3 12X, 'VARIABLE', 11X, 'DEVIATION', 5X, 'DEVIATION', //)
127      260  CC 260 I=1.NCATA
128      260  WRITE(6,265)I, X(1,Y(1)), X(1,Z(1)), RY(1), PERCENT(1)
129      265  FORMAT(' 10, 0G16, 7)
130      SUM=SQRT(SUM/(NCATA-1))
131      CALL CORR(Y,NCATA,RY,RC)
132      WRITE(6,275)SUM, RC
133      275  FORMAT(' 5X, //, 5X, 'STANDARD DEVIATION =', G14, 7, 5X, 'CORRELATION COE
134      275  EFFICIENT', G14, 7)
135      IF(FAIL) GO TO 111
136      300  CONTINUE
137      STOP
138      END
139
140      SUBROUTINE REG(RX,RY,NCATA,NP,DIFF)
141      DIMENSION X(20,10), Y(20), DIFF(10), A(20)
142      DIMENSION A(11,12), B(11,12)
143      N=NP+1
144      N=NP+2
145      CC 10 I=1.NP
146      10  CC 10 J=1.NP
147      10  A(1,J)=0.0
148      10  B(1,J)=0.0

```



```

130      CC 50 ICATA=1,ACATA
131      A(1,1)=1.0
132      CU 20 J=2,NN
133      A(1,J)=A(1,ICATA,J-1)
134      A(1,NN)=RY(1,ICATA)
135      CC 30 I=2,NN
136      CU 30 J=1,NN
137      IF (ABS(AX(ICATA,I-1))-LE-1.0E-10) RY(1,ICATA,I-1)=0.0
138      30 A(1,J)=A(1,J)*AX(ICATA,I-1)
139      CC 40 I=1,NN
140      CU 40 J=1,NN
141      E(1,J)=E(1,J)+A(1,J)*W(ICATA)
142      50 CONTINUE
143      IF(NP.EC.1) GO TO 160
144      N=NP
145      N=N+1
146      UL 60 I=1,NN
147      CU 60 J=1,NN
148      E(1,J)=E(1,J)+1
149      N1=NN-1
150      CC 110 K=1,NN1
151      L=K
152      K=K+1
153      CC 70 L=K+1,NN
154      IF (ABS(E(1,K))-GT. ACS(B(L,K))) L=L+1
155      70 CONTINUE
156      IF (L.EQ.K) GO TO 90
157      CC 80 J=K,NN
158      TEMP=E(K,J)
159      E(K,J)=E(L,J)
160      E(L,J)=TEMP
161      90 CU 100 L=K+1,NN
162      TEMP=E(1,K)/E(K,K)
163      CU 100 J=K+1,NN
164      E(1,J)=1(1,J)-TEMP*E(K,J)
165      110 CONTINUE
166      E(NN,NN)=E(NN,NN)/E(NN,NN)
167      CC 120 A=1,NN1
168      I=NN-K
169      TEMP=0.0
170      IP=1+1
171      CC 130 J=IP,NN
172      TEMP=TEMP+G(1,J)*E(J,NN)
173      120 E(1,NN)=E(1,NN)-TEMP/D(1,1)
174      CC 150 I=1,NN
175      150 DIFF(I)=E(1,NN)
176      RETURN
177      160 DIFF(1)=E(NN,NN)/E(NN,NN)
178      RETURN
179      END

```

```

180      C=PRINTN
181      SUBROUTINE CORR(Y,N,RY,R)
182      DIMENSION Y(50),RY(50)
183      AN=FLCAT(N)
184      SY=0.0
185      SYY=0.0
186      SUM=0.0
187      CC 1 I=1,N
188      SUM=SUM+RY(1)*2
189      SY=SY+Y(1)
190      SYY=SYY+Y(1)*2
191      SIG2=ABS(SYY/AN-(SY/AN)**2)
192      R2=1.0-SUM/SIG2/AN
193      R=SQRT(ABS(R2))
194      RETURN
195      END

```

C\*\*\*\*\*

```

195      FUNCTION WEIGHT(A)
196      C      GENERALISED WEIGHTING FUNCTION FOR THE DEPENDENT DATA
197      WEIGHT=1.0/A/A
198      RETURN
199      END

```

C\*\*\*\*\*

```

199      SUBROUTINE MCDL(Z,P,NF,PART,YSTAR)
200      REAL N1,N2,LMECA2,LMECA1
201      DIMENSION P(10),PART(10)
202      N1=1.019

```

```

203      N2=0.2071
204      T1=0.106E-02
205      T2=0.201E-04
206      LMECA2=0.0142E
207      LMECA1=0.172
208      R=2.*N1
209      S=2.*N2
210      A1=Z*T1*A(2)
211      A2=Z*T2*A(2)
212      IF (ABS(A1)-GE.100.0) A1=100
213      IF (ABS(A2)-GE.100.0) A2=100
214      A=LMECA1*EXP(-A1)
215      B=P(1)*EXP(-A2)
216      YSTAR=A+B
217      PART(1)=E/D(1)
218      PART(2)=-(Z*T1*A)-(Z*T2*B)
219      RETURN
220      END

```

## APPENDIX III

Uncertainty Analysis and Standard Deviations  
of  
Fitted Curves

The data used for the uncertainty analysis are taken from the case of a  $1.04 \times 10^{-6} \text{ m}^3$  bubble rising in a 1% PAA 50/50 glycerol water solution with an injection period of  $\tau = 10 \text{ s}$ . The uncertainty in the following quantities are estimated

$V_c, v_\infty, \langle v_\infty \rangle, D/H, \rho$ , using Kline and McClintock's method (K2).

(1) Terminal Velocity ( $v_\infty$ )

$$v_\infty = \frac{\Delta x}{t}$$

where  $\Delta x$  = the distance travelled by the bubble within two consecutive flashes of the stroboscope

$$\Delta x = (3.50 \pm 0.05) \times 10^{-2} \text{ m}$$

$t$  = the reciprocal of the stroboscopic frequency

$$t = 0.167 \pm 0.01 \text{ s} \quad \checkmark$$

$W_i$  = uncertainty in value  $i$

also

$$\begin{aligned} W_{v_\infty} &= \left[ \left( \frac{\partial v_\infty}{\partial \Delta x} W_{\Delta x} \right)^2 + \left( \frac{\partial v_\infty}{\partial t} W_t \right)^2 \right]^{\frac{1}{2}} \\ &= \left[ \left( \frac{W_{\Delta x}}{t} \right)^2 + \left( -\frac{\Delta x}{t^2} W_t \right)^2 \right]^{\frac{1}{2}} \\ &= v_\infty \left[ \left( \frac{W_{\Delta x}}{\Delta x} \right)^2 + \left( \frac{W_t}{t} \right)^2 \right]^{\frac{1}{2}} \end{aligned}$$

which gives  $v_\infty = (20.96 \pm 1.29) \times 10^{-2} \text{ m/s } (\pm 6.2\%)$

(2) Average Terminal Velocity  $\langle v_{\infty} \rangle$ 

$$\langle v_{\infty} \rangle = a (V - b)^{1/3} \text{ m/s}$$

$$\begin{aligned} \text{where } a &= 18.43 \pm 0 \\ b &= 4.56 \times 10^{-8} \pm 0 \\ V &= (1.04 \pm 0.005) \times 10^{-6} \text{ m}^3 \end{aligned}$$

$$\begin{aligned} \text{also } W_{\langle v_{\infty} \rangle} &= \left[ \left( \frac{\partial \langle v_{\infty} \rangle}{\partial V} W_V \right)^2 \right]^{\frac{1}{2}} \\ &= \left[ \frac{1}{3} a (V - b)^{-\frac{2}{3}} W_V \right] \end{aligned}$$

$$\text{which gives } \langle v_{\infty} \rangle = (18.48 \pm 0.031) \times 10^{-2} \text{ m/s } (\pm 0.17\%)$$

(3) Non-Dimensional (D/H)

$$W_{(D/H)} = \left[ \left( \frac{\partial (D/H)}{\partial D} W_D \right)^2 + \left( \frac{\partial (D/H)}{\partial H} W_H \right)^2 \right]^{\frac{1}{2}}$$

$$D = (1.32 \pm 0.05) \times 10^{-2} \text{ m}$$

$$H = (1.09 \pm 0.05) \times 10^{-2} \text{ m}$$

$$\text{also } W_{(D/H)} = \frac{D}{H} \left[ \left( \frac{W_D}{D} \right)^2 + \left( -\frac{W_H}{H} \right)^2 \right]^{\frac{1}{2}}$$

$$\text{which gives } (D/H) = 1.21 \pm 0.072 (\pm 5.9\%)$$

(4) Density of 1% PAA ( $\rho$ )

$$\rho = \frac{m_{\text{PAA}}}{V_{\text{PAA}}}$$

where  $m_{\text{PAA}} = (57.01 \pm 0.01) \times 10^{-3} \text{ kg}$

$$V_{\text{PAA}} = (50.55 \pm 0.10) \times 10^{-3} \text{ m}^3$$

also  $w_p = \left[ \left( \frac{\partial \rho}{\partial m_{\text{PAA}}} w_{m_{\text{PAA}}} \right)^2 + \left( \frac{\partial \rho}{\partial V_{\text{PAA}}} w_{V_{\text{PAA}}} \right)^2 \right]^{\frac{1}{2}}$

which gives  $\rho = (1128 \pm 2) \text{ kg/m}^3 (\pm 0.2\%)$

(5) Coalescent Volume ( $V_c$ )

$$V_c = A \text{ Exp } (B\Lambda)$$

$$A = 1.50 \times 10^{-6} \pm 0$$

$$B = 49.89 \pm 0$$

$$\Lambda = (10.0 \pm 1.0) \times 10^{-3} \text{ m}$$

$$w_{V_c} = \left[ \left( \frac{\partial V_c}{\partial \Lambda} w_{\Lambda} \right) \right] = B A \text{ Exp } (B\Lambda) w_{\Lambda}$$

which gives  $V_c = (2.47 \pm .12) \times 10^{-6} \text{ m}^3 (\pm 4.86\%)$

Standard deviations for the fitted curves were calculated using the following formula:

$$\hat{\sigma} = \sqrt{\frac{\sum_{i=1}^N (y_i - y_p)^2}{N-p}}$$

where  $\hat{\sigma}$  = Standard deviation  
 $y_i$  = Data point  
 $y_p$  = Fitted point  
 $N$  = Number of points  
 $p$  = Number of parameters

Fitted Quantity			$\hat{\sigma}$ (Standard Deviation)
Viscosity	40%	Glycerol	$\pm 5.1 \times 10^{-6}$ Pa.s
Viscosity	1%	CMC	$\pm 0.05$ Pa.s
PNSD	1%	CMC	$\pm 0.236$ Pa.s <sup>2</sup>
Viscosity	1%	PAA	$\pm 0.069$ Pa.s
PNSD	1%	PAA	$\pm 0.106$ Pa.s <sup>2</sup>
D/H	40%	Glycerol	$\pm 0.304 \times 10^{-2}$
D/H	1%	CMC	$\pm 0.138 \times 10^{-2}$
D/H	1%	PAA	$\pm 0.212 \times 10^{-2}$
$\langle v_{\infty} \rangle$	40%	Glycerol	$\pm 0.531 \times 10^{-2}$ m/s
$\langle v_{\infty} \rangle$	1%	CMC	$\pm 0.21 \times 10^{-1}$ m/s
$\langle v_{\infty} \rangle$	1%	PAA	$\pm 0.36 \times 10^{-1}$ m/s
f	40%	Glycerol	$\pm 0.022$
f	1%	CMC	$\pm 0.014$
f	1%	PAA	$\pm 0.017$
$v_c$	1%	CMC	$\pm 0.29 \times 10^{-6}$ m <sup>3</sup>
$v_c$	1%	PAA	$\pm 0.52 \times 10^{-6}$ m <sup>3</sup>

## VITA AUCTORIS

Joseph George Mordarski  
6340 Matchette Rd.  
Windsor, Ontario  
N9J-2J7  
Canada

Born: September 15, 1957, Nottingham, England

Public School: Woodthorpe Grammar School, England

Public School: St. Alexander (cont.), Canada

High School: F.J. Brennan, Windsor, Ontario, Canada

University: B.A.Sc. (1980) University of Windsor  
M.A.Sc. Candidate (1984) University of Windsor

Employment: Bruce Heavy Water Plant (1979)  
Dupont Canada Inc. (1980)  
University of Windsor (1981)  
St. Clair College (1983)  
Chrysler of Canada (1984)